

POLITECNICO DI TORINO

MASTER OF SCIENCE – BIOMEDICAL ENGINEERING

MASTER OF SCIENCE THESIS

CHITIN DERIVATIVES COATINGS ON TITANIUM SURFACES

SUPERVISOR:

Prof. Silvia Maria SPRIANO

CO-SUPERVISORS:

Doct. Sara FERRARIS

Doct. Gissur ÖRLYGSSON

CANDIDATE

Maria Stefania MASSARO

ACCADEMIC YEAR 2018/19

Index

INTRODUCTION	3
CHAPTER 1 – CHITIN AND ITS DERIVATIVES	4
1.1. CHITIN	5
1.2. STRUCTURE OF CHITOSAN	7
1.3. PROPERTIES OF CHITOSAN	9
1.3.1. <i>Antibacterial activity</i>	9
1.3.2. <i>Antifungal activity</i>	10
1.3.3. <i>Antitumor activity</i>	10
1.4. BIOMEDICAL AND PHARMACEUTICAL APPLICATIONS OF CHITOSAN	10
1.4.1. <i>Tissue engineering</i>	11
1.4.2. <i>Drug delivery systems</i>	11
1.4.3. <i>Cancer therapy</i>	12
1.4.4. <i>Wound healing</i>	12
1.4.5. <i>Bioactive implant coatings</i>	12
1.4.6. <i>Water treatment and food industry</i>	13
1.5. BIBLIOGRAPHY	14
CHAPTER 2 – HOST RESPONSE TO IMPLANTS	18
2.1. PROTEIN ADSORPTION	20
2.2. COMPLEMENT SYSTEM	22
2.3. LEUKOCYTE ADHESION	23
2.4. INFLAMMATION AND HEALING RESPONSE	25
2.5. INFLUENCE OF THE SURFACE PROPERTIES ON THE FOREIGN BODY REACTION	26
2.6. BIBLIOGRAPHY	29
CHAPTER 3 – EFFECTS OF CHITOSAN ON IMMUNE REACTION	33
3.1. EFFECTS OF CHITOSAN ON IMMUNE REACTION	34
3.2. BIBLIOGRAPHY	37
CHAPTER 4 – MATERIALS AND METHODS	38
4.1. TITANIUM ALLOY	39
4.2. PREPARATION OF TITANIUM SAMPLES	40
4.3. PROCEDURES FOR ATTACHMENT OF CHITIN DERIVATIVES TO TITANIUM	41
4.3.1. <i>Physical attachment of chitin derivatives to titanium surface</i>	42
4.3.2. <i>Attachment of chitin derivatives to activated titanium surface using a good leaving group (tresyl chloride).....</i>	43
4.3.3. <i>Attachment of chitin derivatives to activated titanium surface with a coupling agent (polydopamine)</i>	45
4.4. FTIR SPECTROSCOPY	47
4.5. ATOMIC FORCE MICROSCOPY	48
4.6. SCANNING ELECTRON MICROSCOPY	49
4.7. ZETA POTENTIAL	50
4.8. CONTACT ANGLE MEASUREMENT	51
4.9. TAPE TEST	52
4.10. BIBLIOGRAPHY	54
CHAPTER 5 – RESULTS AND DISCUSSION	55
5.1. FOURIER TRANSFORM INFRARED SPECTROSCOPY	57
5.1.1. <i>Physical attachment coating</i>	58
5.1.2. <i>Tresyl chloride activated samples</i>	60
5.1.3. <i>Polydopamine activated samples</i>	61

5.1.4. Comparisons between different types of coatings	62
5.1.5. FTIR on samples stored in PBS at 37°C for two weeks	63
5.2. SCANNING ELECTRON MICROSCOPE ANALYSIS	65
5.3. ATOMIC FORCE MICROSCOPE ANALYSIS	68
5.4. ZETA POTENTIALS	72
5.5. CONTACT ANGLE MEASUREMENTS	75
5.6. TAPE TEST	77
5.7. DISCUSSION	79
5.8. BIBLIOGRAPHY	83
CONCLUSIONS	85
ACKNOWLEDGEMENTS	86

Introduction

A biomaterial is implanted in the body to direct a therapeutic or diagnostic procedure through control of its interaction with the living system.

The immune response of the body to an external material is controlled mainly by leucocytes, white blood cells, that reach the implantation site through the blood vessels and start the proper response. The first step is the adsorption of certain proteins on the surface, immediately followed by platelet activation that start the coagulation cascade to restore the damaged part. The complement system, composed by proteins, is another component of the immune response that integrates the action of leucocytes and platelets. Leucocytes adhesion is the mechanism that leads to the development of the real foreign body response isolating the biomaterial with macrophages and foreign body giant cells. This mechanism needs to be reduced in order to avoid the isolation that can result in damages to the implant and in its inefficacy. In order to control this interaction, the biomaterial can be functionalised with particular coatings such as biopolymers (both natural or synthetic), proteins or sequences of peptides (parts of proteins) able to recognise specific cells.

This thesis is part of NAT4MORE (NATural molecules on the surface of bioactive materials FOR Modulating the host REsponse to implants), a project that consists in the development of nanotextured surfaces for bone implants, functionalized with natural biomolecules, able to fine modulate the host response and reduce infections. The main objective of the project is to use a bioinspired approach for surface functionalization with local biomolecules (polyphenols or chitin derivatives) of bioactive glasses, hydroxyapatite and titanium. Since this project uses biomolecules obtained during a normal agri-food production chain, the activity is also based on a green approach because tries to transform waste into high added value products.

This thesis concerns the coating of titanium alloy (Ti6Al4V) samples with chitin derivatives in cooperation with Innovation Center Iceland and GENIS. Titanium alloys are widely used in the biomedical field as substitute for damaged bones, especially in dental application and hip and knee replacement due to their good mechanical properties. Chitin derivatives, chitosan in particular, extracted from the shell of crustaceans, are known to have good antibacterial property and biocompatibility.

In this study, chitosan provided by GENIS is used attached to an oxidized titanium surface with different methods: physical attachment, attachment using a good leaving group (tresyl chloride) and attachment using a coupling agent (polydopamine). Physical attachment implies the adhesion through chemical bonds or electrostatic attraction between chitosan and the substrate. The good leaving group provides an active site for the attachment and it is removed during the coating. Polydopamine acts as interface between the substrate and chitosan to facilitate the creation of a bond. The last two strategies can help the coating formation when it is performed at pH close to the Isoelectric point of chitosan, where no significant surface charge is on the surface.

After coating, the samples are analysed to verify the effective formation of the coating by using Fourier Transform Infra-Red Spectroscopy, Atomic Force Microscopy, Scanning Electron Microscopy, Zeta Potentials, Contact Angle Measurements and Tape Test. It is also tested the resistance of the coating in a simulated body fluids solution for two weeks in incubator at 37°C.

CHAPTER 1

Chitin and its derivatives

1.1. Chitin

Chitin (Figure 1.1) was discovered by Henri Braconnot in 1811 [1]. It is a biological linear polysaccharide that can be found in the shell of crustaceans, exoskeleton of molluscs and in some fungi. In crustaceans, chitin and other proteins form a complex network with calcium carbonate that lead to the rigid shell [2]. It is composed by randomly distributed β (1-4) linked glucosamine and N-Acetyl-D-glucosamine.

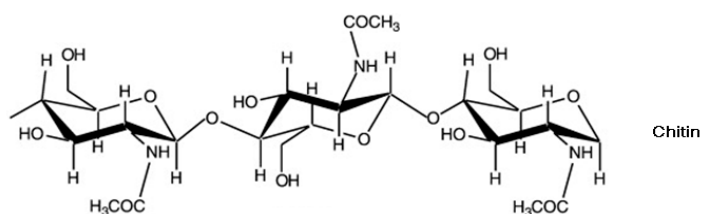


Figure 1.1: chitin

The production of chitin consists of decalcification with diluted HCl, deproteination by diluted NaOH, decolouration with bleaching agent (to remove residual pigments) and drying of crustacean shells as illustrated in Figure 1.2. The deproteination process needs to be performed carefully in order to avoid chemical damage to the biopolymer.

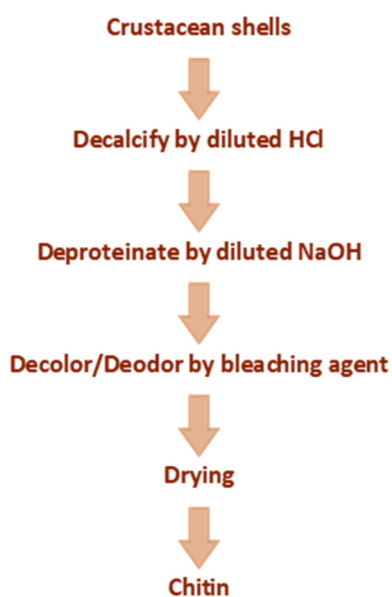


Figure 1.2: production of chitin

The molecular structure of chitin is similar to that of cellulose as shown in Figure 1.3. Cellulose is a linear polymer, formed by D-glucose units linked by β (1-4)-glycosidic oxygen bridges. The chain forms a stable polymer that resists degradation in aqueous solvents. The structure is also rigid due to hydrogen bonding between glucose residues in different chains [3].

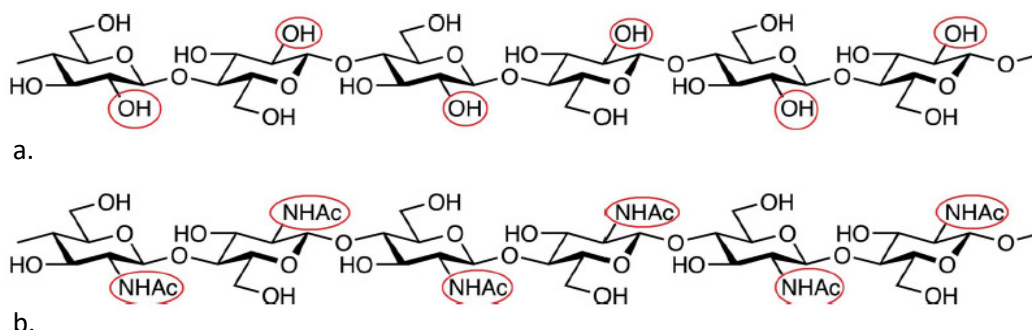


Figure 1.3: differences between cellulose (a) and chitin (b) structures

Chitin can be found in three different polymeric forms with different organization: α , β and γ (Figure 1.4). α -chitin presents an antiparallel configuration while β is parallel, both α and β are crystalline. γ -chitin is a combination of both α and β . α -chitin is the most abundant in nature. Chitin is insoluble in water because it has strong hydrogen bonds between its chains and a rigid structure derived from its crystallinity [4], [5].

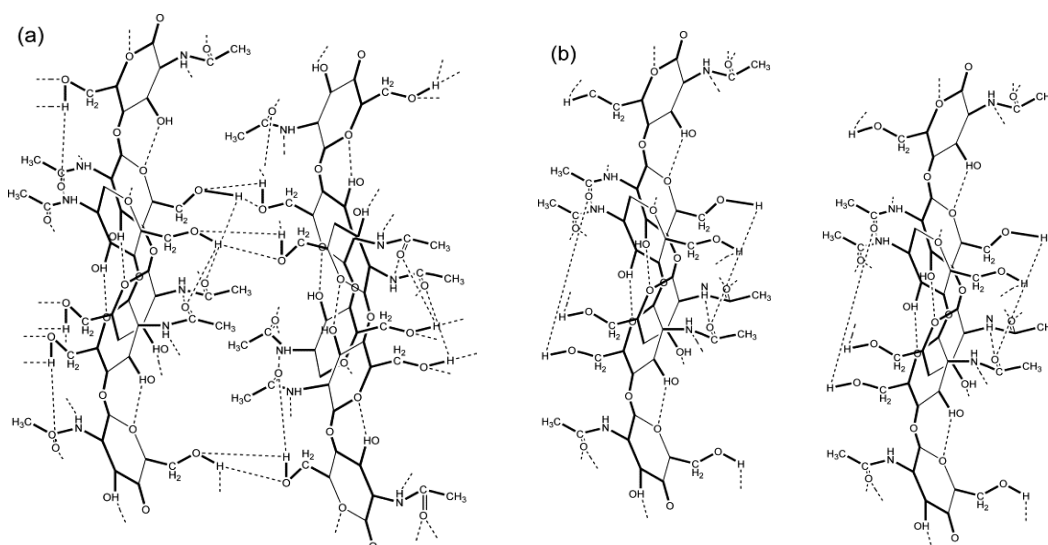


Figure 1.4: molecular structure of α -chitin (a) and β -chitin (b)

Property	Chitin	Chitosan
Deacetylation Degree (%)	Ca. 8-10	50 – 100
Molecular weight (Da)	$< 2 \times 10^6$	$1 \times 10^4 - 1.5 \times 10^6$
Viscosity range (cP)	> 500 (highly depending on the solvent system)	5 -5000 (1% solution in 1% acetic acid)
Solubility	DMAc-LiCl / TCA-MC MeOH-CaCl ₂	Diluted acids
Moisture content (%)	6-10%	6-10%

Table 1.1: properties of chitin and chitosan

1.2. Structure of chitosan

Since chitin has poor solubility in organic solvents and aqueous solutions, in the biological field is used the derived chitosan, which is chitin deacetylated in presence of alkali; in particular, it is common knowledge to define chitosan the chitin derivatives with degree of acetylation less than 50% [6]. Chitosan (Figure 1.5) was discussed for the first time in 1859 by *Rouget* [1]. It is a linear copolymer composed of N-Acetyl-D-glucosamine units with different grade of deacetylation linked by β (1 \rightarrow 4) glycosidic bonds. The structure contains one amino group and two hydroxyl groups in the repeating glucosidic residue [7]. It also presents hydrogen bonds that provide a crystalline rigid structure. It has a structure similar to hyaluronic acid as shown in Figure 1.5 and 1.6 [8].

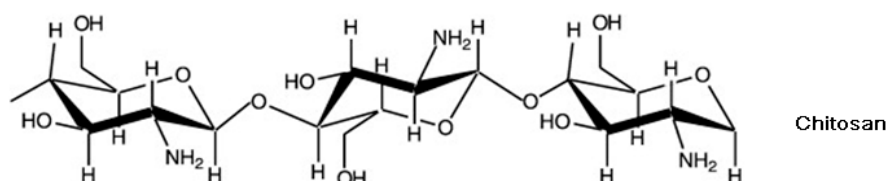


Figure 1.5: chitosan

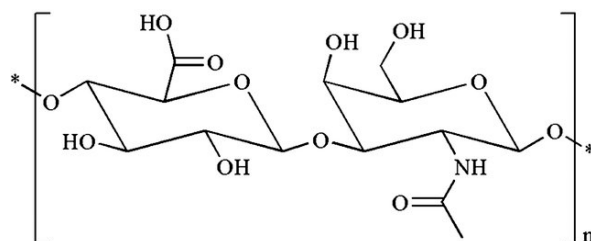
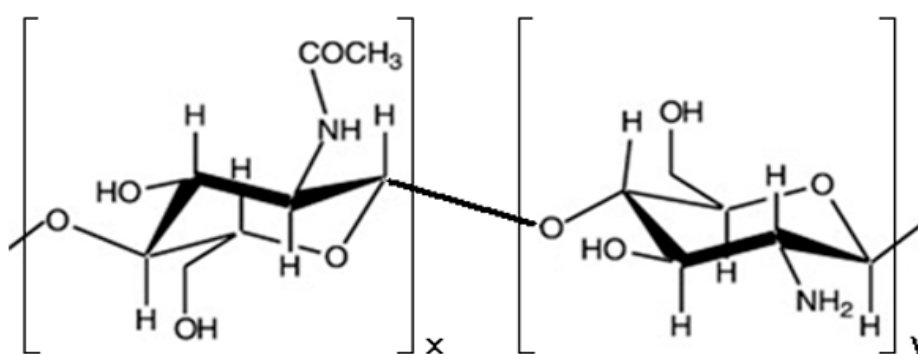


Figure 1.6: hyaluronic acid

Different proportions of N-Acetyl-D-Glucosamine and D-Glucosamine residues provide specific changes in the structure that lead to several types of chitosan distinguished by the degree of deacetylation (Figure 1.7) and the molecular weight. In this research, chitosan with 50% deacetylation degree was used (Genis hf, Iceland).



X = N-acetyl-D-glucosamine
Y = D-glucosamine

$$DD \text{ (degree of deacetylation)} = y / (x+y)$$

$$DA \text{ (degree of acetylation)} = x / (x+y)$$

$$F_A \text{ (mole fraction of N-acetyl-D-glucosamine residues)} = x / (x+y)$$

Figure 1.7: deacetylation degree

The degree of acetylation influences the molecular weight, the elongation at break and the tensile strength [9]. The degree of acetylation also influences biological properties such as stability and precipitation (as shown in Figure 1.8), biodegradation by lysozyme, wound healing and osteogenesis enhancement [10],[11]. Studies performed by *Chatelet* on the attachment and proliferation of fibroblast and keratinocytes evidenced the importance of both the degree of acetylation and the superficial properties on these processes, with the result that an high degree of deacetylation has a weak attachment with no proliferation [12],[13]. With lower degree of acetylation there are more amine groups available for biological interactions. If the adhesion is strong then the proliferation is most likely to be inhibited. The smoothness of the surface also influences proliferation, the last being easier with surfaces more flat. Different deacetylation conditions can influence the viscosity of the chitosan solution by changing the molecular repulsion forces. Fast rates of degradation can produce an inflammatory response due to the accumulation of amino saccharide. Also low degree of deacetylation induces an acute inflammatory response, this last being minimal in case of high DD [12].

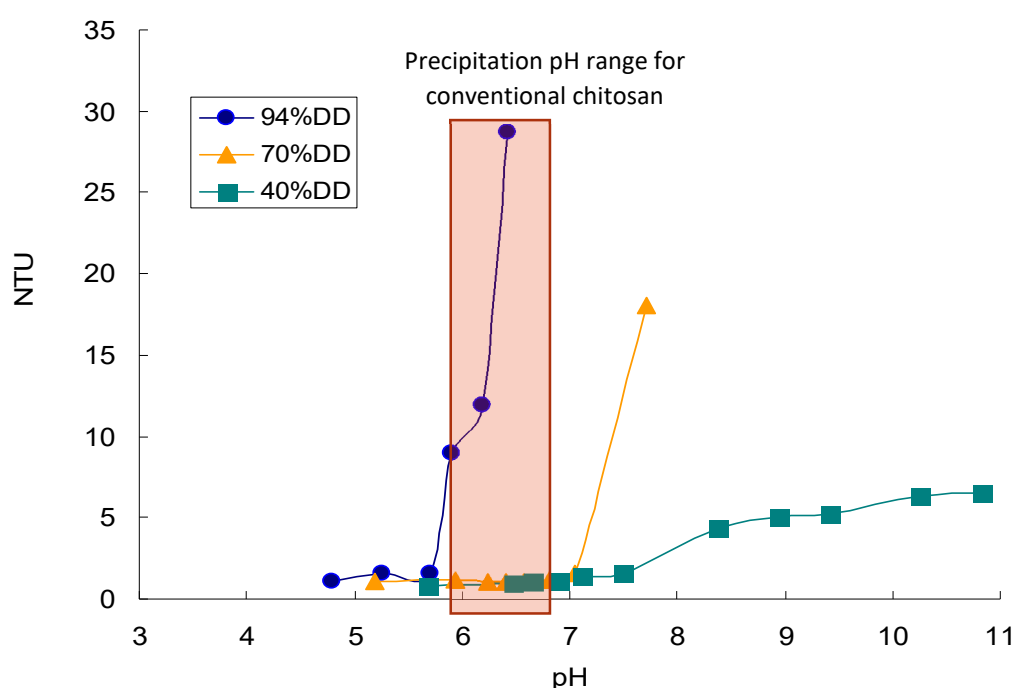


Figure 1.8: the nephelometric turbidity unit (NTU) is used to evaluate the precipitation pH of chitosan by analysing the turbidity of a solution that contains nanoparticles. When chitosan is entirely dissolved in a solution this last becomes homogeneously turbid instead of having chitosan in particles. Chitosan with 94%DD dissolves at pH around 6.4.

Depending on the treatments of the extraction process, chitosan shows different crystallinity and polymorphism.

Chitosan can be dissolved in acidic solution below pH 6 due to the presence of amino groups that become protonated at acidic pH and transform chitosan into a cationic polyelectrolyte. Solubility is dependent on the degree of deacetylation and the method used [1]. As the pH increases above 6, chitosan's amines become deprotonated and the polymer loses its charge becoming insoluble [7].

1.3. Properties of chitosan

Biocompatibility of chitosan is largely attributed to its similarity to hyaluronic acid and glycosaminoglycan extracellular matrix molecules [14]. The cationic nature is believed to help healing processes. Degradation occurs by enzyme action or hydrolysis [7].

Tests performed to promote the use of this biopolymer in the human body do not report any inflammatory or allergic reaction after implantation, injection or ingestion. Studies performed by *Schipper et al.* evidenced that toxicity is dependent on deacetylation degree and molecular weight [15]. At high deacetylation degree, toxicity is related to the molecular weight and the concentration; at lower deacetylation degree, toxicity is less pronounced and less related to the molecular weight.

Chitosan is considered as being a non-toxic, biologically compatible polymer. However, certain modification implemented on chitosan could make it more or less toxic and any residual reactants should be removed carefully. Park reported in vitro oxygen radicals scavenging activity in chitosan that makes it an antioxidant [16].

Table 1.2 shows the biological properties of chitin and chitosan with emphasis on the relationship with the physicochemical characteristics.

Property	Physicochemical characteristic
Biodegradability	Degree of deacetylation, distribution of acetyl groups, molecular weight
Biocompatibility	Degree of deacetylation
Mucoadhesion	Degree of deacetylation, molecular weight
Haemostasis	Degree of deacetylation, molecular weight
Analgesic	Degree of deacetylation
Adsorption enhancer	Degree of deacetylation
Antimicrobial	Molecular weight
Anticholesterolemic	Degree of deacetylation, molecular weight, viscosity
Antioxidant	Degree of deacetylation, molecular weight

Table 1.2: properties and characteristics of chitosan

1.3.1. Antibacterial activity

Chitosan exhibits antimicrobial activity in many reports. Several hypotheses have been proposed based on the cationic nature [17], [18]. Low molecular weight chitosan penetrates bacterial cell walls, binding DNA and inhibiting its transcription [19], while high molecular weight chitosan binds the negatively charged components of the cell walls forming an impermeable layer and blocking transport into the cell. The amount of chitosan bonded with the bacterial cell wall depends on the environmental pH value, the molecular weight and the degree of acetylation. A low environmental pH increases the positive charge of chitosan that favours binding to the bacterial cell wall [20]. A study performed by *Younes* reports that a lower degree of acetylation and a lower pH are favourable to the antibacterial activity [21]. Chitosan based solutions and submicroparticles exhibit antimicrobial activity against *Staphylococcus aureus* and *Escherichia coli* [22].

1.3.2. Antifungal activity

Chitosan exhibits antifungal activity against several fungi [23], [24] due probably to a permeable chitosan film on the crop surface which interfere with fungal growth and activate several defence processes such as chitinase accumulation, proteinase inhibitor synthesis and lignification [16]. High-molecular-weight chitosan derivatives, with low hydrophobicity, and low-molecular-weight derivatives, with high hydrophobicity, displayed the highest potency in suppressing growth in *Aspergillus flavus* *in vitro* [25].

1.3.3. Antitumor activity

Lately, scientist investigated the antitumor activity of chitosan *in vitro* and *in vivo*. *Tokoro et al.* observed the antitumor effect as due to the increase in secretion of interleukine-1 and 2 which cause the increase of cytolytic T-lymphocytes [26]. Carboxymethyl chitosan suppressed migration of human hepatoma cells *in vitro* and murine hepatoma cells *in vivo* [27].

1.4. Biomedical and pharmaceutical applications of chitosan

Chitosan can be formulated as a powder, a gel or a film in order to create chitosan-based scaffolds for tissue engineering, drug delivery systems for drug release, bandages for wound healing, filters for water treatments and to coat other materials and improve their properties. A scheme of the biomedical application of chitosan is shown in Figure 1.9.

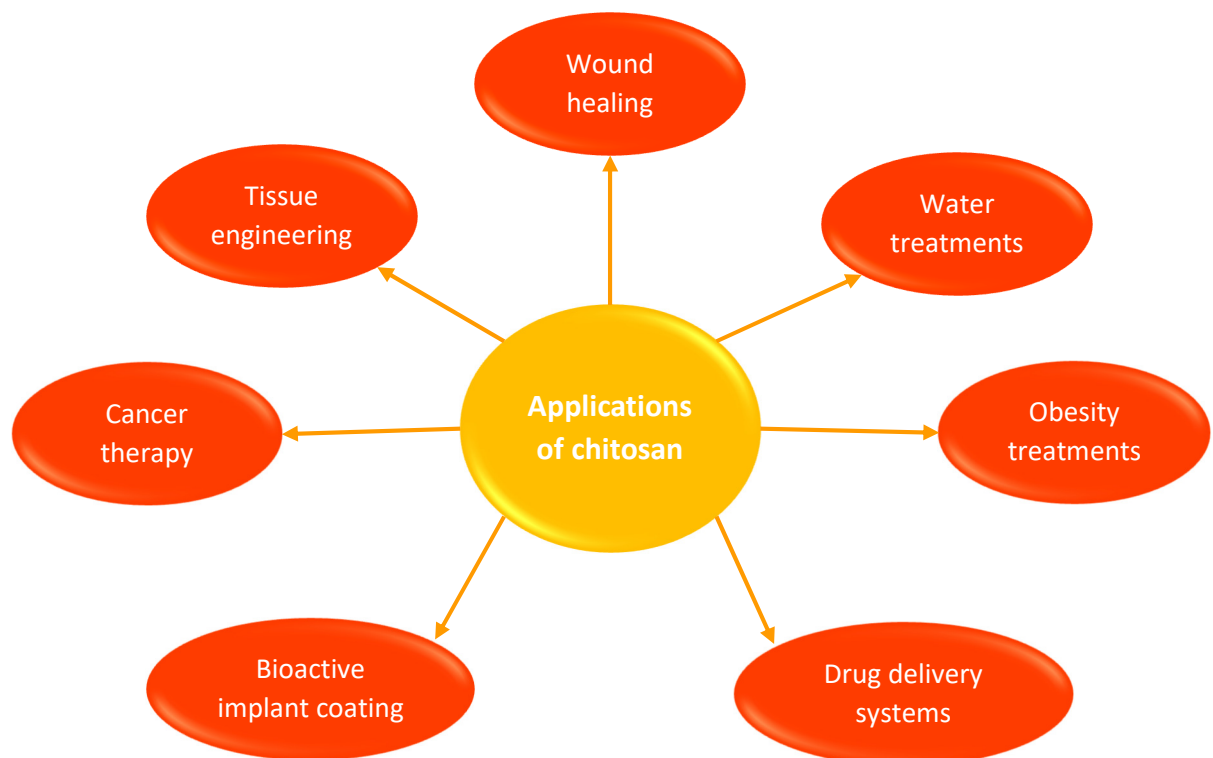


Figure 1.9: schematic representation of the biomedical applications of chitosan

1.4.1. Tissue engineering

Considering its biological properties, chitosan can be used in a lot of biomedical applications that involve tissue engineering. Tissue engineering combines the principles and methods of life sciences with engineering to develop biological substitutes to restore, maintain or improve biofunction [28]. This field needs the use of a scaffold, a structure that supports cells to grow into the desired tissue.

Chitosan has useful properties that allow its use as a scaffold material especially for orthopaedic tissues. These properties include plastic behaviour, antibacterial effects, minimal foreign body reaction, osteoconduction and cell infiltration [29]. Chitosan-based scaffolds can be incorporated with bioactive elements to improve osteogenesis. Chitosan can be fabricated as hydrogels, microcapsules, membranous films, sponges, tubes, or a 3D porous structure [30]. A hydrogel can be crosslinked covalently or ionically: a covalently crosslinked hydrogel has a permanent structure used to release water or bioactive factors, an ionically crosslinked hydrogel has, instead, reversible linkages and can be dissolved. Tubular scaffolds with porous structure can be applied to regenerate nerves and blood vessels [29].

Depending on the specific function of the scaffold, chitosan can be blended with other materials to create a structure more similar to the properties required [31],[32]. Examples of this application are a scaffold made with collagen blended with chitosan to improve extracellular matrix production, cell adhesion and proliferation for vascular regeneration [33]. Scaffold made by blending gelatine with chitosan allows the proper swelling properties, burst strength and growth of smooth muscles cells [31].

Scaffolds can also be produced and loaded with bioactive molecules. Chitosan is a linear polymer with repetitive units. Since it has a cationic nature, ionic complexes can be formed with bioactive compounds, forming polyelectrolyte complexes with strong reversible links [34]. Chitosan also has reactive hydroxyl and amino units that can lead to modifications to improve its bioactivity [30].

Chupa et al. demonstrated that chitosan blended with glycosaminoglycans or dextran sulphate can control vascular endothelial proliferation [35].

1.4.2. Drug delivery systems

In the drug delivery industry chitosan can be used as tablets, microspheres, micelles, vaccines, nucleic acids, hydrogels, nanoparticles and conjugates. Chitosan can be used in these systems in implantable and injectable forms. It is widely used as an excipient in tablet formulation for oral medications [36]. Microspheres are studied for developing drug release systems for oral delivery [37]. Micelles can be formed with an external hydrophilic shield and an internal hydrophobic centre by the electrostatic repulsion between the opposite charges of polymers [38]. Hydrogels are 3D structure capable of adsorbing fluids through diffusion, entrapment and tethering [39]. These hydrogels injected in the body form semi-solid structures that can protect the drug from physiological degradation and provide a steady release. Nanoparticles have good biodegradability and biocompatibility and can be obtained through gelation, emulsion and self-assembly [40]. Furthermore, they can be delivered with non-invasive methods such as oral, nasal and ocular routes. In the oral delivery, granules of chitosan show adhesion in the distal esophageal mucosa allowing the adsorption of drugs in this section by enhancing the residence time. Nasal applications show problems such as low membrane permeability, short local residence time and high secretion that prevent many therapies. Mucoadhesive properties of chitosan can improve drug delivery in nasal systems delaying mucociliary clearance and improving

adhesion of the drug allowing more time for the therapy. Hydrogels have been studied as carrier of drugs for topical application in the eye due to their ability to be applied as a liquid and then becoming a gel improving the resident time of the drug and the therapeutic efficacy [41].

1.4.3. Cancer therapy

Recent treatments for cancer therapy involve gene delivery. In this therapy, a gene implicated in cancer pathology is manipulated by delivering exogenous nucleic acid into the tumor cells [42]. This delivery has a lot of obstacles inside the body (enzymatic degradation, rapid bio-clearance, cellular entry limitations) that lead to the necessity to develop delivery vehicles. For gene delivery, usually, viral vectors are used, but these systems are subjected to mutagen and carcinogen derived problems [43]. For this reason, nowadays non-viral vectors are investigated [44]. Non-viral vectors can be liposomes, polymeric carriers and nanoparticles. Polymeric carriers, such as polyethylene imine (PEI) and poly-L-lysine (PLL) have the collateral effect of toxicity due to their high cationic charge [45]. Chitosan, however, does not exhibit toxicity as a gene delivery vehicle [46].

1.4.4. Wound healing

Although chitosan hydrogels have an acidic nature, its use in wound healing is being investigated. Generally, hydrogels provide a 3D growth matrix for tissue that activate macrophages activity and stimulate cell proliferation. Chitosan promotes activity of polymorphonuclear leukocytes, macrophages and fibroblasts that enhance granulation as well as the organization of the repaired tissues [47]. Its degradation product, N-acetyl- β -D-glucosamine, stimulates fibroblast proliferation, collagen deposition and hyaluronic acid synthesis [48]. Chitosan gels, however, need toxic chemicals acting as crosslinkers in order to be created, limiting its use as a biomaterial. A way to eliminate the use of toxic additives when producing a chitosan gel is the use of cryogelation, because chitosan shows neutral pH. *Takei* demonstrated the effectiveness of chitosan gels made with cryogelation blended with gluconic acid as wound healing enhancers [49]. *Charernsriwilaiwat et al.* demonstrated that electrospun fibres made with chitosan blended with ethylenediaminetetraacetic acid, polyvinyl alcohol and lysozyme is useful for wound healing applications due to lysozyme presence [50].

1.4.5. Bioactive implant coating

There are a lot of methods that have been used to coat surfaces with chitosan for implants. These include physical adsorption, chemical reaction and electrodeposition. Every time chitosan is used to coat a surface, it needs to be firmly bounded in order to withstand the mechanical forces derived from implant placement and to secure the implant position during osseointegration.

Silanes have been used to guarantee a better attachment of the chitosan to the surface [51]. Silanes contain silicon with a maximum of four additional groups. The simplest compound is the silicon tetrahydride, that contains four hydrogen molecules [52]. Silicon tetrahydride (silane) is not used as it is for attachment, but is used after the addition of active groups, as the ones containing oxygen with an alkane attachment, in order to allow covalent bonding. Typically, three oxygen atoms can be found attached to silicon to create a network in the surface, leaving the last unit to form a bond with the molecules of the final coating [53].

In the electrodeposition process a charged material in a conductive solution is deposited on a surface with an electrical current. Chitosan can be deposited on a surface using an electrophoretic process because the positively charged chitosan dispersed into a solution is attracted to a negatively charged surface through an electric field [54],[55]. The property of chitosan to deprotonate at pH above 6.3 allow the stability of the attachment after the removal of the electric field. This method often includes the blending of chitosan with other materials such as CaP (calcium phosphate) to take advantage of the properties of both materials. Involving calcium phosphate into the coating lead to the formation of hydroxyapatite that allow a better integration bone-implant, meaning that using both hydroxyapatite and chitosan enhance the properties of the coating. The electrophoretic deposition can also be achieved via layer-by-layer. In this technique two materials, one positively charged and the other negatively charged, are attached to a surface through interactions between opposite charges creating a coating with a certain amount of layers [56]. The two polyelectrolytes can derive both from natural and synthetic materials. When the technique is used in the biologic field natural polyelectrolytes are most used such as chitosan and alginate (a biopolymer extracted from algae).

Electrostatic interactions have been used by *Mitra et al.* in 2016 to attach quaternized chitosan (QCS) on polymers and metals. Quaternized chitosan was prepared suspending low molecular weight chitosan in N-methyl-2-pyrrolidone and left overnight with stirring. Then it was added NaOH at 60°C overnight also with stirring. To obtain the final product potassium iodide and hexyl bromide were added to the mixture and left with stirring for 48h. The supernatant was then extracted by centrifugation and an excess of acetone was added to precipitate the QCS collected via centrifugation. This precipitate was dissolved in deionized water, dialysed for 2-3 days and freeze-dried to obtain the final QCS. QCS has permanent positively charged ammonium groups allowing higher antimicrobial activity against the negatively charged bacterial surface. Since quaternized chitosan is water-soluble, this type of coating needs the use of a polymerized substrate such as acrylic acid or multivalent anionic acids (sodium tripolyphosphate, sodium pyrophosphate and sodium hexametaphosphate) [57].

Rikhari et al. in 2018 evaluated the increase in the anticorrosion behaviour of polypyrrole/chitosan coating on titanium compared to polypyrrole titanium, enhanced microhardness and adhesion strength were also noted in this electropolymerization process [58].

Chitosan, in combination with ceramide, was used to coat gold nanoparticles improving their biocompatibility and stability for imaging, drug delivery and photothermal therapy [59].

1.4.6. Water treatment and food industry

Chitosan can be used for pollutant adsorption in water treatment systems due to the presence of amino and hydroxyl groups. These groups interact and adsorb dyes, metals and organic compounds [60], [61]. Adsorption properties can be improved by modification of the functional groups, with, for example, cross-linking techniques or grafting [62]. For heavy metals, chitosan can be a chelating polymer through the amine groups. For organic compounds, the adsorption depends on cationic exchange, diffusion, hydrogen bond, Van der Waals force, dipole-dipole and electrostatic interactions [63].

Chitosan has been approved by FDA as a preservative in the food industry. It is used as a coating for its ability to form films that protect food from microbe proliferation prolonging the shelf life [64].

1.5. Bibliography

- [1] V. Dodane and V. D. Vilivalam, "Pharmaceutical application of chitosan," *Pharm. Sci. Technol. Today*, vol. 1, no. 6, pp. 246–253, 1998.
- [2] I. Younes and M. Rinaudo, "Chitin and Chitosan Preparation from Marine Sources. Structure, Properties and Applications," *Mar. Drugs*, vol. 13, no. 3, pp. 1133–1174, Mar. 2015.
- [3] P. Pooyan, I. T. Kim, K. I. Jacob, R. Tannenbaum, and H. Garmestani, "Design of a cellulose-based nanocomposite as a potential polymeric scaffold in tissue engineering," *Polymer (Guildf)*, vol. 54, no. 8, pp. 2105–2114, 2013.
- [4] M. Rinaudo, "Chitin and chitosan: Properties and applications," *Prog. Polym. Sci.*, vol. 31, no. 7, pp. 603–632, Jul. 2006.
- [5] M. Sugimoto, M. Morimoto, H. Sashiwa, H. Saimoto, and Y. Shigemasa, "Preparation and characterization of water-soluble chitin and chitosan derivatives," *Carbohydr. Polym.*, vol. 36, no. 1, pp. 49–59, May 1998.
- [6] R. Lieder *et al.*, "In vitro bioactivity of different degree of deacetylation chitosan, a potential coating material for titanium implants," *J. Biomed. Mater. Res. - Part A*, vol. 100 A, no. 12, pp. 3392–3399, 2012.
- [7] M. Dash, F. Chiellini, R. M. Ottenbrite, and E. Chiellini, "Chitosan - A versatile semi-synthetic polymer in biomedical applications," *Prog. Polym. Sci.*, vol. 36, no. 8, pp. 981–1014, 2011.
- [8] P. Zucca and E. Sanjust, "Inorganic materials as supports for covalent enzyme immobilization: methods and mechanisms," *Molecules*, vol. 19, no. 9, pp. 14139–14194, 2014.
- [9] H. S. Blair, D. J. Guthrie, T. Law, and P. Turkington, "Chitosan and modified chitosan membranes. Preparation and characterization," *Appl. Polym. Sci.*, vol. 33, no. 2, pp. 641–656, 1987.
- [10] Y. Hidaka, M. Ito, K. Mori, H. Yagasaki, and A. H. Kafrawy, "Histopathological and immunohistochemical studies of membranes of deacetylated chitin derivatives implanted over rat calvaria.," *J. Biomed. Mater. Res.*, vol. 46, no. 3, pp. 418–423, Sep. 1999.
- [11] P. Rojsitthisak, N. Chuen How, S. Chandkrachang, and W. Stevens, "Effect of Chemical Treatment on the Characteristics of Shrimp Chitosan," *J. Met. Mater. Miner.*, vol. 12, no. 1, pp. 11–18, Jan. 2002.
- [12] C. Chatelet, O. Damour, and a Domard, "Influence of the degree of acetylation on some biological properties of chitosan films.," *Biomaterials*, vol. 22, no. 3, pp. 261–268, 2001.
- [13] L. John, R. Foster, S. Ho, J. Hook, M. Basuki, and H. Marçal, "Chitosan as a Biomaterial : Influence of Degree of Deacetylation on Its Physiochemical , Material and Biological Properties," *PLoS One*, vol. 10, no. 8, pp. 1–22, 2015.
- [14] J. D. Bumgardner *et al.*, "Chitosan: Potential use as a bioactive coating for orthopaedic and craniofacial/dental implants," *J. Biomater. Sci. Polym. Ed.*, vol. 14, no. 5, pp. 423–438, 2003.
- [15] N. G. Schipper, K. M. Varum, P. Stenberg, G. Ocklind, H. Lennernas, and P. Artursson, "Chitosans as absorption enhancers of poorly absorbable drugs. 3: Influence of mucus on absorption enhancement.," *Eur. J. Pharm. Sci.*, vol. 8, no. 4, pp. 335–343, Aug. 1999.
- [16] R.-K. Bai, M.-Y. Huang, and Y.-Y. Jiang, "Selective permeabilities of chitosan-acetic acid complex membrane and chitosan-polymer complex membranes for oxygen and carbon dioxide," *Polym. Bull.*, vol. 20, no. 1, pp. 83–88, 1988.
- [17] R. Muzzarelli, R. Tarsi, O. Filippini, E. Giovanetti, G. Biagini, and P. E. Varaldo, "Antimicrobial properties of N-carboxybutyl chitosan," *Antimicrob. Agents Chemother.*, vol. 34, no. 10, pp. 2019–2023, 1990.

- [18] L.-Y. Zheng and J.-F. Zhu, "Study on antimicrobial activity of chitosan with different molecular weights," *Carbohydr. Polym.*, vol. 54, no. 4, pp. 527–530, Dec. 2003.
- [19] N. R. Sudarshan, D. G. Hoover, and D. Knorr, "Antibacterial action of chitosan," *Food Biotechnol.*, vol. 6, no. 3, pp. 257–272, 1992.
- [20] J. Rhoades and S. Roller, "Antimicrobial Actions of Degraded and Native Chitosan against Spoilage Organisms in Laboratory Media and Foods," *Appl. Environ. Microbiol.*, vol. 66, no. 1, pp. 80–86, Jan. 2000.
- [21] I. Younes, S. Sellimi, M. Rinaudo, K. Jellouli, and M. Nasri, "Influence of acetylation degree and molecular weight of homogeneous chitosans on antibacterial and antifungal activities," *Int. J. Food Microbiol.*, vol. 185, no. 1, pp. 57–63, Aug. 2014.
- [22] W. A. Sarhan and H. M. E. Azzazy, "High concentration honey chitosan electrospun nanofibers: Biocompatibility and antibacterial effects," *Carbohydr. Polym.*, vol. 122, no. 1, pp. 135–143, May 2015.
- [23] M. M. M. Atia, H. Buchenauer, A. Z. Aly, and M. I. Abou-Zaid, "Antifungal Activity of Chitosan Against *Phytophthora infestans* and Activation of Defence Mechanisms in Tomato to Late Blight," *Biol. Agric. Hortic.*, vol. 23, no. 2, pp. 175–197, Jan. 2005.
- [24] V. Saharan *et al.*, "Synthesis and in vitro antifungal efficacy of Cu-chitosan nanoparticles against pathogenic fungi of tomato," *Int. J. Biol. Macromol.*, vol. 75, no. 1, pp. 346–353, Apr. 2015.
- [25] J. dos S. Gabriel, M. J. Tiera, and V. A. de O. Tiera, "Synthesis, Characterization, and Antifungal Activities of Amphiphilic Derivatives of Diethylaminoethyl Chitosan against *Aspergillus flavus*," *J. Agric. Food Chem.*, vol. 63, no. 24, pp. 5725–5731, Jun. 2015.
- [26] A. Tokoro, N. Tatewaki, K. Suzuki, T. Mikami, S. Suzuki, and M. Suzuki, "Growth-inhibitory effect of hexa-N-acetylchitohexaose and chitohexaose against Meth-A solid tumor," *Chem. Pharm. Bull. (Tokyo)*, vol. 36, no. 2, pp. 784–790, Feb. 1988.
- [27] Z. Jiang, B. Han, H. Li, X. Li, Y. Yang, and W. Liu, "Preparation and anti-tumor metastasis of carboxymethyl chitosan," *Carbohydr. Polym.*, vol. 125, no. 1, pp. 53–60, Jul. 2015.
- [28] R. Langer and J. P. Vacanti, "Tissue engineering," *Science*, vol. 260, no. 5110, pp. 920–926, May 1993.
- [29] P. J. VandeVord, H. W. T. Matthew, S. P. DeSilva, L. Mayton, B. Wu, and P. H. Wooley, "Evaluation of the biocompatibility of a chitosan scaffold in mice," *J. Biomed. Mater. Res.*, vol. 59, no. 3, pp. 585–590, Mar. 2002.
- [30] T. Jiang, S. G. Kumbar, L. S. Nair, and C. T. Laurencin, "Biologically active chitosan systems for tissue engineering and regenerative medicine," *Curr. Top. Med. Chem.*, vol. 8, no. 4, pp. 354–364, 2008.
- [31] L. Zhang *et al.*, "A sandwich tubular scaffold derived from chitosan for blood vessel tissue engineering," *J. Biomed. Mater. Res. A*, vol. 77, no. 2, pp. 277–284, May 2006.
- [32] A. S. Gobin, V. E. Froude, and A. B. Mathur, "Structural and mechanical characteristics of silk fibroin and chitosan blend scaffolds for tissue regeneration," *J. Biomed. Mater. Res. A*, vol. 74, no. 3, pp. 465–473, Sep. 2005.
- [33] S. A. H. Norazril, B. S. Aminuddin, M. M. Norhayati, A. L. Mazlyzam, O. Fauziah, and B. H. I. Ruszymah, "Comparison of chitosan scaffold and chitosan-collagen scaffold: a preliminary study," *Med. J. Malaysia*, vol. 59, no. Suppl B, pp. 186–187, May 2004.
- [34] J. Berger, M. Reist, J. M. Mayer, O. Felt, and R. Gurny, "Structure and interactions in chitosan hydrogels formed by complexation or aggregation for biomedical applications," *Eur. J. Pharm. Biopharm.*, vol. 57, no. 1, pp. 35–52, Jan. 2004.

- [35] J. M. Chupa, A. M. Foster, S. R. Sumner, S. V. Madhally, and H. W. T. Matthew, "Vascular cell responses to polysaccharide materials: in vitro and in vivo evaluations," *Biomaterials*, vol. 21, no. 22, pp. 2315–2322, 2000.
- [36] I. Jabbal-Gill, P. Watts, and A. Smith, "Chitosan-based delivery systems for mucosal vaccines," *Expert Opin. Drug Deliv.*, vol. 9, no. 9, pp. 1051–1067, Sep. 2012.
- [37] H.-L. Jiang *et al.*, "In vitro study of the immune stimulating activity of an atrophic rhinitis vaccine associated to chitosan microspheres," *Eur. J. Pharm. Biopharm.*, vol. 58, no. 3, pp. 471–476, Nov. 2004.
- [38] A. Harada and K. Kataoka, "Formation of Polyion Complex Micelles in an Aqueous Milieu from a Pair of Oppositely-Charged Block Copolymers with Poly(ethylene glycol) Segments," *Macromolecules*, vol. 28, no. 15, pp. 5294–5299, Jul. 1995.
- [39] S. Supper, N. Anton, N. Seidel, M. Riemenschnitter, C. Curdy, and T. Vandamme, "Thermosensitive chitosan/glycerophosphate-based hydrogel and its derivatives in pharmaceutical and biomedical applications," *Expert Opin. Drug Deliv.*, vol. 11, no. 2, pp. 249–267, Feb. 2014.
- [40] P. Lai, W. Daear, R. Löbenberg, and E. J. Prenner, "Overview of the preparation of organic polymeric nanoparticles for drug delivery based on gelatine, chitosan, poly(D,L-lactide-co-glycolic acid) and polyalkylcyanoacrylate," *Colloids Surfaces B Biointerfaces*, vol. 118, no. 1, pp. 154–163, Jun. 2014.
- [41] A. Bernkop-Schnurch and S. Dunnhaupt, "Chitosan-based drug delivery systems," *Eur. J. Pharm. Biopharm.*, vol. 81, no. 3, pp. 463–469, 2012.
- [42] D. Cross and J. K. Burmester, "Gene therapy for cancer treatment: past, present and future," *Clin. Med. Res.*, vol. 4, no. 3, pp. 218–227, Sep. 2006.
- [43] N. Nayerossadat, T. Maedeh, and P. A. Ali, "Viral and nonviral delivery systems for gene delivery," *Adv. Biomed. Res.*, vol. 1, no. 1, p. 27, Jul. 2012.
- [44] H. Yin, R. L. Kanasty, A. A. Eltoukhy, A. J. Vegas, J. R. Dorkin, and D. G. Anderson, "Non-viral vectors for gene-based therapy," *Nat. Rev. Genet.*, vol. 15, no. 8, pp. 541–555, Aug. 2014.
- [45] K. Singha, R. Namgung, and W. J. Kim, "Polymers in Small-Interfering RNA Delivery," *Nucleic Acid Ther.*, vol. 21, no. 3, pp. 133–147, Jun. 2011.
- [46] S. Mao, W. Sun, and T. Kissel, "Chitosan-based formulations for delivery of DNA and siRNA," *Adv. Drug Deliv. Rev.*, vol. 62, no. 1, pp. 12–27, Jan. 2010.
- [47] H. Ueno, T. Mori, and T. Fujinaga, "Topical formulations and wound healing applications of chitosan," *Adv. Drug Deliv. Rev.*, vol. 52, no. 2, pp. 105–115, Nov. 2001.
- [48] R. A. Muzzarelli, M. Mattioli-Belmonte, A. Pugnali, and G. Biagini, "Biochemistry, histology and clinical uses of chitins and chitosans in wound healing," *EXS*, vol. 87, no. 1, pp. 251–264, 1999.
- [49] T. Takei, H. Nakahara, H. Ijima, and K. Kawakami, "Synthesis of a chitosan derivative soluble at neutral pH and gellable by freeze–thawing, and its application in wound care," *Acta Biomater.*, vol. 8, no. 2, pp. 686–693, 2012.
- [50] N. Charernsriwilaiwat, P. Opanasopit, T. Rojanarata, and T. Ngawhirunpat, "Lysozyme-loaded, electrospun chitosan-based nanofiber mats for wound healing," *Int. J. Pharm.*, vol. 427, no. 2, pp. 379–384, 2012.
- [51] R. Gupta and N. K. Chaudhury, "Entrapment of biomolecules in sol–gel matrix for applications in biosensors: Problems and future prospects," *Biosens. Bioelectron.*, vol. 22, no. 11, pp. 2387–2399, May 2007.

- [52] A. V Topchiev and K. A. Andrianov, "Basic nomenclature and classification of low-molecularweight organo-silicon compounds," *Bull. Acad. Sci. USSR, Div. Chem. Sci.*, vol. 2, no. 3, pp. 439–445, 1953.
- [53] P. Van Der Voort and E. F. Vansant, "Silylation of the Silica Surface A Review," *J. Liq. Chromatogr. Relat. Technol.*, vol. 19, no. 17–18, pp. 2723–2752, Oct. 1996.
- [54] J. Redepenning, "Electrochemical preparation of chitosan/hydroxyapatite composite coatings on titanium substrates," *J. Biomed. Mater. Res. - Part A*, vol. 66, no. 2, pp. 411–416, 2003.
- [55] X. Pang and I. Zhitomirsky, "Electrodeposition of composite hydroxyapatite-chitosan films," *Mater. Chem. Phys.*, vol. 94, no. 2–3, pp. 245–251, 2005.
- [56] J. Zhou, G. Romero, E. Rojas, L. Ma, S. Moya, and C. Gao, "Layer by layer chitosan/alginate coatings on poly(lactide-co-glycolide) nanoparticles for antifouling protection and Folic acid binding to achieve selective cell targeting," *J. Colloid Interface Sci.*, vol. 345, no. 2, pp. 241–247, 2010.
- [57] D. Mitra, M. Li, R. Wang, Z. Tang, E.-T. Kang, and K. G. Neoh, "Scalable Aqueous-Based Process for Coating Polymer and Metal Substrates with Stable Quaternized Chitosan Antibacterial Coatings," *Ind. Eng. Chem. Res.*, vol. 55, no. 36, pp. 9603–9613, Sep. 2016.
- [58] B. Rikhari, S. Pugal Mani, and N. Rajendran, "Electrochemical behavior of polypyrrole/chitosan composite coating on Ti metal for biomedical applications," *Carbohydr. Polym.*, vol. 189, no. 1, pp. 126–137, 2018.
- [59] G. Battogtokh, O. Gotov, and Y. T. Ko, "Chitosan–ceramide coating on gold nanorod to improve its physiological stability and reduce the lipid surface-related toxicity," *Arch. Pharm. Res.*, vol. 40, no. 3, pp. 356–363, 2017.
- [60] P. O. Boamah *et al.*, "Sorption of heavy metal ions onto carboxylate chitosan derivatives—A mini-review," *Ecotoxicol. Environ. Saf.*, vol. 116, no. 1, pp. 113–120, Jun. 2015.
- [61] M. Vakili *et al.*, "Application of chitosan and its derivatives as adsorbents for dye removal from water and wastewater: A review," *Carbohydr. Polym.*, vol. 113, no. 1, pp. 115–130, Nov. 2014.
- [62] G. Z. Kyzas and D. N. Bikiaris, "Recent modifications of chitosan for adsorption applications: a critical and systematic review.," *Mar. Drugs*, vol. 13, no. 1, pp. 312–337, Jan. 2015.
- [63] V. S. Tran *et al.*, "Typical low cost biosorbents for adsorptive removal of specific organic pollutants from water," *Bioresour. Technol.*, vol. 182, no. 1, pp. 353–363, Apr. 2015.
- [64] A. L. Mihai and M. E. Popa, "Chitosan coatings, a natural and sustainable food preservation method," *J. Biotechnol.*, vol. 208, no. Supplement, p. S81, 2015.

CHAPTER 2

CHAPTER 2

Host response to implants

In 2009, Williams defined a biomaterial as *“a substance that has been engineered to take a form which, alone or as part of a complex system, is used to direct, by control of interactions with components of living systems, the course of any therapeutic or diagnostic procedure”*[1]. Also Williams, in 2008, gave the definition of biocompatibility as the *“ability of a biomaterial to perform its desired function with respect to a medical therapy, without eliciting any undesirable local or systemic effects in the recipient or beneficiary of that therapy, but generating the most appropriate beneficial cellular or tissue response in that specific situation, and optimising the clinically relevant performance of that therapy”*[2]. These two definitions mean that when an external material is implanted in the body, this should react appropriately to improve the healing processes.

Implanting a device in the body implies surgery procedures that lead to an injury. This injury initiates an inflammatory reaction that influences the host response of the body. Immediately after implantation, proteins, platelets and leukocytes from the blood are adsorbed by the biomaterial surface initiating a cascade reaction that aims to remove the cause of the inflammation [3]. Since the cause is a device that is permanent or that degrades in a long period of time, compared to the ones of immune reaction, the cascade continues until the foreign material is entirely surrounded by cells that do not allow the interaction between the body and the biomaterial. This is the main reason why modern biomaterials need to generate the most appropriate reaction after implantation.

The host response to a biomaterial, schematically described in Figure 2.1, is characterized first by protein adsorption on the surface. This process activates the platelets starting the coagulation cascade. Neutrophils and monocytes are attracted, with proteins from the complement system, to the surface following the coagulation cascade [3].

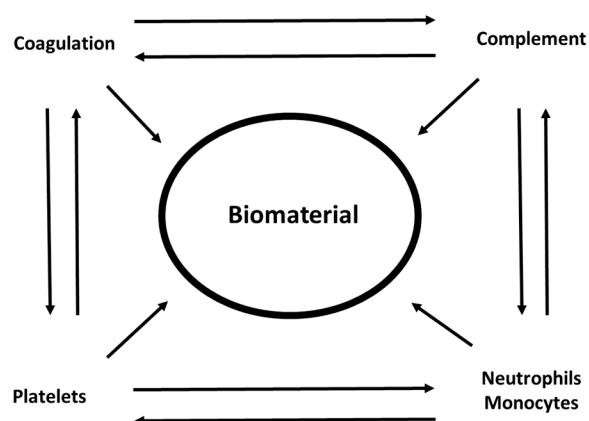


Figure 2.1: scheme of the biomaterial-tissue interaction, adapted from Gorbet and Sefton [3]

2.1: Protein adsorption

The adsorption of proteins derived from blood at the interface body-biomaterial is inevitable and influences the biological behaviour of the biomaterial itself. Proteins absorption is influenced by the properties of both protein and surface and by environmental conditions.

Properties of proteins can be the charge, size, amino acid composition and the hard or soft stability of the structure. Hard proteins like ribonuclease, α -chymotrypsin or lysozyme are more easily adsorbed on hydrophobic surfaces, rather than the hydrophilic ones, due to hydrophobic interaction of their unaltered configuration. Soft proteins, that have low internal stability, such as bovine and human serum albumin, immunoglobulin or haemoglobin are adsorbed onto all the surfaces by changing their conformation [4]. Human serum albumin (HSA) is an α -chain protein with 585 amino acids. It is a non-glucosylated protein with crystalline structure of α -helix and disulphide bonds as shown in Figure 2.2a. It is the most abundant protein in blood plasma, making it the most important factor of protein adsorption on a surface. Albumin is physiologically used to carry fatty acids, drugs, metals and hormones. Albumin can be used to deliver drug or as a medical device coating because it prevents adhesion of platelets or other proteins [5].

Immunoglobulin G is an antibody consisting of four peptide chains arranged in a Y shape, as in Figure 2.2b [6]. This antibody controls the infections of a tissue [7]. IgG represents 75% of immunoglobulins in human serum and is the main antibody in blood and body fluids. It is divided into four types in humans (IgG1, IgG2, IgG3 and IgG4). This protein can be used for immune deficiencies, infections and autoimmune disorders. The four chains of IgG consist of two heavy chains (κ or λ class) and two light chains (both γ) linked together by disulphide bonds and non-covalent forces. Different types of IgG differs for the size of the hinge region, the position of the disulphide bonds and the molecular weight [8], [9].

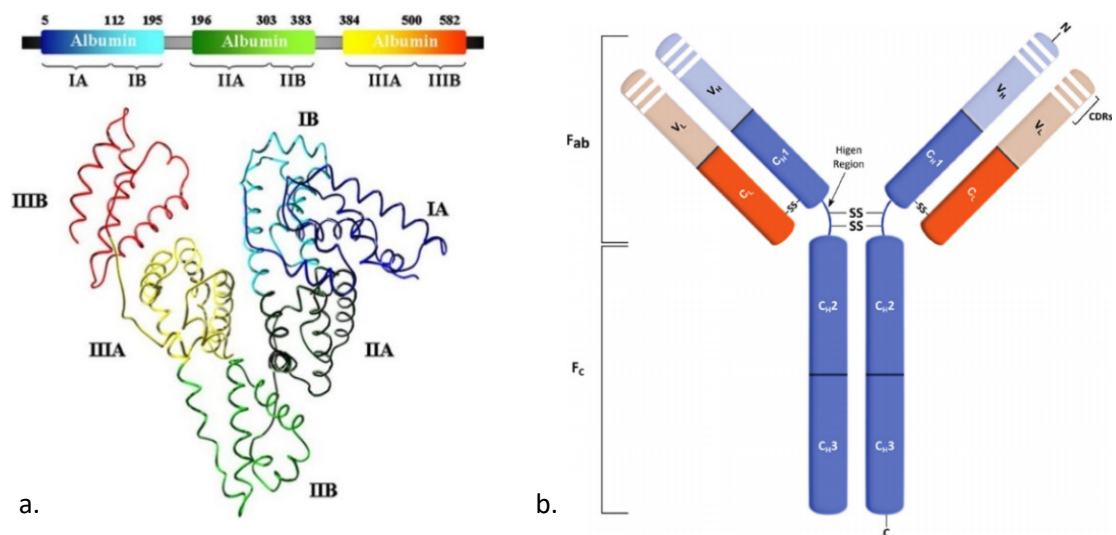


Figure 2.2: a) structure of human serum albumin, the 585 amino acids that form the structure are divided in six subdomains [5]; b) structure of Immunoglobulin G, is evident the Y shape of the four chains linked by disulphide bonds [6]

Fibrinogen is a glycoprotein made by two symmetric half molecules with three polypeptide chains (α , β and γ) kept together by disulphide bonds. It is synthesised in the liver and is the main cause of thrombus in the blood. Other properties of fibrinogen include modulation of the cell adhesion and spreading and chemotactic activity. The predominant chain is the α , made by 610 amino acids while β is made by 461 amino acids and γ by 411 residues [10]. Fibrinopeptides A and B, shown in Figure 2.3, being separated from the main protein for the action of thrombin, cause the formation of fibrin starting the clot cascade. Fibrins arranged in aggregates form the clot, but fibrin can be degraded by plasmin (proteolytic enzyme derived from the fibrinolytic system). The fibrin degradation products, depending on the concentration of plasmin, tend to weaken the structure of clots, inhibit coagulation and adhesion and prolong coagulation times [11].

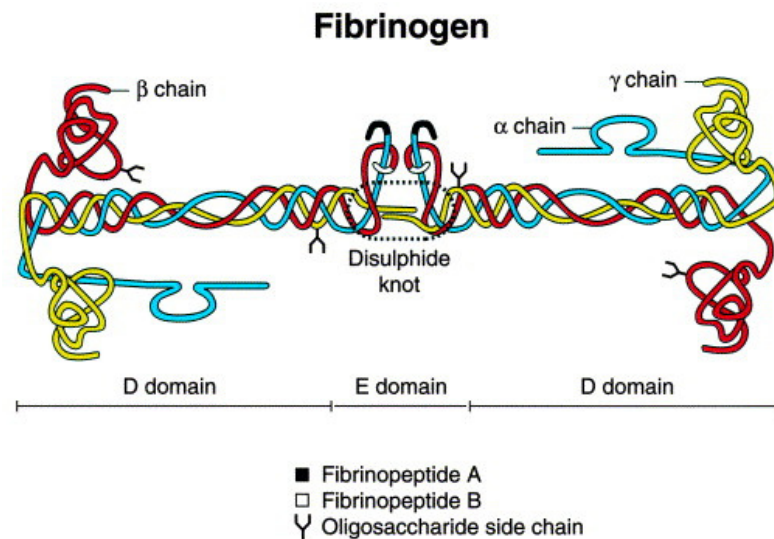


Figure 2.3: scheme of fibrinogen, three sets of different chains are linked by disulphide bonds at the amino-terminal end. Thrombin removes fibrinopeptides A and B starting the fibrin cloth [10]

Platelets (Figure 2.4) are components of the blood that modulate the immune response releasing cytokines and chemokines. Platelets have an irregular, anucleated disk shape with diameter of 2-3 μm . When platelets are activated, they secrete coagulation factors, adhesive proteins, growth factors and proteoglycans. Platelets contain granules α , dense and lysosomal: α -granules have the factors implicated in haemostasis, thrombosis and in the interactions with the vessel walls; dense granules have the responsibility to recruit more platelets for the aggregation process and lysosomes possess hydrolytic enzymes. The process of platelets activation and aggregation needs to be highly controlled because an excess leads to diseases [12], [13],[14].

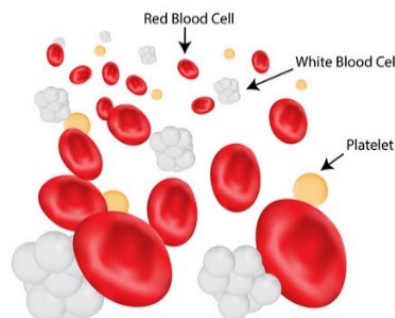


Figure 2.4: main components of the blood stream: red blood cells (responsible of carrying oxygen through haemoglobin), white blood cells (responsible of the defence reaction) and platelets (responsible of the coagulation cascade for the healing process) reported from The Platelet Society [<https://plateletsociety.co.uk/>]

2.2: Complement system

The complement system was discovered by Jules Bordet in 1896 finding that fresh serum complemented antibodies killing activity of bacteria. It is formed by at least 35 plasmas and membrane-bound proteins that act in a cascade sequence as control proteins and cellular receptor. It is a rapid key mediator of the inflammatory response. This system, shown in Figure 2.5, can be activated by an antibody-dependent process, an alternative path or a protease (Mannan Binding Lectine Associated Serine Protease – MBL/MASP) [15],[16]. The classical pathway is activated when antibodies (mostly IgG) bounded to a microbe are attached to C1, the first component of complement. The alternative pathway directly recognises some microbial surface structure and the lectin pathway starts with MBL recognising the terminal mannose residues of microbes. All the pathways lead to the C3 convertases (the formation of unstable protease complexes) and the next assembly of C5, C6, C7, C8 and C9 forming the membrane attack complex [17].

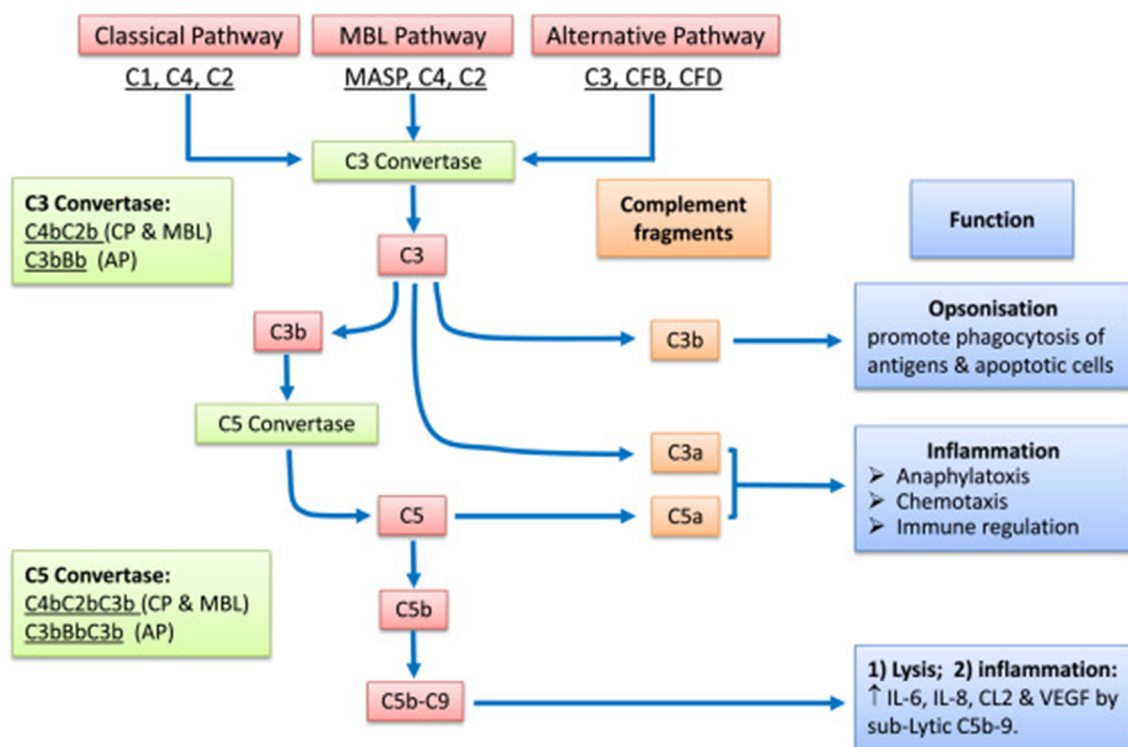


Figure 2.5: scheme of the three pathways of the complement system, each component has its role in the immune response [16]

The complement activation increases the inflammatory response and can cause harm to the host mediating the tissue destruction. In physiological conditions, regulatory proteins (RCA) mediate the complement activation to protect the tissue. RCAs regulate the stability of C3 convertases.

To prevent the excess of complement activation, researchers have been studying ways of inhibiting the activity through synthetic complement inhibitors and high doses of IgGs [18]–[25]. In particular, *Inagi et al.* studied the effect of inhibition operated by FUT-175 (Futhan) on the C3/C5 convertase activity [25]. The same effect was obtained by *Thomas et al.* with dextran derivatives made bearing carboxylic groups and benzylamide sulfonate groups [22], [23]. *Mouthon et al.* reported the immunomodulatory capacities of intravenous immune globulin (IVIG). There are five mechanisms of action to modulate the IVIG in immune-mediated diseases: functional blocking of F_c receptors on macrophages, inhibition of the damage induced by complement activation of C3b and C4b, modulation

of the production of cytokines, neutralization of circulating autoantibodies and selection of immune repertoires [21]. *Basta et al.* studied the effect of IVIG delivery on guinea pigs showing that higher levels of IVIG prevent C3 active fragments from binding to the target cells [19], [20].

2.3: Leukocyte adhesion

Leukocytes, or white blood cell, represents the defence system in the blood. They are the only nucleated cells in the blood stream and are capable to migrate in the tissues. Leukocytes are divided into five types according to their specific role in the defence process as in Figure 2.6. They can be neutrophils, eosinophils, basophils, lymphocytes and monocytes [26], [27], [28].

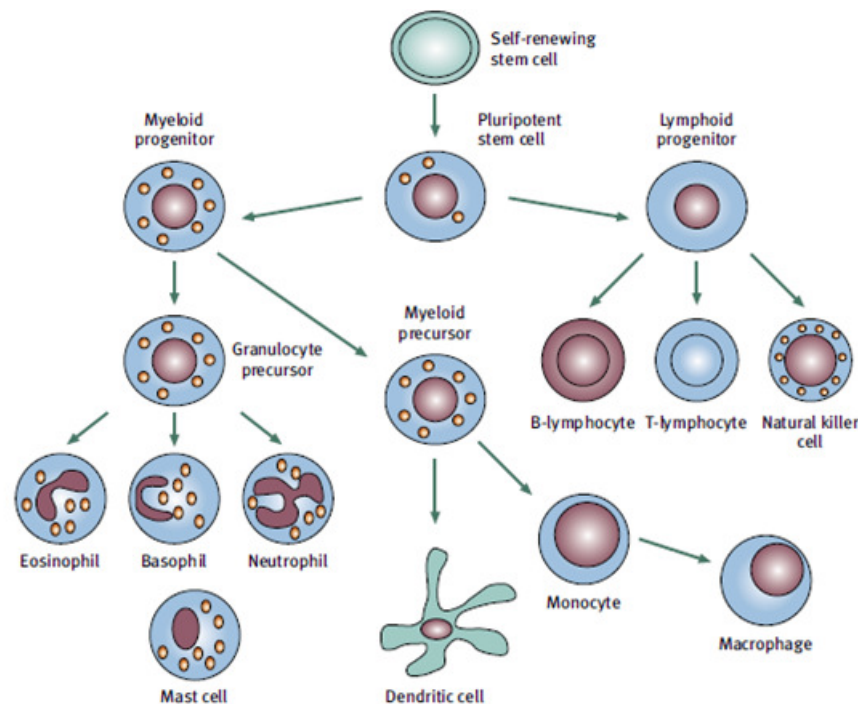


Figure 2.6: Pluripotent stem cells can differentiate into two main classes: the myeloid and lymphoid progenitors. The myeloid progenitor originates monocytes (via the myeloid precursor), or eosinophils, basophils and neutrophils (via the granulocyte precursor). Lymphocytes and natural killer cells are originated, instead, from the lymphoid progenitor [28].

Neutrophils represents about 50-80% of all leukocytes and can phagocyte microorganisms and external cells present in blood and tissues. When there is an infective episode, neutrophils number increases to protect the organism and through counting this number it can immediately be verified the presence of an infection [26], [29]. Neutrophils remain in the blood for 6-10 hours and then migrate through the vascular wall. The phagocytosis is subdivided in migration, chemotaxis, ingestion, degranulation and oxidative burst activity. Migration, shown in Figure 2.7, is activated when an inflammatory reaction causes the adhesion of the cell to the vascular endothelium. Following this reaction, the endothelial cells allow migration in the tissue when the neutrophil changes its shape. Selectins present in the vascular endothelium cause the rolling of the white cell on the endothelium surface itself until integrins and other adhesion molecules (such as immunoglobulins) lead to the proper migration [30]. Chemotaxis acts with agents produced by the complement activation and makes the neutrophil move depending on the concentration gradient. The true phagocytosis is the process of ingestion by which the microbe is engulfed inside the neutrophil due to antibody recognition and immunoglobulin binding. The phagosome, the result of phagocytosis, is degranulated by the action

of internal neutrophils granules containing enzymes. Degranulation is enhanced by oxidative burst activity. In this process, neutrophils produce reactive oxygen species, such as O_2^- , hydrogen peroxide and OH radicals, that are toxic to the microbe [28], [31].

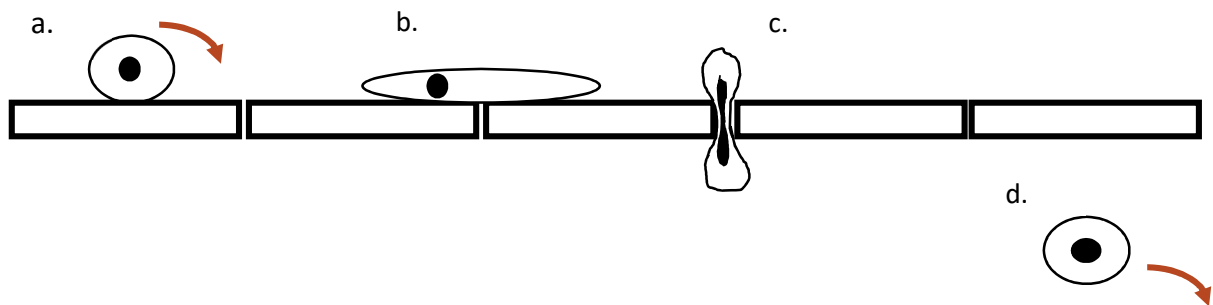


Figure 2.7: the migration process consists of a sequence of four movements: a) rolling of the cell on the endothelium, b) activation of the adhesion to the vascular wall, c) transendothelial migration through the gaps between endothelial cells and d) movement to the inflammation site. Adapted from Ref. [27]

Eosinophils represents 1-4% of white blood cells and can phagocyte parasites by releasing toxic molecules after the adhesion to the parasite's body. This type of defence is very low and in some cases the toxic molecules can lead to damage of the normal tissues with allergic reactions [26].

Basophils represents less than 1% of total leukocytes and operate as the eosinophils without phagocytosis. They release toxic molecules, but also histamine, heparin and other composites that have a role in allergic reactions [26].

Monocytes represents 2-8% of white blood cells and act as phagocytes. These cells can migrate in the tissues where they highly expand their dimensions (5-10 times) to become macrophages for microbe phagocytosis [26]. The recruitment of these cells is mediated by cytokines and chemoattractants, in particular by cysteine-cysteine chemokines (that modulate β -integrin binding) and interleukins [32].

Lymphocytes represents 20-40% of leukocytes and act on the immune system. They allow the recognition of foreign cells to the immune system. Lymphocytes are divided into three main types: B, T and null (mostly natural killers). Lymphocytes B recognise antigens by secretion of antibodies. These antibodies adhere to the bacterial surface allowing the targeting of other killing cells. Lymphocytes T, instead, damage the host cell membrane becoming cytotoxic T-lymphocytes that allow the swelling of the targeted cell leading to the cell destruction. The natural killer cells act against viral infections killing the cells that have been infected by the virus limiting the proliferation [33].

Leukocytes adhesion is directly related to the host response to biomaterial implantation. Leukocytes adhere to polymeric surfaces in processes involving blood-material interactions (haemodialysis, hemofiltration, cardiopulmonary bypass and artificial heart implantation) [34]. These cells recognize proteins adsorbed on the biomaterial surface and adhere to it through interactions via adhesion ligand-receptor superfamily. Leukocytes activation lead to spreading, formation of micro thrombi via platelet-platelet or platelet-leukocyte interactions, detachment of thrombi and adherent platelets, release of leukocytes proteases and promotion of fibroblast growth on prosthetic materials. Macrophages activation and fusion into giant cells determines the stability and/or degradation of the implant. Leukocytes can also modulate the response of other cell types with the release of cytokines, growth factors and bioactive agents. Complement activation, derived from protein adsorption on the biomaterial surface, binds leukocytes through protein C3 of the alternative pathway. An inactive

surface, on the contrary, leads to the inhibition of C5 conversion terminating the complement activity [35]–[38].

2.4: Inflammation and healing response

The normal process of inflammation is an essential part of the healing response protecting the body from foreign organisms. Sometimes, however, it can contribute to the damage with a chronic inflammatory response that develop into a fibrous capsule [35], [39]. This fibrous capsule can be a barrier between the biomaterial and the body. The biomaterial properties and the surgery made for implantation have a direct influence on the inflammatory response and the healing.

Acute inflammation is the consequence of rolling, adhesion and migration of neutrophils and monocytes through the endothelium. The release of cytokines from these cells mediate the adhesion of proteins that initiates the coagulation cascade. Normally, neutrophils and macrophages, with their action, remove the foreign body and restore the tissue. When a biomaterial is implanted, the source of the inflammation site cannot be removed and it remains an inflammatory stimulus and a chronic state. The healing response is the granulation tissue via fibroblasts proliferation. The final stage is the foreign body reaction in which giant body cells surround the biomaterial with a fibrous encapsulation creating a barrier [40]. In Figure 2.8 we can see all the steps that terminate in the foreign body response, in particular:

- Implant of the biomaterial to substitute the damaged part.
- Protein adsorption on the biomaterial surface from the immediate interaction with blood stream. This depends mainly on albumin, immobilized immunoglobulin G and fibrinogen.
- Coagulation of the blood near the biomaterial due to platelet activation and formation of fibrin.
- Acute inflammation as a consequence of neutrophils and monocytes adhesion to the biomaterial surface through fibrinogen.
- Chronic inflammation due to formation of macrophages and multinucleated giant cells.
- Foreign body response with the complete formation of a layer of collagen.

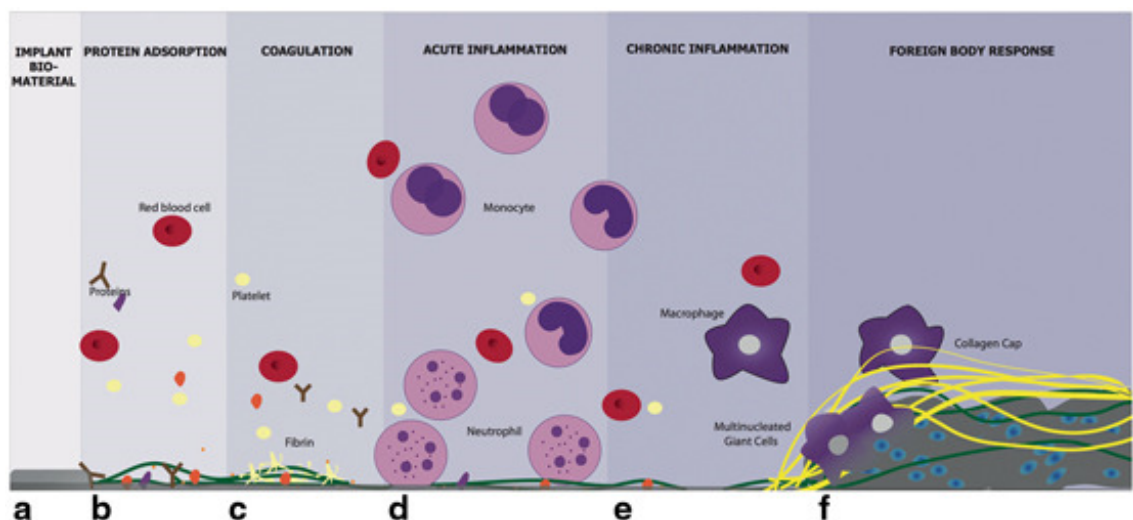


Figure 2.8: steps of the foreign body reaction [40]

Tang and Eaton demonstrated the influence of fibrinogen in the development of the foreign body response studying mice with low levels of fibrinogen, mice unable to synthesize complement and mice unable to synthesize Immunoglobulin G. They discovered that mice without complement or Immunoglobulin G activity could still produce a layer of phagocytes while mice without fibrinogen were unable to produce an inflammatory response until fibrinogen was injected in the body [41].

The cascade started with protein adsorption produce a provisional matrix useful for the wound healing process. This matrix, containing growth factors, cytokines, chemoattractants and other bioactive agents, mediates the macrophages activity controlling the phases of the healing. After the initial interactions, the extent of the implantation site influences the dimensions and characteristics of the acute and chronic inflammation reaction [42].

Foreign body response is composed of three phases: onset, progression and resolution. In the progression phase, the acute inflammation becomes chronic. At this stage, macrophages release pro-inflammatory cytokines and chemokines that increase the attraction of leukocytes. Macrophages also produce enzymes that degrade the biomaterial and giant cells that phagocyte the degradation products. The microenvironment of the biomaterial maintains the inflammation stimulus leading to the creation of granulation tissue and the fibrous capsule around the surface. This fibrous capsule is made prevalently by fibroblasts and macrophages [43]. The acute inflammation is generally resolved in two-three weeks with the formation of a granulation tissue due to macrophages, fibroblasts and neovascularization [44]. Macrophages activated in the inflammation site can fuse together to create foreign body giant cells, part of multinucleated giant cells. These cells remain in the biomaterial-tissue interface for the lifetime of the device [45]. Macrophages phenotype influences the healing response to the foreign body.

2.5: Influence of the surface properties on the foreign body reaction

Surface properties such as chemistry, shape and topography show an important role in the foreign body reaction.

To limit the attachment of proteins on the surface, its functional groups must have (super)-hydrophilic nature, hydrogen bond acceptors (the donor in a hydrogen bond is the atom to which the hydrogen atom is covalently bonded and it is usually a strongly electronegative atom such as N, O, or F; the hydrogen acceptor is the electronegative ion or molecule bonded through the hydrogen bridge and it must have an electron pair) and/or neutral charge. Fibrinogen binds with -OH, -NH₂ and -CH₃ surfaces. It does not bond with -COOH.

Neutral and non-ionic surfaces limit the adhesion of platelets.

Table 2.1 summarizes the response of functional groups to proteins [46].

Surface functional group	Reactions
Carboxyl (-COOH) <i>Hydrophilic, negatively charged</i>	<ul style="list-style-type: none"> ➤ Preferentially interacts with fibronectin and albumin ➤ Attenuates inflammatory responses and reduces fibrotic capsule formation <i>in vivo</i>
Hydroxyl (-OH) <i>Hydrophilic, neutral charge</i>	<ul style="list-style-type: none"> ➤ Reduces plasma protein affinity ➤ High level of cell infiltration due to thick fibrotic capsule
Amine (-NH₂) <i>Hydrophilic, positive charge</i>	<ul style="list-style-type: none"> ➤ High fibronectin affinity ➤ Triggers acute inflammatory responses, thick fibrotic capsule formation and cell infiltration <i>in vivo</i>
Methyl (-CH₃) <i>Hydrophobic, neutral charge</i>	<ul style="list-style-type: none"> ➤ Binds fibrinogen leading to platelet activation ➤ Binds IgG ➤ High recruitment of inflammatory cells <i>in vivo</i> ➤ Increased leukocytes adhesion and phagocyte migration
Mixed -NH₂ and -COOH <i>Positive and negative</i>	<ul style="list-style-type: none"> ➤ At the equal molar fraction (neutral net charge) platelet adsorption is lower compared to other fractional mixes of the functionalities
Mixed -OH and -CH₃ <i>Hydrophobic and hydrophilic</i>	<ul style="list-style-type: none"> ➤ Platelet adhesion and fibrinogen adsorption decrease when the fraction of -OH increases
Mixed -PO₃H₂ and -OH <i>Negative and neutral</i>	<ul style="list-style-type: none"> ➤ Equal molar fraction of the groups leads to a low number of platelet adhesion

Table 2.1: proteins response to surface functional groups. Adapted from Ref. [46]

An important parameter in the characterization of the immune response is the ratio between the surface and the volume of the biomaterial, with higher values (such as in porous materials) showing higher amount of macrophages. Even shape and size have a direct impact on body reaction with spherical microparticles more exposed to phagocytosis than elliptically shaped when dimensions are compatible with this kind of reaction [47].

Sanders et al. demonstrated the influence of the form and dimensions of different polymeric fibres on the foreign body reaction. It was found that fibres with diameter 1-5 micrometres showed low or absent fibrous capsule compared to fibres with diameter 10-15 micrometres [48].

Surface topography influences cell adhesion depending on cell type. Normally, cells prefer roughened surfaces probably for the greater surface useful to the adhesion of more cells. However, human gingival fibroblasts seem to prefer electropolished surfaces. Knowing the preference of a cell to a particular surface, substrate topography can be selected to attract or reject cell types. Since macrophages prefer roughened substrates, it can be useful to use smooth surfaces when the goal is to avoid the attachment [49]. The increase in surface roughness decreases osteoblast proliferation, increases differentiation and protein synthesis. A roughened surface presents more surface area compared to a smooth one and this also affects cytokines production, with more interleukins secreted by macrophages exposed to higher surface area ratios [45].

Host response can also be modulated by incorporation of bioactive molecules providing adhesion sites and anti-inflammatory mediators or drugs. Adhesion of specific protein peptides, such as RGD (arginine-glycine-aspartic acid) sequence, can modulate the foreign response mediating macrophages adhesion and migration. The use of polyethylene glycol (PEG) coatings determines the anti-fouling properties by which a surface becomes non-interactive with proteins [50], [51].

Glucocorticoids suppress the immune response by inhibition of inflammatory cell activation (stopping the synthesis of inflammatory mediators) and promote the healing by the enhancement of anti-inflammatory cytokines release. The coupling of dexamethasone to a surface reduces inflammation by absence of macrophages and fibrous capsule formation on the implant. Since

dexamethasone also suppress VEGF (vascular endothelial growth factor) production at the implant site, it is usually combined with this particular growth factor to allow the proper healing response [50].

Functionalise a surface with growth factors like EGF (epidermal growth factor), FGF (fibroblast growth factor), GM-CSF (granulocyte macrophage colony stimulating factor) or VEGF, is useful to control adhesion, migration, proliferation and differentiation of fibroblasts, keratinocytes and endothelial cells in wound healing. Monocytes and macrophages reacts to growth factors through interactions with active fibroblasts, endothelial cells and keratinocytes suggesting a path to control their response [50].

2.6: Bibliography

- [1] D. F. Williams, "On the nature of biomaterials," in *Biomaterials*, vol. 30, no. 30, 2009, pp. 5897–5909.
- [2] D. F. Williams, "On the mechanisms of biocompatibility," *Biomaterials*, vol. 29, no. 20, pp. 2941–2953, 2008.
- [3] M. B. Gorbet and M. V Sefton, "Biomaterial-associated thrombosis: roles of coagulation factors, complement, platelets and leukocytes," *Biomaterials*, vol. 25, no. 26, pp. 5681–5703, 2004.
- [4] K. Nakanishi, T. Sakiyama, and K. Imamura, "On the adsorption of proteins on solid surfaces, a common but very complicated phenomenon," *J. Biosci. Bioeng.*, vol. 91, no. 3, pp. 233–244, 2001.
- [5] Z. Adamczyk, M. Nattich-Rak, M. Dąbkowska, and M. Kujda-Kruk, "Albumin adsorption at solid substrates: A quest for a unified approach," *J. Colloid Interface Sci.*, vol. 514, no. 1, pp. 769–790, 2018.
- [6] L. Loureiro *et al.*, "Challenges in Antibody Development against Tn and Sialyl-Tn Antigens," *Biomolecules*, vol. 5, no. 3, pp. 1783–1809, Aug. 2015.
- [7] P. F. Gomes, J. M. Loureiro, and A. E. Rodrigues, "Adsorption equilibrium and kinetics of Immunoglobulin G on a mixed-mode adsorbent in batch and packed bed configuration," *J. Chromatogr. A*, vol. 1524, no. 1, pp. 143–152, 2017.
- [8] R. H. Painter, "IgG," *Encyclopedia of Immunology*. pp. 1208–1211, 1998.
- [9] D. K. Flaherty, "Antibodies," in *Immunology for Pharmacy*, 2012, pp. 70–78.
- [10] S. Herrick, O. Blanc-Brude, A. Gray, and G. Laurent, "Fibrinogen," *Int. J. Biochem. Cell Biol.*, vol. 31, no. 7, pp. 741–746, 1999.
- [11] "Fibrinogen," *Br. Med. J.*, vol. 4, no. 5627, pp. 341–342, 1968.
- [12] M. El Haouari, J. J. López, H. Mekhfi, J. A. Rosado, and G. M. Salido, "Antiaggregant effects of Arbutus unedo extracts in human platelets," *J. Ethnopharmacol.*, vol. 113, no. 2, pp. 325–331, 2007.
- [13] M. El Haouari and J. A. Rosado, "Platelet signalling abnormalities in patients with type 2 diabetes mellitus: A review," *Blood Cells, Mol. Dis.*, vol. 41, no. 1, pp. 119–123, 2008.
- [14] C. Faggio *et al.*, "Flavonoids and platelet aggregation: A brief review," *Eur. J. Pharmacol.*, vol. 807, no. 1, pp. 91–101, 2017.
- [15] M. Kirschfink, "Controlling the complement system in inflammation," *Immunopharmacology*, vol. 38, no. 1, pp. 51–62, 1997.
- [16] H. Xu and M. Chen, "Targeting the complement system for the management of retinal inflammatory and degenerative diseases," *Eur. J. Pharmacol.*, vol. 787, no. 1, pp. 94–104, Mar. 2016.
- [17] S. Zhang and P. Cui, "Complement system in zebrafish," *Dev. Comp. Immunol.*, vol. 46, no. 1, pp. 3–10, 2014.

- [18] C. E. Hack, A. C. Ogilvie, B. Eisele, A. J. Eerenberg, J. Wagstaff, and L. G. Thijs, "C1-inhibitor substitution therapy in septic shock and in the vascular leak syndrome induced by high doses of interleukin-2.," *Intensive Care Med.*, vol. 19 Suppl 1, pp. S19-28, 1993.
- [19] M. Basta and M. C. Dalakas, "High-dose intravenous immunoglobulin exerts its beneficial effect in patients with dermatomyositis by blocking endomysial deposition of activated complement fragments.," *J. Clin. Invest.*, vol. 94, no. 5, pp. 1729–1735, Nov. 1994.
- [20] M. Basta, P. Kirshbom, M. M. Frank, and L. F. Fries, "Mechanism of therapeutic effect of high-dose intravenous immunoglobulin. Attenuation of acute, complement-dependent immune damage in a guinea pig model.," *J. Clin. Invest.*, vol. 84, no. 6, pp. 1974–1981, Dec. 1989.
- [21] L. Mouthon *et al.*, "Mechanisms of action of intravenous immune globulin in immune-mediated diseases.," *Clin. Exp. Immunol.*, vol. 104 Suppl 1, pp. 3–9, May 1996.
- [22] H. Thomas, F. Maillet, D. Letourneur, J. Jozefonvicz, and M. D. Kazatchkine, "Effect of substituted dextran derivative on complement activation in vivo," *Biomaterials*, vol. 16, no. 15, pp. 1163–1167, 1995.
- [23] H. Thomas, F. Maillet, D. Letourneur, J. Jozefonvicz, E. Fischer, and M. D. Kazatchkine, "Sulfonated dextran inhibits complement activation and complement-dependent cytotoxicity in an in vitro model of hyperacute xenograft rejection," *Mol. Immunol.*, vol. 33, no. 7, pp. 643–648, 1996.
- [24] B. Crepon, F. Maillet, M. D. Kazatchkine, and J. Jozefonvicz, "Molecular weight dependency of the acquired anticomplementary and anticoagulant activities of specifically substituted dextrans," *Biomaterials*, vol. 8, no. 4, pp. 248–253, 1987.
- [25] R. Inagi, T. Miyata, K. Maeda, S. Sugiyama, A. Miyama, and I. Nakashima, "FUT-175 as a potent inhibitor of C5/C3 convertase activity for production of C5a and C3a," *Immunol. Lett.*, vol. 27, no. 1, pp. 49–52, 1991.
- [26] C. L. Stanfield, "Cardiovascular system: the blood," in *Principles of Human Physiology*, IV., Pearson, Benjamin Cummings, 2011, pp. 435–450.
- [27] J. Cavenagh, "White blood cells," *Surg.*, vol. 25, no. 2, pp. 61–64, 2007.
- [28] C. A. King and M. R. Wills, "Immunology I: innate immunology," *Surg.*, vol. 23, no. 8, pp. 304–308, 2005.
- [29] S. Nazlibilek, D. Karacor, T. Ercan, M. H. Sazli, O. Kalender, and Y. Ege, "Automatic segmentation, counting, size determination and classification of white blood cells," *Measurement*, vol. 55, no. 1, pp. 58–65, 2014.
- [30] E. J. Brown, "Adhesive interactions in the immune system," *Trends Cell Biol.*, vol. 7, no. 7, pp. 289–295, 1997.
- [31] Y. Reyat and G. Bellingan, "The basic science of acute lung injury," *Surg.*, vol. 22, no. 6, pp. 3–7, 2004.
- [32] A. M. Vignola, M. Gjomarkaj, B. Arnoux, and J. Bousquet, "Monocytes," *J. Allergy Clin. Immunol.*, vol. 101, no. 2, pp. 149–152, 1998.
- [33] C. L. Stanfield, "The immune system," in *Principles of Human Physiology*, IV., Pearson, Benjamin

Cummings, 2011, pp. 667–691.

- [34] F. Lim and S. L. Cooper, "Effect of sulphonate incorporation on in vitro leucocyte adhesion to polyurethanes," *Biomaterials*, vol. 16, no. 6, pp. 457–466, 1995.
- [35] N. P. Ziats, K. M. Miller, and J. M. Anderson, "In vitro and in vivo interactions of cells with biomaterials," *Biomaterials*, vol. 9, no. 1, pp. 5–13, 1988.
- [36] R. J. Johnson, "Complement activation during extracorporeal therapy: biochemistry, cell biology and clinical relevance.," *Nephrol. Dial. Transplant*, vol. 9 Suppl 2, pp. 36–45, 1994.
- [37] W. J. Kao, "Evaluation of leukocyte adhesion on polyurethanes: the effects of shear stress and blood proteins," *Biomaterials*, vol. 21, no. 22, pp. 2295–2303, 2000.
- [38] L.-Y. L. Yung, R. W. Colman, and S. L. Cooper, "The effect of high molecular weight kininogen on neutrophil adhesion to polymer surfaces," *Immunopharmacology*, vol. 43, no. 2, pp. 281–286, 1999.
- [39] J. E. Babensee, J. M. Anderson, L. V. McIntire, and A. G. Mikos, "Host response to tissue engineered devices," *Adv. Drug Deliv. Rev.*, vol. 33, no. 1, pp. 111–139, 1998.
- [40] T. Yu, V. J. Tutwiler, and K. Spiller, "The role of macrophages in the foreign body response to implanted biomaterials," in *Biomaterials in Regenerative Medicine and the Immune System*, I., L. Santambrogio, Ed. Springer International Publishing, 2015, pp. 17–34.
- [41] W. Kenneth Ward, "A review of the foreign-body response to subcutaneously-implanted devices: the role of macrophages and cytokines in biofouling and fibrosis," *J. Diabetes Sci. Technol.*, vol. 2, no. 5, pp. 768–777, Sep. 2008.
- [42] J. M. Anderson, A. Rodriguez, and D. T. Chang, "Foreign body reaction to biomaterials," *Semin. Immunol.*, vol. 20, no. 2, pp. 86–100, 2008.
- [43] S. M. van Putten, D. T. A. Ploeger, E. R. Popa, and R. A. Bank, "Macrophage phenotypes in the collagen-induced foreign body reaction in rats," *Acta Biomater.*, vol. 9, no. 5, pp. 6502–6510, 2013.
- [44] J. M. Anderson, "Biocompatibility and Bioresponse to Biomaterials," in *Principles of regenerative medicine*, I., A. Atala, R. Lanza, J. Thomson, and R. Nerem, Eds. Elsevier, Academic Press, 2008, pp. 704–723.
- [45] Z. Sheikh, P. J. Brooks, O. Barzilay, N. Fine, and M. Glogauer, "Macrophages, Foreign Body Giant Cells and their response to implantable biomaterials," *Materials (Basel)*, vol. 8, no. 1, pp. 5671–5701, 2015.
- [46] P. Thevenot, W. Hu, and L. Tang, "Surface Chemistry Influences Implant Biocompatibility," *Curr. Top. Med. Chem.*, vol. 8, no. 4, pp. 270–280, Feb. 2008.
- [47] H.-D. Wu, D.-Y. Ji, W.-J. Chang, J.-C. Yang, and S.-Y. Lee, "Chitosan-based polyelectrolyte complex scaffolds with antibacterial properties for treating dental bone defects," *Mater. Sci. Eng. C*, vol. 32, no. 2, pp. 207–214, 2012.
- [48] J. E. Sanders, S. D. Bale, and T. Neumann, "Tissue response to microfibers of different polymers: Polyester, polyethylene, polylactic acid, and polyurethane," *J. Biomed. Mater. Res.*, vol. 62, no. 2, pp. 222–227, Nov. 2002.

- [49] B. Chehroudi, "Effects of Surface Topography on Cell Behavior," in *Encyclopedic Handbook of Biomaterials and Bioengineering*, D. L. Wise, Ed. Marcel Dekker, 1995, pp. 813–842.
- [50] S. Franz, S. Rammelt, D. Scharnweber, and J. C. Simon, "Immune responses to implants - A review of the implications for the design of immunomodulatory biomaterials," *Biomaterials*, vol. 32, no. 28, pp. 6692–6709, 2011.
- [51] K. Sarkar, Y. Xue, and S. Sant, "Host response to synthetic versus natural biomaterials," in *The immune response to implanted materials and devices*, B. Corradetti, Ed. Springer International Publishing, 2017.

CHAPTER 3

Effects of chitosan on immune reaction

3.1: Effects of chitosan on immune reaction

Structure and biological properties of chitosan (Figures 3.1 and 3.2) have been reported previously in Chapter 1, here is reported its effect on the foreign body response described in Chapter 2.

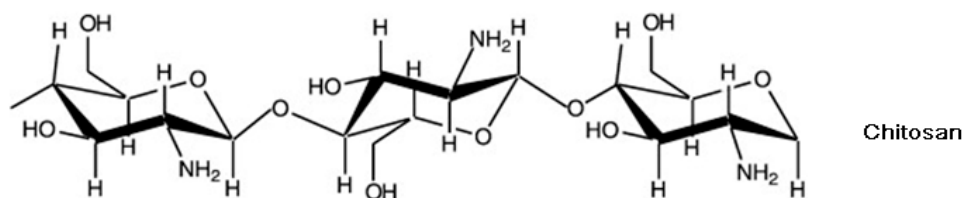


Figure 3.1: structure of chitosan

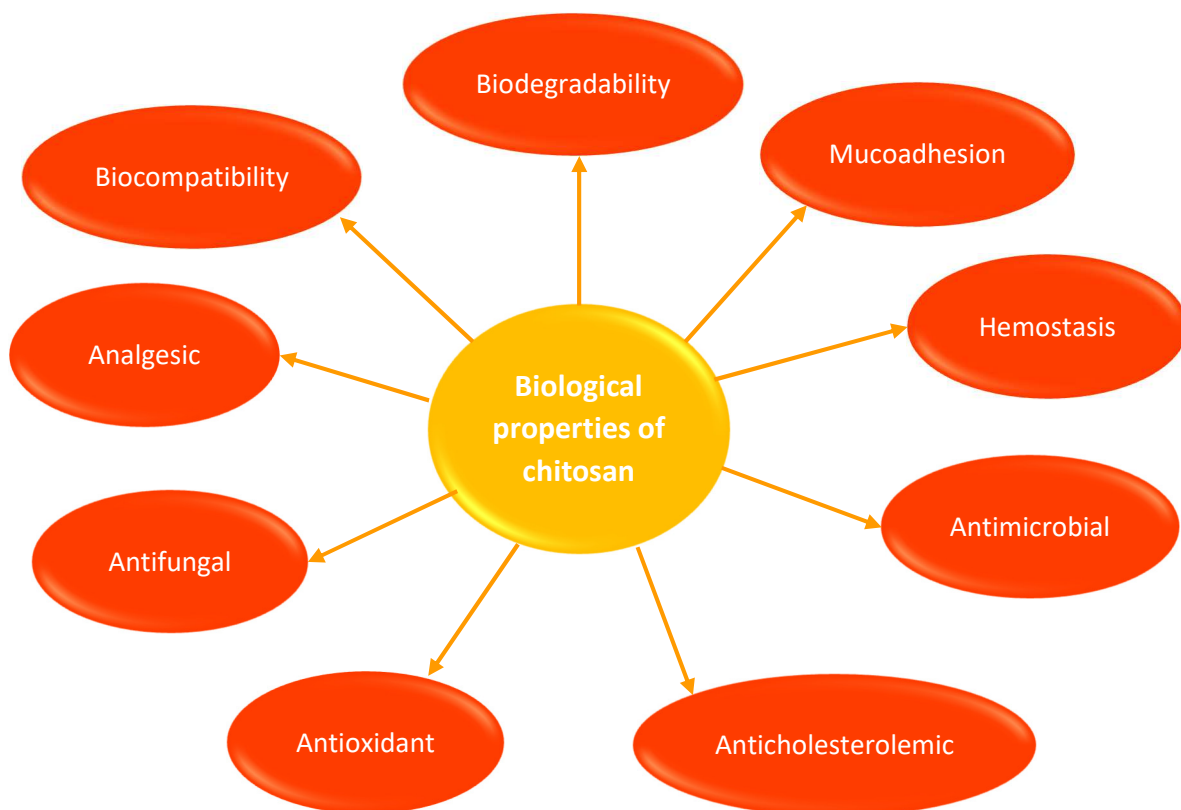


Figure 3.2: biological properties of chitosan

The effect of chitosan in improving wound healing was first discovered in 1970. The properties of chitosan include mechanic plastic behaviour, antibacterial effects, minimal foreign body reaction, osteoconduction and cell infiltration [1]. Although chitosan presents cell infiltration, macrophages become inactive, resulting in an anti-inflammatory effect [1]. Chitosan-based scaffolds can be incorporated with bioactive elements to improve osteogenesis. Chitosan can be fabricated as hydrogels, microcapsules, membranous films, sponges, tubes or a 3D porous structure [2].

The general response of the body to chitosan is minimal, but it can depend on the properties of chitosan and on the application.

Vandevord et al. discovered that porous scaffolds made with chitosan implanted into mice models do not show pathological inflammatory response. It was found an accumulation of neutrophils within the implant with an increase in the implant time. No evidence of infection or endotoxin were revealed. It was observed collagen deposition in the porous structure starting the creation of connective tissue. ELISA (enzyme-linked immunosorbent assay) showed minimal incidence of specific reaction to chitosan and minimal signs of inflammation even with a large migration of white blood cells at the implant site [1].

A porous scaffold made with chitosan and alginate through co-precipitation and freeze-drying was studied for bone tissue regeneration. This scaffold did not present cytotoxic activity on MG-63 cells (cell line derived from human osteosarcoma) indicating good biocompatibility. In order to reduce the time of formation of bone tissue, this chitosan-alginate scaffold was blended with hydroxyapatite showing the presence of new bone tissue 8 weeks after implantation that was not present in the pure chitosan-alginate scaffold [3].

Chitosan can be used to produce an *in situ* hydrogel for biomedical applications. On a study conducted in rats, it was found that this chitosan hydrogel attracted monocytes to form macrophages after the injection but in a period of 30 days do not lead to formation of foreign body giant cells indicating the absence of inflammation. Macrophages just started the degradation process of the polymer [4]. The same result was obtained over a period of 6 weeks after which hydrogel nanoparticles made with chitosan showed a decrease in the number of macrophages around the implant without chronic development [5].

A polyelectrolyte complex gel scaffold made with chitosan, γ -polyglutamic acid (γ -PGA) and carboxymethyl-cellulose for bone regeneration tested in dogs resulted in a minimal inflammatory reaction three days after implantation, suggesting its use for dental applications [6].

Barbosa et al. developed a Dhvar-5-chitosan coating that acted with bactericidal effects on *Staphylococcus epidermidis*, *Staphylococcus aureus*, *Escherichia coli* and *Pseudomonas aeruginosa* (most prevalent pathogens in infections associated to implants). Dhvar-5 immobilization with exposure of the hydrophobic end showed high antimicrobial activity against *Gram-positive* bacteria and reduced the *Gram-negative* bacteria adhesion. This antimicrobial activity does not present cytotoxic effects nor inflammation response on surrounding cells [7].

Oliveira et al. investigated the influence of a substrate of chitosan with 88%DD (deacetylation degree) on monocytes differentiation. Differentiation into macrophages was allowed for 7 to 10 days on chitosan and on polystyrene for tissue culture as control. Results showed that after 10 days the macrophages differentiation reduced the expression of pro-inflammatory cytokines on chitosan compared to control. Chitosan also induced the production of anti-inflammatory cytokines compared to control. It was also discovered that chitosan, up to day 7, increased the migratory behaviour of monocytes and, subsequently, of macrophages, with a slow migration on the fully differentiated

macrophages [8]. *Chatelet et al.* discovered that the same chitosan inhibits proliferation of fibroblasts. These cells adhere to chitosan with a subsequent variation in their morphology and behaviour [9].

Mori, Okumura et al. analysed the effects of chitin and chitosan on the proliferation of fibroblasts and cytokines *in vitro*. Although chitin and chitosan did not enhance directly the proliferation of fibroblasts, it was discovered that chitosan blended with heparin improved fibroblasts growth. This is explained with the polyelectrolyte interactions between the two complexes that lead to the enhancement of wound healing. Chitosan in high concentration with fetal calf serum (FCS) showed a reduction in cell proliferation only in the blended state indicating an indirect inhibition. Chitin and its derivatives do not stimulate directly the production of cytokines by fibroblasts (typically interleukins) characteristic of the inflammatory reaction [10].

Chitosan can, however, have negative effects following its application depending on its deacetylation degree. When chitosan is used with PET in electrospun fibres for abdominal meshes, as in research by *Veleirinho et al.*, it increases the foreign body reaction [11]. This can also depend on the fibres dimensions as is known that high surface-to-volume ratios (present in the electrospun nanofibers) contribute to protein adsorption and thus to foreign body reaction [12], [13].

Barbosa et al. also obtained similar results when testing the reaction of chitosan with different deacetylation degrees (this being the opposite of the acetylation degree, $\%DD=100-\%AD$) and showing the importance of acetyl and amine functional groups. Chitosan with 85% deacetylation degree attracted more leukocytes and inflammatory cells compared to chitosan with 96% deacetylation degree [14].

The anti-inflammatory behaviour of chitosan has been demonstrated through tests and applications. Even if the first reaction when chitosan is implanted in the body as scaffold, hydrogel or coating for substrates, is of attraction to leukocytes, the overall response in the long term is of biocompatibility. It has been discovered that chitosan shows the ability to inhibit the activation of neutrophils and macrophages when used as scaffold or hydrogel. Chitosan used as a coating showed antibacterial effects without cytotoxicity and inflammation on surrounding cells. Chitosan can produce a negative effect when used in fibres obtained via electrospinning.

It is important, to obtain a minimal inflammatory reaction, the use of chitosan, depending on the application, with the proper deacetylation degree and with the best form (scaffold, hydrogel or coating).

3.2: Bibliography

- [1] P. J. VandeVord, H. W. T. Matthew, S. P. DeSilva, L. Mayton, B. Wu, and P. H. Wooley, "Evaluation of the biocompatibility of a chitosan scaffold in mice.," *J. Biomed. Mater. Res.*, vol. 59, no. 3, pp. 585–590, Mar. 2002.
- [2] T. Jiang, S. G. Kumbar, L. S. Nair, and C. T. Laurencin, "Biologically active chitosan systems for tissue engineering and regenerative medicine.," *Curr. Top. Med. Chem.*, vol. 8, no. 4, pp. 354–364, 2008.
- [3] H.-H. Jin *et al.*, "In vivo evaluation of porous hydroxyapatite/chitosan–alginate composite scaffolds for bone tissue engineering.," *Int. J. Biol. Macromol.*, vol. 51, no. 5, pp. 1079–1085, 2012.
- [4] M. J. Moura, J. Brochado, M. H. Gil, and M. M. Figueiredo, "In situ forming chitosan hydrogels: Preliminary evaluation of the in vivo inflammatory response," *Mater. Sci. Eng. C*, vol. 75, no. 1, pp. 279–285, 2017.
- [5] Y.-L. Chiu *et al.*, "pH-triggered injectable hydrogels prepared from aqueous N-palmitoyl chitosan: In vitro characteristics and in vivo biocompatibility," *Biomaterials*, vol. 30, no. 28, pp. 4877–4888, 2009.
- [6] H.-D. Wu, D.-Y. Ji, W.-J. Chang, J.-C. Yang, and S.-Y. Lee, "Chitosan-based polyelectrolyte complex scaffolds with antibacterial properties for treating dental bone defects," *Mater. Sci. Eng. C*, vol. 32, no. 2, pp. 207–214, 2012.
- [7] M. Barbosa, F. Costa, C. Monteiro, F. Duarte, M. C. L. Martins, and P. Gomes, "Antimicrobial coatings prepared from Dhvar-5-click-grafted chitosan powders," *Acta Biomater.*, vol. 84, no. 1, pp. 242–256, 2019.
- [8] M. I. Oliveira, S. G. Santos, M. J. Oliveira, A. L. Torres, and M. A. Barbosa, "Chitosan drives anti-inflammatory macrophage polarisation and pro-inflammatory dendritic cell stimulation," *Eur. Cells Mater.*, vol. 24, no. 1, pp. 136–153, 2012.
- [9] C. Chatelet, O. Damour, and a Domard, "Influence of the degree of acetylation on some biological properties of chitosan films.," *Biomaterials*, vol. 22, no. 3, pp. 261–268, 2001.
- [10] T. Mori *et al.*, "Effects of chitin and its derivatives on the proliferation and cytokine production of fibroblasts in vitro," *Biomaterials*, vol. 18, no. 13, pp. 947–951, 1997.
- [11] B. Veleirinho *et al.*, "Foreign body reaction associated with PET and PET/chitosan electrospun nanofibrous abdominal meshes," *PLoS One*, vol. 9, no. 4, pp. e95293–e95293, Apr. 2014.
- [12] K. T. Shalumon, N. S. Binulal, M. Deepthy, R. Jayakumar, K. Manzoor, and S. V Nair, "Preparation, Characterization and Cell Attachment Studies of Electrospun Multi-scale Poly(caprolactone) Fibrous Scaffolds for Tissue Engineering," *J. Macromol. Sci. Part A*, vol. 48, no. 1, pp. 21–30, Nov. 2010.
- [13] G. Voskerician, P. H. Gingras, and J. M. Anderson, "Macroporous condensed poly(tetrafluoroethylene). I. In vivo inflammatory response and healing characteristics.," *J. Biomed. Mater. Res. A*, vol. 76, no. 2, pp. 234–242, Feb. 2006.
- [14] J. N. Barbosa, I. F. Amaral, A. P. Águas, and M. A. Barbosa, "Evaluation of the effect of the degree of acetylation on the inflammatory response to 3D porous chitosan scaffolds," *J. Biomed. Mater. Res. Part A*, vol. 93A, no. 1, pp. 20–28, Apr. 2010.

CHAPTER 4

Materials and methods

4.1: Titanium alloy [1]

Titanium and its alloys have been widely used as biomaterials for bone implants due to their mechanical properties. Pure titanium is used as dental substitute while Ti6Al4V and Ti6Al7Nb are used for hip and knee replacement because of their higher mechanical properties and reduced density.

Generally, titanium alloys have Young's modulus more similar to the bone rather than other alloys. This and good biocompatibility, high mechanical and corrosion resistance make titanium alloys useful materials for health applications. Titanium's ability to react with oxygen creates a layer of TiO_2 that improve corrosion resistance and lead to a biocompatible material.

The crystal structure of titanium at ambient temperature and pressure is close-packed hexagonal (α). At about 890°C , the titanium undergoes an allotropic transformation to a body-centred cubic (β) phase which remains stable to the melting temperature (1670°C). Introduction of interstitial atoms in the structure leads to stabilization of α or β phases. Aluminium in particular stabilizes the α phase while vanadium stabilizes the β phase. In this thesis were used disk samples of 10 mm diameter of Ti6Al4V, an alloy that contains 6% in weight of Aluminium and 4% in weight of Vanadium. (the elements of Ti6Al4V are shown in Table 4.1).

Element	Aluminium	Vanadium	Iron	Oxygen	Nitrogen	Hydrogen	Carbon
Weight %	5.5 – 6.75	3.5 – 4.5	0 – 0.4	0 – 0.2	0 – 0.05	0 – 0.015	0 – 0.1

Table 4.1: Weight % of Ti6Al4V alloy elements

Ti6Al4V minimum yield strength vary from 760 to 895 MPa depending on processing, heat treatment, section size and chemistry. Table 4.2 reports a comparison between the mechanical properties of Ti6Al4V and of stainless steel and cortical bone.

Ti6Al4V is an alloy with relatively low electrical conductivity or high resistivity compared to other metals. This alloy has also excellent corrosion resistance due primarily to oxide-film formation. At low temperatures, a thin protective oxide film is present in normal atmospheric environments. When penetrated or broken, the oxide layer is quickly reformed, influencing surface treatments performed.

Ti6Al4V is highly resistant to natural environments and to many aqueous chemicals up to at least their boiling temperatures. It is resistant to general corrosion by sea water and brine, oxidizing acids, aqueous chloride solutions, wet chlorine gas and sodium hypochlorite at typical product-operating temperatures. It is, however, vulnerable to reducing acids such as hydrofluoric, hydrochloric, sulfuric, oxalic, formic and phosphoric acids.

Material	Density [g/cm ³]	Young's modulus [GPa]	Shear modulus [GPa]	Poisson's ratio
Cortical bone [2]	-	18	6	0.41
Ti6Al4V	4.428	105 – 116	41 – 45	0.26 – 0.36
Stainless steel	7.916	190 – 215	74 – 83	0.27 – 0.3

Table 4.2: mechanical properties of Ti6Al4V compared to cortical bone and stainless steel

4.2: Preparation of titanium samples

In order to use chitosan as a coating for bone implants, the polymer needs to be firmly bound to the implant surface in order to withstand the mechanical forces associated with implant placement and to secure the implant in place during osseointegration. To improve the attachment of the chitin to the surface, each titanium sample is mirror polished with a polishing machine as in Figure 4.1. Once the degree of the abrasive grip is selected and fitted in the machine, the sample is polished by contact with the rotating grip. The speed of the grip can be selected by the operator. To correctly polish the sample, this procedure is done under water so the debris produced can be removed from the machine. The degree of polishing is evaluated visually by the operator. At the end of the procedure the samples are as in Figure 4.2.



Figure 4.1: polishing machine

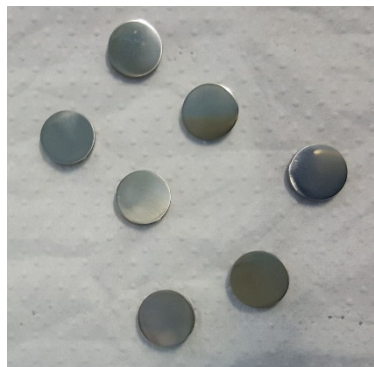


Figure 4.2: polished samples

Samples are ultrasonically cleaned in acetone for five minutes, then in deionized water two times for ten minutes.

The next step is the oxidation of the surface with an acid treatment. Samples are immersed for a minute in hydrofluoric acid, then for two in hydrochloric acid and for two hours in a solution of hydrogen peroxide at 60 °C. The oxidation results in a nanoporous layer with violet or green colour as can be seen in Figure 4.3.

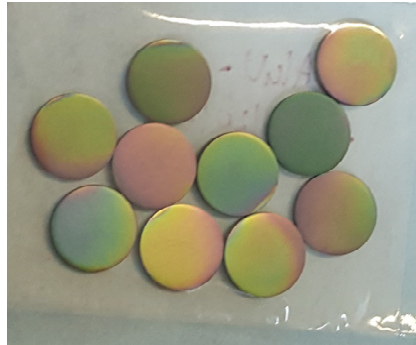


Figure 4.3: oxidised samples

4.3: Procedures for attachment of chitin derivatives to titanium

Chitosan was provided as a powder by Genis hf (Reykjavik, Iceland) and is shown in Figure 4.4. The deacetylation degree is 50%. This chitosan also has swelling properties as can be seen in Figure 4.5.

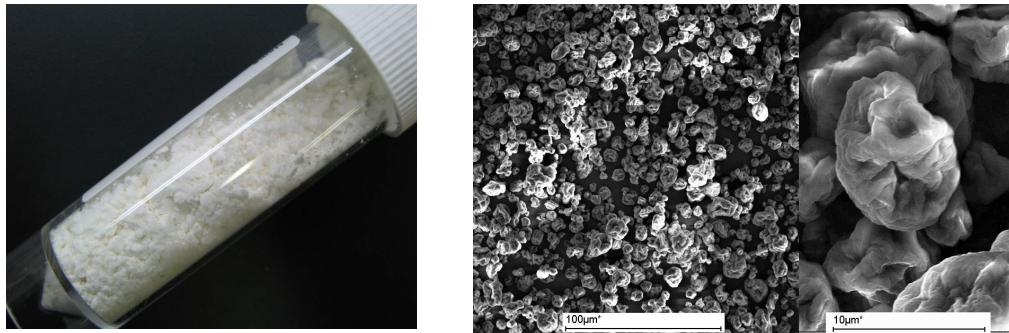


Figure 4.4: Genis chitosan

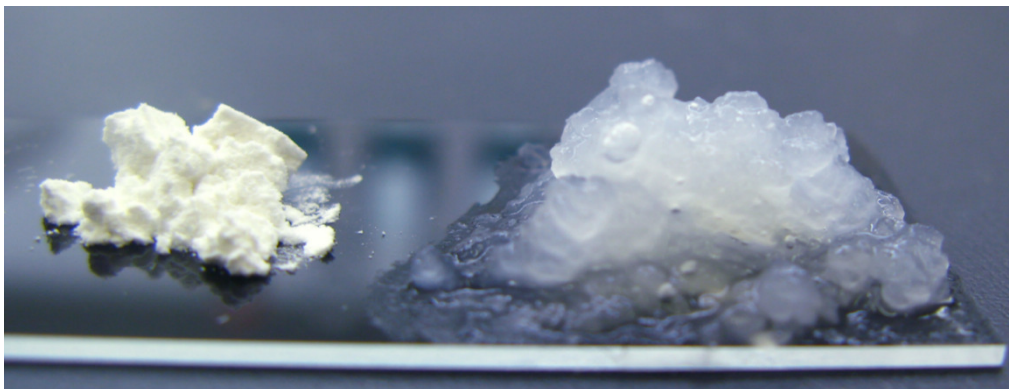


Figure 4.5: swelling properties of Genis chitosan

Since chitin derivatives possess a non-reducing and a reducing end, the grafting to a surface can occur by covalently linking OH groups to the surface or either of the non-reducing or reducing terminus. In case of the OH linkages, the polymer molecules might tend to be attached to the surface by multiple linkages while grafting the terminus will only produce one linkage per molecule. In order to facilitate grafting and have a better control over the density of grafting points on the substrates it can be used a good leaving group (tresyl chloride) or a coupling agent (polydopamine) which are able to react with the reducing end of the polymer.

4.3.1. Physical attachment of chitin derivatives to titanium surface

Two procedures were used in this type of attachment, the first dissolving chitin derivatives into acetic acid and the second using a PBS (phosphate buffered saline) solution.

In the first procedure chitosan was dissolved into a solution of acetic acid and deionized water. It was used a solution 1% w/v of chitosan in 1% acetic acid. The sample was immersed into the solution for five minutes and then dried overnight at room temperature in air. After this, the sample was neutralized into a solution of 0.25M NaOH (sodium hydroxide - molecular weight 40 g/mol) for half an hour and then washed with deionized water. Equation 4.1 indicates the weight of sodium hydroxide used for a solution of 500 ml.

$$w[g] = M \left[\frac{mol}{l} \right] * MW \left[\frac{g}{mol} \right] * V[l] = 0.25 * 40 * 0.5 = 5g$$

Equation 4.1: weight of NaOH for neutralization

The sample changes its coating as shown in Figure 4.6.

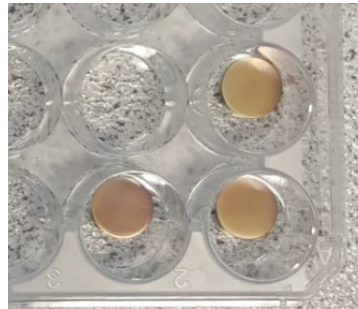


Figure 4.6: coated samples

In the second procedure a phosphate buffered saline solution was made by adding 137 mM sodium chloride (NaCl), 2.7 mM potassium chloride (KCl), 10 mM disodium hydrogen phosphate ($\text{Na}_2\text{HPO}_4 \cdot 2\text{H}_2\text{O}$) and 1.8 mM potassium dihydrogen phosphate (KH_2PO_4) to distilled water, obtaining a solution with pH of 7.32. Equations 4.2 show the weights of the PBS components for 500 ml.

0.5 % w/v of chitosan was added into the PBS solution and left overnight in a magnetic stirrer as in Figure 4.7 to allow the dissolution. At this pH the 50% DD chitosan went into suspension. The samples were immersed in the suspension for 1, 3 or 5 minutes and then dried. Different times of immersion were used because after 1 minute the coating was not well attached. It seemed that the chitosan required more time to be attached. The samples obtained are in Figure 4.8.

$$w[g] = M \left[\frac{\text{mol}}{l} \right] * MW \left[\frac{g}{\text{mol}} \right] * V[l] = 0.137 * 58.4 * 0.5 = 4g \text{ of NaCl}$$

$$w[g] = M \left[\frac{\text{mol}}{l} \right] * MW \left[\frac{g}{\text{mol}} \right] * V[l] = 0.0027 * 74.55 * 0.5 = 0.1g \text{ of KCl}$$

$$w[g] = M \left[\frac{\text{mol}}{l} \right] * MW \left[\frac{g}{\text{mol}} \right] * V[l] = 0.01 * 177.99 * 0.5 = 0.89g \text{ of Na}_2\text{HPO}_4 \cdot 2\text{H}_2\text{O}$$

$$w[g] = M \left[\frac{\text{mol}}{l} \right] * MW \left[\frac{g}{\text{mol}} \right] * V[l] = 0.0018 * 186.08 * 0.5 = 0.12g \text{ of KH}_2\text{PO}_4$$

Equations 4.2: weights of PBS solution components

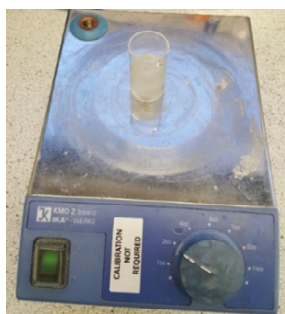


Figure 4.7: magnetic stirrer to suspend chitosan into PBS

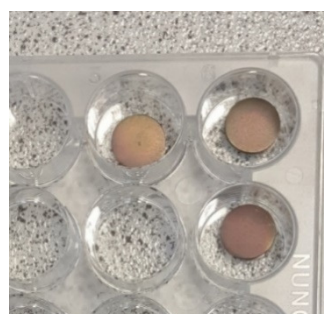


Figure 4.8: coated samples

4.3.2. Attachment of chitin derivatives to activated titanium surface using a good leaving group (Tresyl Chloride)

2,2,2-Trifluoroethanesulfonyl chloride ($\text{CF}_3\text{CH}_2\text{SO}_2\text{Cl}$), also known as tresyl chloride (Figure 4.9), is the most used sulfonyl chloride and is able to convert alcohols into the corresponding sulfonyl esters for the activation of inorganic supports [3].

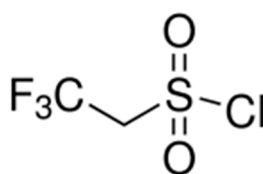


Figure 4.9: 2,2,2-trifluoroethanesulfonyl chloride - Tresyl chloride

Tresyl Chloride was directly dropped in a liquid form onto the titanium surface without other solvents and stored at 37°C for 2 days to allow the activation. A possible scheme of the reaction is shown in Figure 4.10: tresyl chloride reacts with the basic terminal OH on the titanium surface to form a Ti-O-S bond [4], [5] and then leaves the sample to allow the adhesion of chitosan.

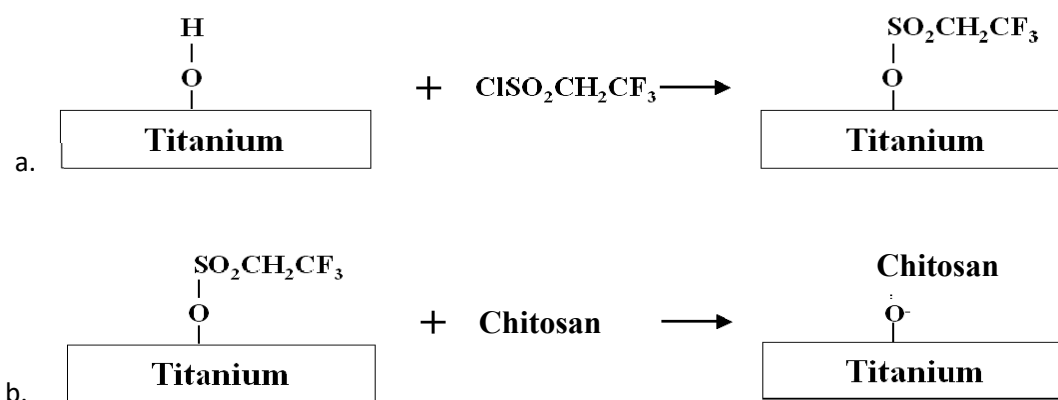


Figure 4.10: possible technique of tresyl chloride activation (a) and immobilization of chitosan (b) as reported in Ref. [4], tresyl chloride leaves the surface to allow the bonding with chitosan

After two days the samples were washed with deionized water, water:acetone (50:50) and acetone and dried [4]. This treatment stopped the exposure of OH operated by tresyl chloride in the titanium surface.

In order to coat the samples with chitosan the same solution of PBS prepared for the first method was used here. Titanium was immersed into the solution and left for 24 hours at 37°C in incubator (Figure 2.11) to allow the reaction. After the coating the tresyl chloride should be totally removed from the surface because is a leaving group that is useful only for a better activation of the sample.



Figure 4.11: incubator

The same procedure was made with samples at room temperature to confront the reaction conditions.

After the activation with tresyl chloride, the samples show a change in the brightness as in Figure 4.12a. Figure 4.13 shows a scheme of the procedure used for the coating to obtain the samples as in Figure 4.12b [6].

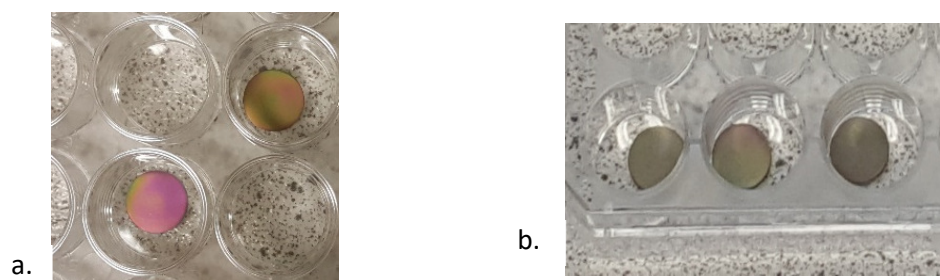


Figure 4.12: a. Tresyl chloride activated samples; b. Tresyl chloride activated samples coated with chitosan

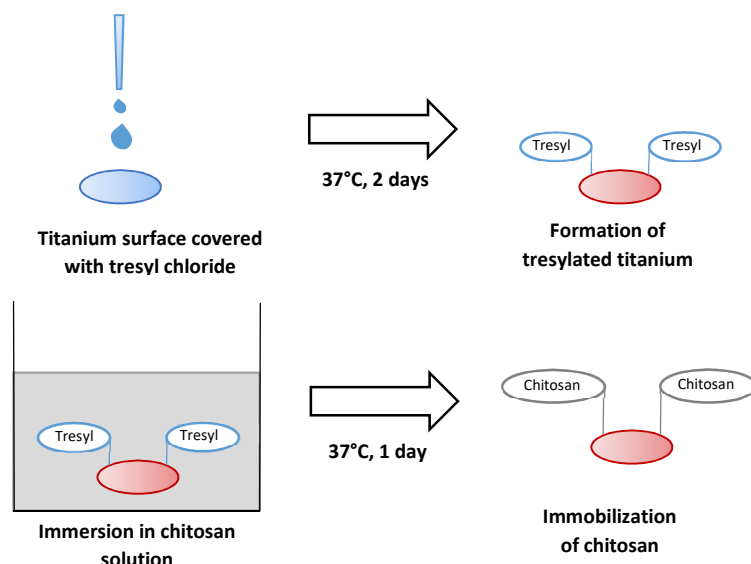


Figure 4.13: procedure of chitosan immobilization by using Tresyl chloride activation method. Adapted and reproduced from Ref. [6]

4.3.3. Attachment of chitin derivatives to activated titanium surface with a coupling agent (Polydopamine)

In order to attach the chitosan to the titanium surface here was used a coupling agent, a compound that provides a chemical bond between two different materials. Polydopamine (PDA) was introduced as coupling agent by Messersmith's study of a mussel-inspired surface functionalization technique [7]. PDA exhibits high reactivity towards biomolecules containing amine and thiol functional groups [8]. A possible scheme of the activation and coating with polydopamine and chitosan is shown in Figure 4.14 [9].

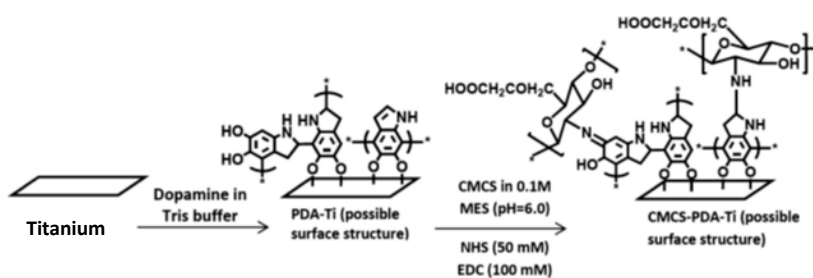


Figure 4.14: possible activation and coating with polydopamine as reported from Ref. [9]

The PDA is spontaneously formed by pH-induced, oxidative polymerization of dopamine-hydrochloride in alkaline solutions ($\text{pH} > 7.5$). Here were dissolved 2 mg/ml of dopamine hydrochloride into a 10 mM Tris solution. Figure 4.15 shows the molecular structure of Tris and Equation 4.3 its weight for a solution of 100 ml. Since the pH of the solution was 9.67, it was adjusted to 8.52 with HCl [8] to allow the dopamine reaction into polydopamine.

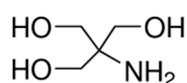


Figure 4.15: Tris(hydroxymethyl)aminomethane; 2-Amino-2-(hydroxymethyl)-1,3-propanediol

$$w[g] = M \left[\frac{\text{mol}}{l} \right] * MW \left[\frac{g}{\text{mol}} \right] * V[l] = 0.01 * 121.14 * 0.1 = 0.121g \text{ of Tris buffer}$$

Equation 4.3: weight of Tris

The samples were soaked into the Tris solution for four hours with continuous shaking as in Figure 4.16, rinsed with deionised water and dried at room temperature to obtain the samples in Figure 4.17.

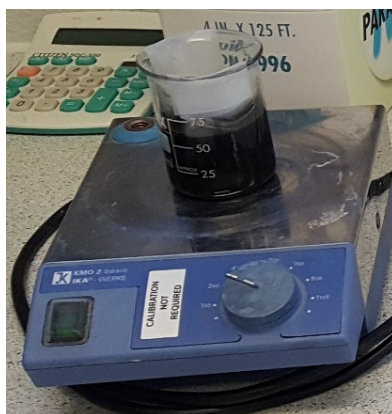


Figure 4.16: magnetic stirrer for the polydopamine activation

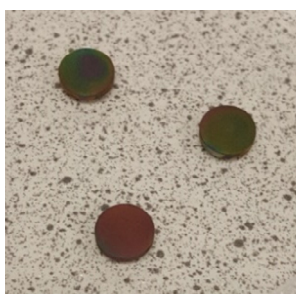


Figure 4.17: polydopamine samples

Different methods were used to attach the chitosan to find the best one in terms of time and difficulty of procedure.

In the first 0.5 % w/v chitosan was dispersed into distilled water and the samples were left into it for 24 hours at room temperature with stirring [10]. Samples as in Figure 4.18 are obtained.



Figure 4.18: chitosan coated sample

Another method used was to make a suspension of 0.5% w/v chitosan into PBS solution and leave the titanium immersed into it for four hours with stirring [11].

It was also tried a MES buffer solution dispersing 1% chitosan into distilled water and then adding 0.1 M MES, 50 mM NHS and 100 mM EDC [9] with weights shown in Equations 4.4 for a solution of 50 ml. Samples were left four hours into the solution and then neutralized into NaOH.

$$w[g] = M \left[\frac{\text{mol}}{l} \right] * MW \left[\frac{g}{\text{mol}} \right] * V[l] = 0.1 * 213.25 * 0.05 = 1.06g \text{ of MES}$$

$$w[g] = M \left[\frac{\text{mol}}{l} \right] * MW \left[\frac{g}{\text{mol}} \right] * V[l] = 0.05 * 115.09 * 0.05 = 0.2877g \text{ of NHS}$$

$$w[g] = M \left[\frac{\text{mol}}{l} \right] * MW \left[\frac{g}{\text{mol}} \right] * V[l] = 0.1 * 191.7 * 0.05 = 0.958g \text{ of EDC}$$

Equation 4.4: weights of MES solution components

EDC reacts with carboxylic acid groups to form an active ester intermediate which in turn is easily displaced by nucleophilic attack from primary amino groups in the reaction mixture. The primary amine forms an amide bond with the original carboxyl group and an EDC by-product is released as a soluble urea derivative. NHS esters are reactive groups formed by carbodiimide-activation of carboxylate molecules. NHS ester-activated cross-linkers and labelling compounds react with primary amines to yield stable amide bonds [12]. Figure 4.19 shows the structures of these components.

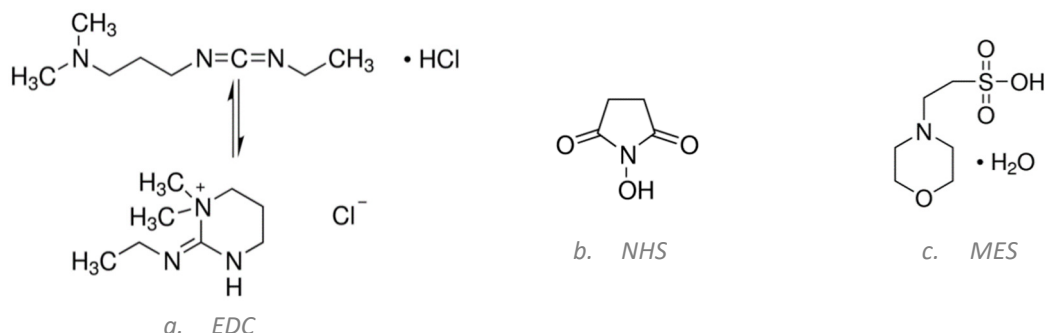


Figure 4.19: molecular structures of MES solution components

4.4: FTIR Spectroscopy

Fourier Transform Infrared Spectroscopy shows the functional groups present on the surface analysed in a spectrum. When a material is exposed to an infrared radiation, this last can be absorbed or transmitted. A detector captures this radiation scattered and, with an analysis via Fourier transform, generates a spectrum. Fourier transform is a mathematical function that transforms time dependent data into frequency dependant data. This spectrum represents the intensity of molecular vibrations of the bonds of functional groups in the material allowing their recognition. This is possible because bond vibrate at particular frequencies depending on the mass of the atoms, the strength of the bonds and the environment around the molecule.

The most important part of a FTIR spectrometer is the interferometer. A device that split the beam into two parts allowing an interference in the detector due to their recombination.

The measurements were done using Nicolet iN10 MX produced by Thermo Scientific.

Samples of each method were analysed to confront the intensities of the transmission and to make qualitative considerations on the coatings. In particular, regarding the physical attachment with chitosan in acetic acid, three different samples were analysed to verify differences between samples of the same procedure. A sample from this method was then confronted with a sample made with chitosan suspended in PBS to evaluate the two procedures. Tressylated samples with and without

chitosan at room temperature are confronted with the ones at 37°C. In the procedure with polydopamine it was analysed a sample without chitosan with a sample coated with chitosan for each method used. In the end a confrontation between the best method for each procedure can be useful to evaluate the intensity of the different types of coatings.

4.5: Atomic Force Microscopy [13]

The atomic force microscope uses the intermolecular forces measurements to obtain an image of the surface scanned by the probe. The probe consists of a cantilever with a sharp tip on a piezoelectric actuator. The cantilever is controlled by a laser sensitive photodetector to provide a feedback on the position. The analysis can be conducted keeping the force constant or keeping the tip at constant distance from the surface. Scanning can be performed in contact, non-contact or tapping mode. Non-contact mode allows the extraction of topographical information moving the cantilever away from the surface and oscillating it at the natural resonance frequency. The contact mode analyses the surface properties keeping the tip in contact with the sample during scanning. Tapping mode is a combination of the two other modes with the oscillation of the tip and the contact for short amount of time of the tip to the surface.

The microscope used was a PSIA-XE10 (Figure 4.20) and the analysis was conducted in non-contact mode. The software Gwyddion (<http://gwyddion.net/>) was used to extract information and values from the topographical images obtained. Samples were analysed selecting scan areas of 1 and 5 µm and the roughness obtained with Equations 4.5. Since the nanoporous structure is coated the roughness is expected to decrease after the coating.

$$S_a = \frac{1}{N} \sum_{j=1}^N |s_j| \quad S_q = \sqrt{\frac{1}{N} \sum_{j=1}^N s_j^2}$$

Equations 4.5: surface average roughness (Sa) and surface root mean square roughness (Sq)

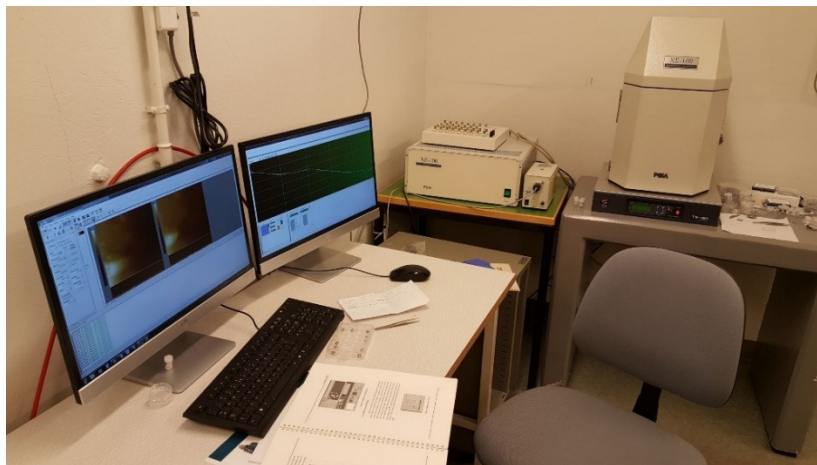


Figure 4.20: PSIA XE-10 Atomic Force Microscope

The first sample analysed was the oxidized titanium without chitosan coating to verify the level of roughness of this basis substrate. For the physical attachment procedure were analysed both the chitosan dissolved in acetic acid and the chitosan suspended in PBS methods. Samples activated with tresyl chloride at 37°C and room temperature with and without chitosan coating were analysed next.

Regarding the polydopamine activation was analysed a sample without chitosan to verify the roughness of the polydopamine layer and samples with chitosan dispersed in water and suspended in PBS. The polydopamine activated sample with chitosan dissolved in the MES buffer was not further investigated due to difficulty of the procedure and FTIR results shown in Chapter 5 in this thesis.

4.6: Scanning Electron Microscopy

The scanning electron microscope is used to obtain the morphology of the surface with a focused electronic beam that scans the sample. The beam of electrons interacts with the sample and generate secondary electrons, backscattered electrons and X-rays. The X-rays generated do not cause damage to the sample and allow chemical analysis. In order to detect organic compounds in the surface the samples were analysed with a beam of 5 kV. To have a better electronic conduction the samples were covered with gold in vacuum atmosphere for two minutes (Figure 4.21a) and then scanned with the microscope shown in Figure 4.21b (Gemini, Zeiss).

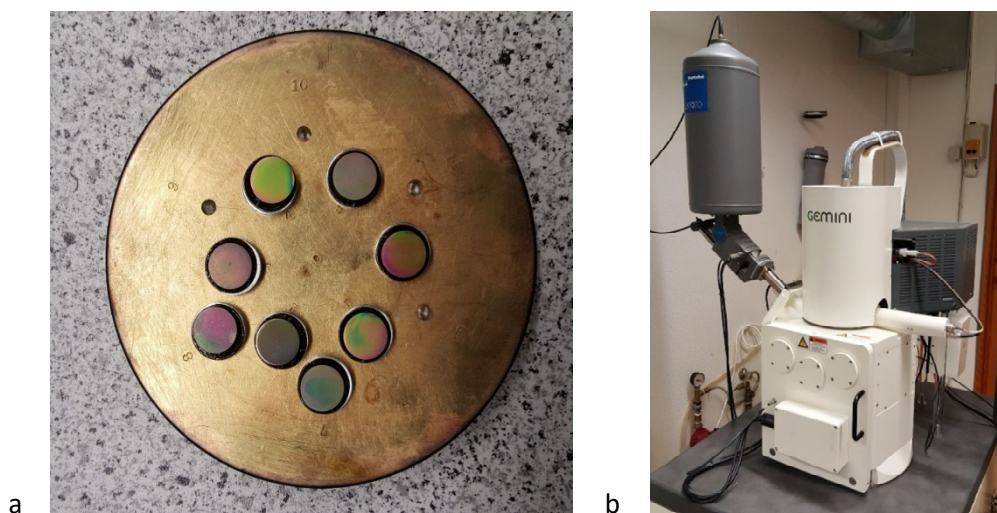


Figure 4.21: a. gold coated samples, b. Zeiss Gemini scanning electron microscope

After importing the image in ImageJ, setting the threshold values needed, the software can identify differences in the colour of each pixel to distinguish the area coated with the one uncoated as shown in Figure 4.22. Based on these differences it can be found the percentage of area coated in the image to make assumptions on the efficacy of the coating.

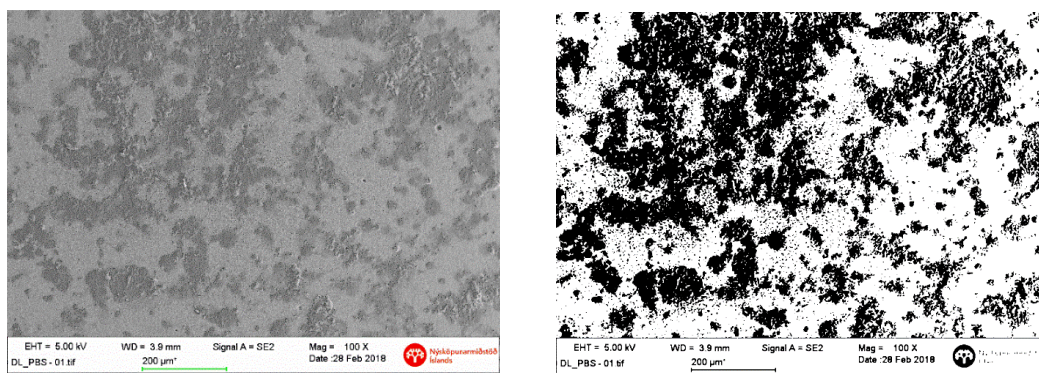


Figure 4.22: ImageJ automatic threshold analysis

The first sample analysed was the oxidised titanium to investigate the nanoporous layer after the acid treatment. Regarding the samples coated with chitosan were analysed samples coated with chitosan dissolved in acetic acid and suspended in PBS, samples activated with tresyl chloride at 37°C and at room temperature with and without chitosan suspended in PBS, polydopamine activated samples and polydopamine activated samples with chitosan suspended in PBS and dispersed in deionized water. Coated samples stored for two weeks in PBS at 37°C were also analysed (chitosan dissolved in acetic acid, tresyl chloride activated sample with chitosan suspended in PBS and polydopamine sample with chitosan dispersed in deionized water).

4.7: Zeta potential [14]

Zeta potential analyses the charge of a solid surface when exposed to aqueous solution. The solid surface interaction with a liquid lead to a different distribution of charge in the liquid at the interface. The surface charge generates a change in potential that is related to the distance from the surface itself, being lower with the increase in distance as illustrated in Figure 4.23. The shear plane is the boundary that indicates the slipping of the moving liquid phase compared to the stationary liquid phase during the measurement.

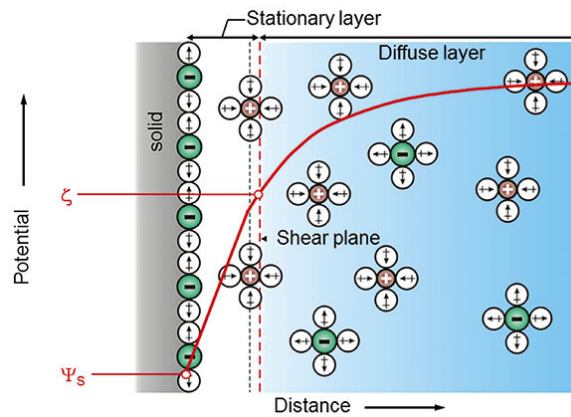


Figure 4.23: surface charge at the solid-liquid interface

The surface charge at the interface solid-liquid depends on acid-base reactions and water ions adsorption. The functional groups present on the surface are responsible for the positive or negative charge of the interface as illustrated in Figure 4.24. Quantity of functional groups and pH influence the equilibrium of potential.

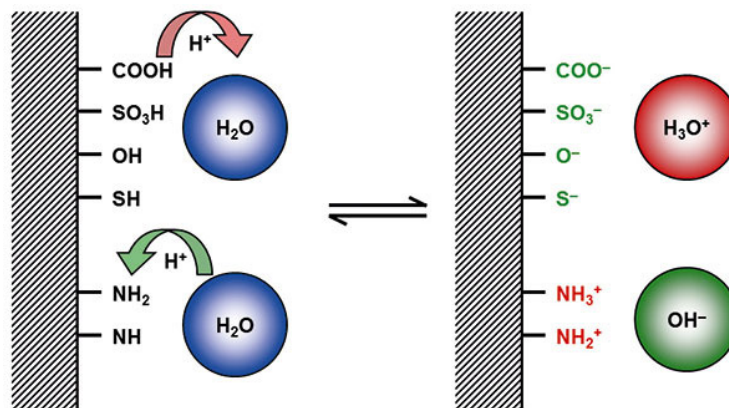


Figure 4.24: scheme of interfacial charges for different functional groups

The measure of a potential involves the determination of an electrokinetic effect due to relative movements between two phases. For samples with flat surfaces, the zeta potential is obtained with the tangential streaming potential. In this case two samples are mounted on the device with the planar surfaces opposite and a stream of electrolyte solution passes through the channel tangentially as illustrated in Figure 4.25.

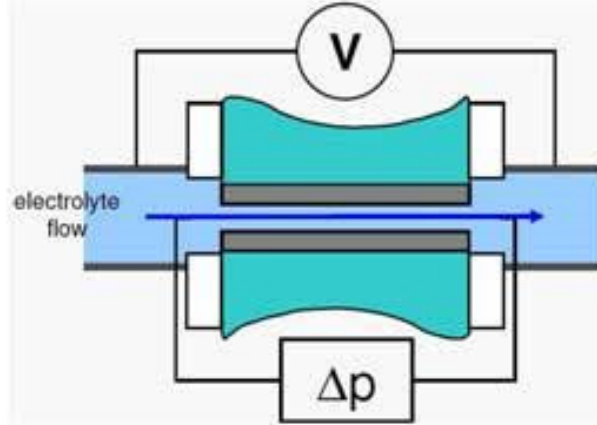


Figure 4.25: tangential streaming potential

Since the samples have a planar solid surface, the zeta potential can accurately be calculated with Equation 4.6 of Helmholtz-Smoluchowski where $dI_{str}/d\Delta p$ is the streaming current coefficient, L/A represents the gap between the two solid samples, η and $\epsilon \times \epsilon_0$ are the viscosity and dielectric coefficient of the electrolyte solution. This measure is affected by the contribution of the solid sample to surface conductance, electrical conductance and ionic conductance. In the case analysed here, in presence of a layer capable of swelling, ionic conductance derives from ions permeating the swollen layer and depends on the ionic strength of the electrolyte solution and pH. This leads to underestimated values.

$$\zeta = \frac{dI_{str}}{d\Delta p} \times \frac{\eta}{\epsilon \times \epsilon_0} \times \frac{L}{A}$$

Equation 4.6: equation of Helmholtz-Smoluchowski

The samples were analysed in a basic solution for samples of polished titanium with chitosan dissolved in acetic acid, oxidised titanium with chitosan dissolved in acetic acid, oxidised titanium activated with tresyl chloride with chitosan suspended in PBS at 37°C and oxidised titanium activated with polydopamine with chitosan dispersed in deionised water.

4.8: Contact angle measurement [15]

Contact angle is an indicator of the wettability of a surface. Two types of measurements can be used to find the contact angle: a drop of water placed on the surface in air as in Figure 4.26a, or a bubble of air in a submerged surface in water as in Figure 4.26b. In this thesis the first method was used. The contact angle is defined by the equation of Young shown in Equation 4.7 where γ represents the interfacial tension and in particular: $\gamma_{s/a}$ the interfacial tension solid-air, $\gamma_{s/l}$ the interfacial tension solid-liquid and $\gamma_{l/a}$ the interfacial tension liquid-air.

$$\gamma_{s/a} = \gamma_{s/l} + \gamma_{l/a} \cos \theta$$

Equation 4.7: equation of Young

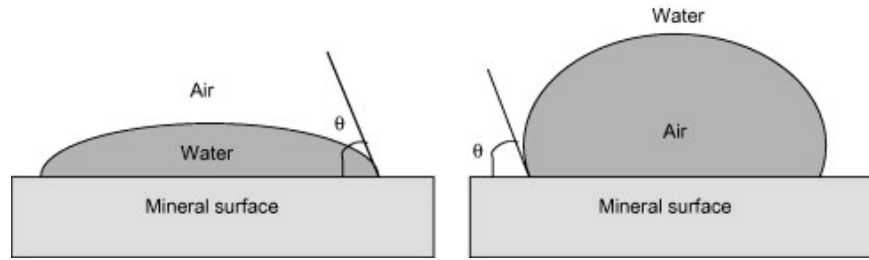


Figure 4.26: a. drop of water in air, b. bubble of air in water

Contact angle is measured using a drop (5 μ l) of ultrapure water at room temperature by direct view of the drop profile using a telescope goniometer. Since the surface of the sample is not perfectly homogeneous, two drops per sample were used when possible. The contact angle was measured for samples of polished titanium coated with chitosan dissolved in acetic acid, oxidised titanium coated with chitosan dissolved in acetic acid, oxidised titanium activated via tresyl chloride with chitosan suspended in PBS at 37°C and oxidised titanium activated via polydopamine with chitosan dispersed in deionized water. For all these samples contact angle was measured also after tape test and z-potential. It was also measured the contact angle of samples stored for two weeks in a PBS solution at 37°C, in particular oxidised titanium with chitosan dissolved in acetic acid, tresyl chloride activated sample with chitosan in PBS at 37°C and polydopamine activated sample with chitosan dispersed in deionized water.

4.9: Tape test [16]

This test is performed to evaluate the adhesion of the coating on the substrate. It's a destructive test that tries to remove the coating using the attachment of the coating to a tape, as shown in Figure 4.27. On the surface to be analysed parallels cut are made a few mm apart to create a grid. Placing the tape in the middle of the grid and removing it after 90 seconds of application lead to the adhesion test results in the form of flaked parts. The percentage of flakes and detached parts lead to a classification of the adhesion as illustrated in Figure 4.28: from samples with a 0% of area removed (5B) to samples with more than 65% of area removed (0B). This test was performed on samples of polished titanium coated with chitosan dissolved in acetic acid, oxidised titanium coated with chitosan in acetic acid and tresyl chloride activated sample with chitosan suspended in PBS at 37°C.

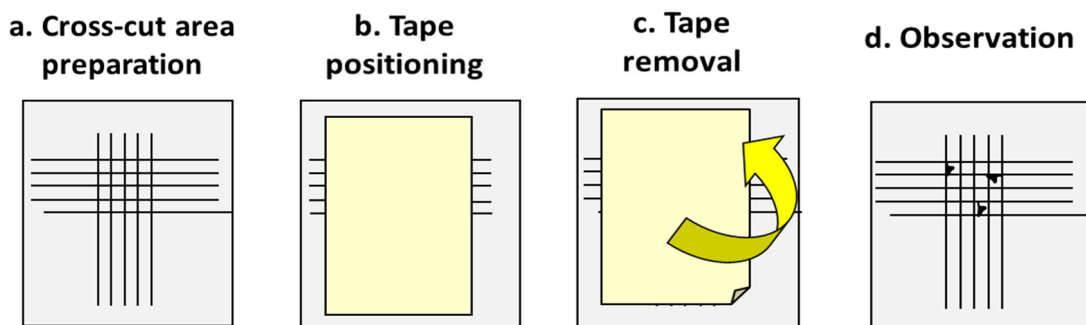


Figure 4.27: Scheme of tape test procedure

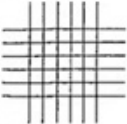
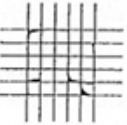


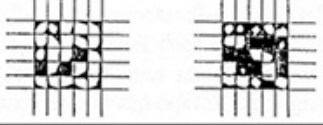
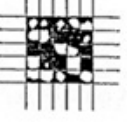
Classification	% of Area Removed	Surface of Cross-cut Area From Which Flaking has Occured for 6 Parrallel Cuts & Adhesion range by %
5B	0% None	
4B	Less than 5%	
3B	5 - 15%	
2B	15 - 35%	
1B	35 - 65%	
0B	Greater than 65%	

Figure 4.28: Classification of adhesion test results

4.10: Bibliography

- [1] R. Boyer, G. Welsch, and E. W. Collings, *Titanium alloys*. ASM International, 1994.
- [2] M. J. Mirzaali *et al.*, "Mechanical properties of cortical bone and their relationships with age, gender, composition and microindentation properties in the elderly," *Bone*, vol. 93, no. 1, pp. 196–211, 2016.
- [3] M. R. Leedy, H. J. Martin, P. A. Norowski, J. A. Jennings, W. O. Haggard, and J. D. Bumgardner, "Use of chitosan as a bioactive implant coating for bone implant applications," in *Advances in Polymer Science: Chitosan for Biomaterials II*, R. Jayakumar, M. Prabakaran, and R. A. A. Muzzarelli, Eds. Springer-Verlag, 2011, pp. 129–165.
- [4] T. Hayakawa and M. Yoshinari, "Fibronectin Immobilization onto Titanium using Tresyl Chloride-activation Technique," *Nano Biomed.*, vol. 1, no. 1, pp. 34–40, 2009.
- [5] P. Zucca and E. Sanjust, "Inorganic materials as supports for covalent enzyme immobilization: methods and mechanisms," *Molecules*, vol. 19, no. 9, pp. 14139–14194, 2014.
- [6] T. Hayakawa, "Biochemical surface modifications to titanium implants using the tresyl chloride activated method," *Dent. Mater. J.*, vol. 34, no. 6, pp. 725–739, 2015.
- [7] H. Lee, S. M. Dellatore, W. M. Miller, and P. B. Messersmith, "Mussel-inspired surface chemistry for multifunctional coatings," *Science*, vol. 318, no. 5849, pp. 426–430, 2007.
- [8] X. Yu, J. Walsh, and M. Wei, "Covalent Immobilization of collagen on titanium through polydopamine coating to improve cellular performances of MC3T3-E1 cells," *RSC Adv.*, vol. 4, no. 14, pp. 7185–7192, 2013.
- [9] D. Zheng, K. G. Neoh, Z. Shi, and E. T. Kang, "Assessment of stability of surface anchors for antibacterial coatings and immobilized growth factors on titanium," *J. Colloid Interface Sci.*, vol. 406, no. 1, pp. 238–246, 2013.
- [10] H. Li *et al.*, "Enhancement of growth and osteogenic differentiation of MC3T3-E1 cells via facile surface functionalization of polylactide membrane with chitooligosaccharide based on polydopamine adhesive coating," *Appl. Surf. Sci.*, vol. 360 Part B, pp. 858–865, 2016.
- [11] J. Liu *et al.*, "Simple and tunable surface coatings via polydopamine for modulating pharmacokinetics, cell uptake and biodistribution of polymeric nanoparticles," *RSC Adv.*, vol. 7, no. 26, pp. 15864–15876, 2017.
- [12] L. Tack, K. Schickle, F. Böke, and H. Fischer, "Immobilization of specific proteins to titanium surface using self-assembled monolayer technique," *Dent. Mater.*, vol. 31, no. 10, pp. 1169–1179, 2015.
- [13] N. Jalili and K. Laxminarayana, "A review of atomic force microscopy imaging systems: Application to molecular metrology and biological sciences," *Mechatronics*, vol. 14, no. 8, pp. 907–945, 2004.
- [14] T. Luxbacher, *The ZETA Guide - Principles of the streaming potential technique*, I. Anton Paar GmbH, 2014.
- [15] T. T. Chau, "A review of techniques for measurement of contact angles and their applicability on mineral surfaces," *Miner. Eng.*, vol. 22, no. 3, pp. 213–219, Feb. 2009.
- [16] "ASTM D3359-17, Standard Methods for Rating Adhesion by Tape Test, ASTM International, West Conshohocken, PA, 2017, www.astm.org."

CHAPTER 5

Results and discussion

It was decided to test different methods of coating in order to screen the best one both in terms of efficacy of attachment and simplicity of the procedure. Three main procedures were applied with different methods to dissolve chitosan.

In the first procedure, chitosan was dissolved in two solutions, acetic acid and PBS, resulting in a physical attachment on the surface. The rationale is that it is well known that chitosan has an isoelectric point in the basic range (pH 6-7 or higher) and it is expected to be positively charged in an acidic solution (acetic acid). On the other side, it was previously tested that the chemically treated Ti used as substrate has a very low isoelectric point (pH 2) and it has a negative charge in acidic environment. A direct graft of positively charged chitosan to a negative charged surface can be expected in a solution of acetic acid. The chitosan used in this research can be also suspended in PBS at pH 7.2-7.4 that is not far from the expected Isoelectric Point of chitosan (depending on deacetylation degree): it is of interest to test the effect of the different surface charge of chitosan on the coating procedure. In PBS the substrate is expected to show deprotonated surface groups that could affect grafting as well. As reference, it was also coated, with chitosan dissolved in acetic acid, a polished Ti sample without the oxidising treatment.

The second procedure involved tresyl chloride for the activation of the substrate as performed by *Hayakawa et al.* and chitosan was suspended in PBS at 37°C (for a higher reactivity of tresyl chloride) or room temperature, as reference and in view of a simpler procedure [1]. Tresyl chloride is used as leaving group only for the activation of the substrate and is removed during the coating of chitosan. Considering that in PBS the electrostatic interaction between the coating and the substrate is expected to be quite low, the use of a leaving group could help to enhance the adhesion of the coating.

In the third procedure, the substrate was coated with polydopamine as discovered by *Messersmith et al.* in his study on mussel-inspired functionalization technique [2]. In this last procedure, chitosan was dispersed in distilled water as used by *Li et al.* to coat polylactide membranes with chitooligosaccharides [3], suspended in PBS as used by *Liu et al.* [4] and dissolved in a MES buffer (pH 5.5–6.7) as used by *Yu et al.* to attach collagen and by *Zheng et al.* to attach chitosan to titanium [5], [6].

Table 5.1 reports the names of the samples used in this chapter explaining the coating method.

Name of samples	Method of coating
MP_DIRECT_AA	Polished titanium coated with chitosan dissolved in acetic acid (physical attachment)
CT_DIRECT_AA	Oxidised titanium coated with chitosan dissolved in acetic acid (physical attachment)
CT_DIRECT_PBS	Oxidised titanium coated with chitosan suspended in PBS (physical attachment)
CT_TRESYL_37	Oxidised titanium activated with tresyl chloride at 37°C
CT_TRESYL_RT	Oxidised titanium activated with tresyl chloride at room temperature
CT_TRESYL_37_PBS	Oxidised titanium activated with tresyl chloride at 37°C coated with chitosan suspended in PBS
CT_TRESYL_RT_PBS	Oxidised titanium activated with tresyl chloride at room temperature coated with chitosan suspended in PBS
CT_POLYDOP	Oxidised titanium activated with polydopamine
CT_POLYDOP_PBS	Oxidised titanium activated with polydopamine and coated with chitosan suspended in PBS
CT_POLYDOP_WATER	Oxidised titanium activated with polydopamine and coated with chitosan dispersed in deionized water
CT_POLYDOP_MES	Oxidised titanium activated with polydopamine and coated with chitosan dissolved in the MES buffer
CT_DIRECT_AA_2WEEKS	Oxidised titanium coated with chitosan dissolved in acetic acid (physical attachment) stored for two weeks in PBS at 37°C in incubator
CT_TRESYL_37_PBS_2WEEKS	Oxidised titanium activated with tresyl chloride at 37°C coated with chitosan suspended in PBS stored for two weeks in PBS at 37°C in incubator
CT_POLYDOP_WATER_2WEEKS	Oxidised titanium activated with polydopamine coated with chitosan dispersed in deionized water stored for two weeks in PBS at 37°C in incubator

Table 5.1: names of analysed samples used in this chapter

Chitosan resulted to be differently soluble in the different solvents used. A detailed description is reported in the chapter “Materials and methods”; in summary, it can be completely dissolved in acetic acid solution, while in PBS a suspension was obtained.

5.1. Fourier Transform Infrared spectroscopy

The first analysis made was controlling the presence of chitosan on the samples with Fourier Transform Infrared Spectroscopy that allows to detect the functional groups on the surface analysed. The data obtained are analysed with the help of Matlab™.

Pure chitosan FTIR spectrum has been largely reported in literature and generally presents the vibrational patterns typically found in most polysaccharides structures [7], [8]. Starting from this literature some peaks are present in all the spectra, in particular the peak at 1653 cm^{-1} due to C=O vibrations from amide, the peak at 1560 cm^{-1} due to bending of amino group, the broad band centred at 3400 cm^{-1} due to axial stretching of OH groups and the sharp peak at 2900 cm^{-1} due to axial deformation of CH_2 from the glucosamine unit structure. The three peaks at $1420\text{-}1320\text{ cm}^{-1}$ are due to CH_3 bending vibrations and the one at 1100 cm^{-1} to C-O. At 945 cm^{-1} the small peak is due to C-O-C stretching and is typical of polysaccharides. These results are evident in Figures 5.1, 5.2, 5.3, 5.4 and 5.5 and the data are reported in Table 5.2, 5.3 and 5.4. The intensity of OH groups depends also on the activated substrate of titanium that is oxidised. It must be considered that the instrument requires an oxidised sample without coating as background and makes a subtraction of the spectrum of the substrate. This can lead to unpredictable errors in the spectra.

Since the FTIR involves the transmittance of functional groups, the environment can influence the results because it is not carried out under vacuum conditions. This is reflected in the presence of small and sharp peaks derived from CO_2 around $2500\text{-}2300\text{ cm}^{-1}$ that depend on air interference and are not properly compensated.

5.1.1. Physical attachment coating

Figure 5.1 shows that every sample produces different peaks with different intensity due to the analysis of single points: this analysis is not the average of a wide area and it has a qualitative meaning referred to the significant modification of the coating.

All the peaks expected are present in samples with chitosan dissolved in acetic acid physically attached to the substrate. This is also shown in Table 5.2 with the indication of intensity and type of each peak.

Wavenumber (cm^{-1})	Type of peak	Intensity	Description
3400-3300	Broad	High	O-H of carboxylic acids
2900	Sharp	High	CH_2
2500-2300	Sine curve	High	NH_3^+
1650	Sharp	High	Conjugated C=O of carboxylic acids
1560	Sharp	High	NH
1420-1320	Three sharp peaks	Medium	CH_3
1100	Broad	High	C-O of carboxylic acids
945-900	Two sharp peaks	Medium	C-O-C

Table 5.2: type and intensity of functional groups oscillation obtained via FTIR in CT_DIRECT_AA samples

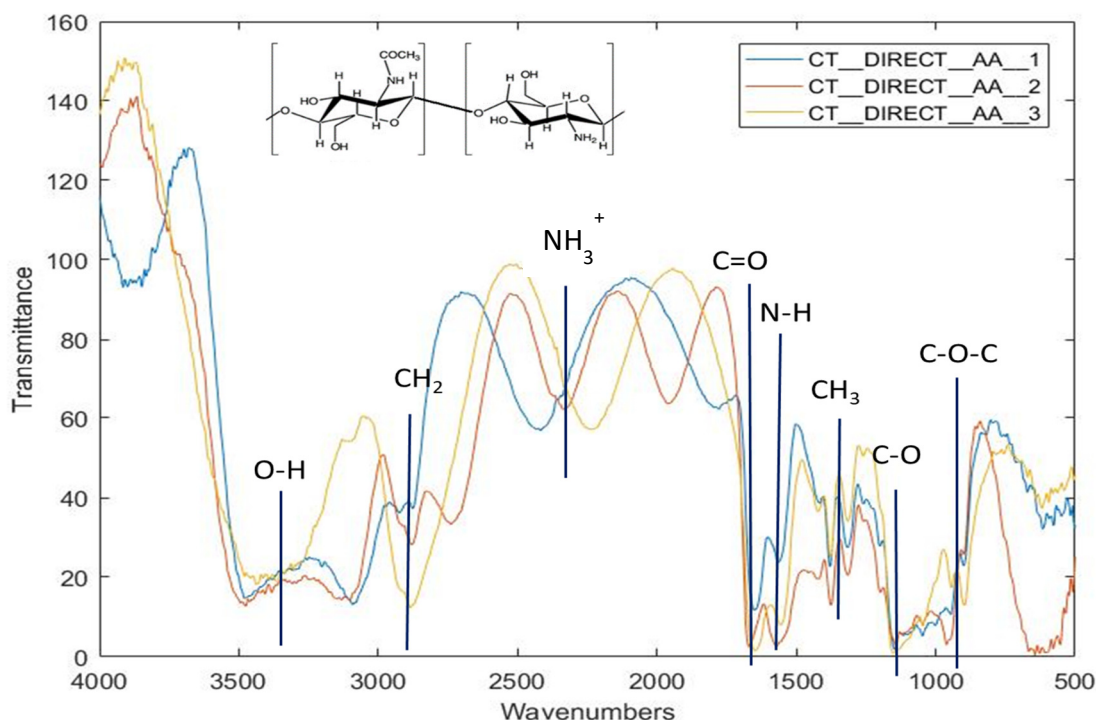


Figure 5.1: FTIR of three samples coated with chitosan dissolved in acetic acid (CT_DIRECT_AA), the OH vibration around 3300 cm^{-1} evidences the presence of errors in the measurements due to background subtraction

Table 5.3 illustrates the wavenumber of the peaks, with the indication of type and intensity, of samples coated with chitosan suspended in PBS physically attached.

Wavenumber (cm^{-1})	Type of peak	Intensity	Description
3400	Broad	Medium	O-H of carboxylic acids
2900	Sharp	Small	CH_2
1650	Sharp	High	Conjugated C=O of carboxylic acids
1560	Sharp	High	NH
1420-1320	Three sharp peaks	Small	CH_3
1100	Broad	High	C-O of carboxylic acids
945-900	Two sharp peaks	Small	C-O-C

Table 5.3: type and intensity of functional groups oscillation obtained via FTIR on CT_DIRECT_PBS samples

In Figure 5.2 FTIR of CT_DIRECT_AA and CT_DIRECT_PBS are compared to verify on a qualitative level the efficacy of the coatings. It emerges that when chitosan is dissolved in acetic acid, the characteristic peaks of chitosan (OH axial stretching, C=O amides and NH bending) are more intense when compared to chitosan suspended in PBS. Moreover, the peak in the range 2000-2500 cm^{-1} is absent in the coating made in PBS solution, while it is well evident in the coating made in acetic acid. This peak (that is affect by internal reflections within the coating when the coating is thick and transparent like in the case of the one made in acetic acid) can be attributed to NH_3^+ functional groups and its presence is related to the zeta potential of the coating made in acetic acid that is quite far from the isoelectric point.

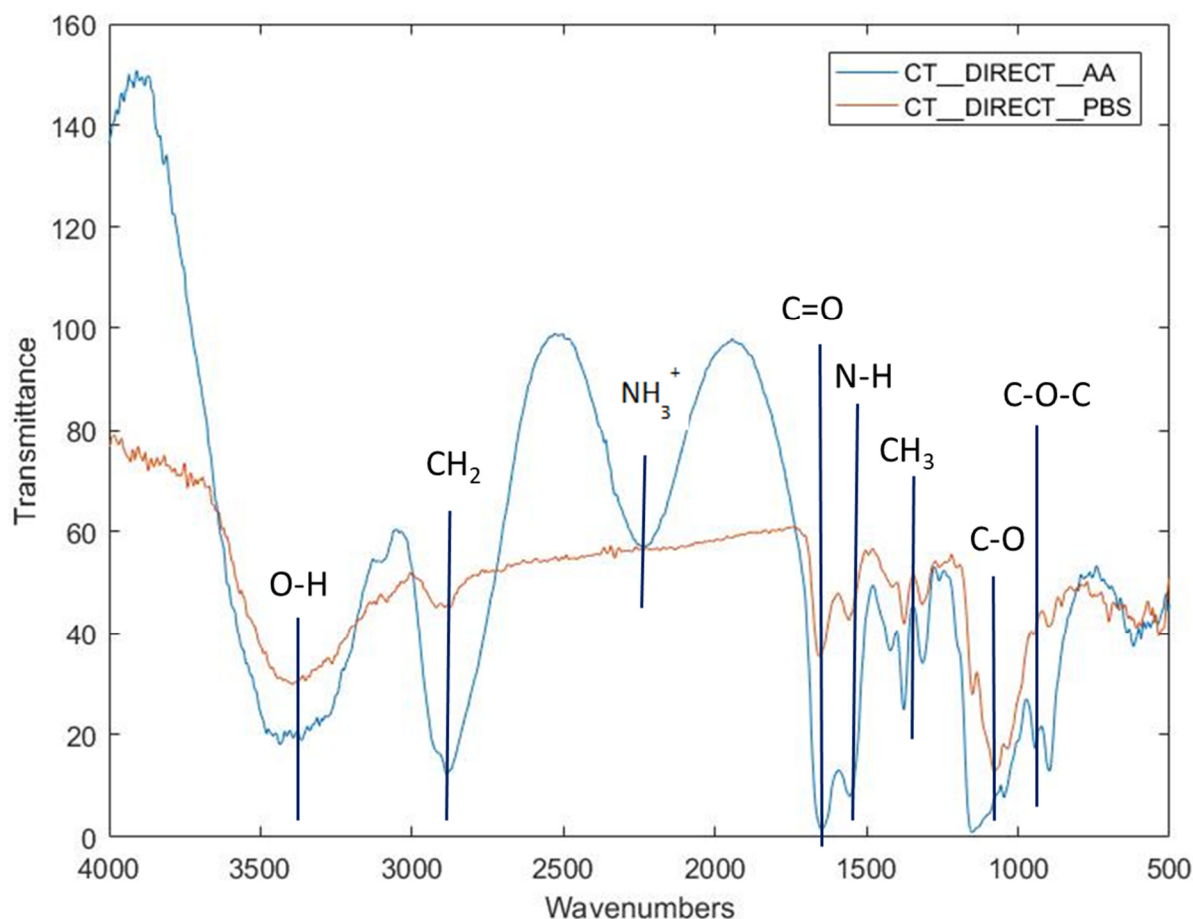


Figure 5.2: FTIR spectra of titanium with chitosan physically attached

5.1.2. Tresyl Chloride activated samples

Analysing the FTIR spectra of samples treated with tresyl chloride (CT_TRESYL_37_PBS and CT_TRESYL_RT_PBS) at 37°C and at room temperature, the difference in the intensities of the peaks is highly evident as shown in Figure 5.3, indicating that the coating was better formed at 37°C. All the expected peaks are found in these samples with different intensities. At this point, due to the analysis conditions of only one spot in the sample, it is early to say if the sample at room temperature is really uncoated as appears from Table 5.4.

Wavenumber (cm ⁻¹)	Type of peak	CT_TRESYL_37_PBS	CT_TRESYL_RT_PBS	Description
3400	Broad	High	Small	O-H of carboxylic acids
2900	Sharp	High	Small	CH ₂
1650	Sharp	High	Small	Conjugated C=O of carboxylic acids
1560	Sharp	High	Small	NH
1375-1310	Three sharp peaks	High	Small	CH ₃
1100	Broad	High	Small	C-O of carboxylic acids
945-900	Two sharp peaks	High	Small	C-O-C

Table 5.4: type and intensity of functional groups obtained via FTIR for samples activated by tresyl chloride and coated with chitosan in PBS at 37°C (CT_TRESYL_37_PBS) or at room temperature (CT_TRESYL_RT_PBS)

From Figure 5.3 also emerges that the activation of the surface with tresyl chloride at 37°C or at room temperature do not produce differences in the spectra of the sample surface before the coating with chitosan.

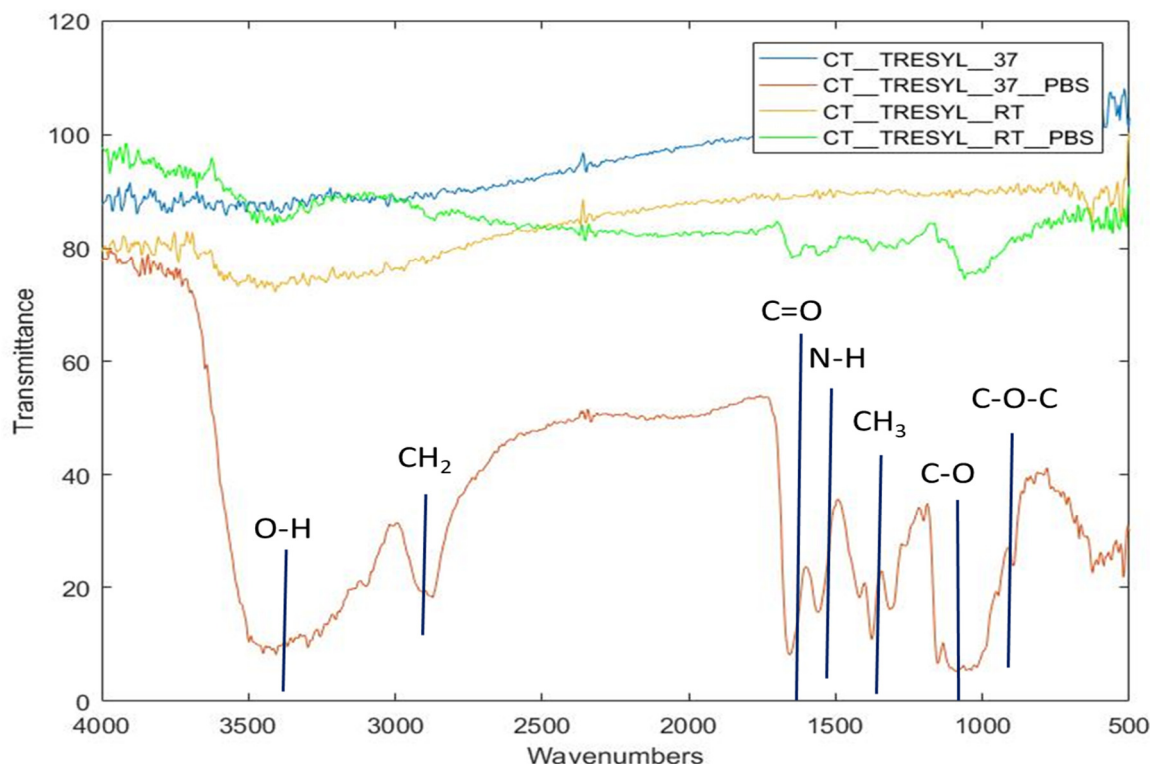


Figure 5.3: FTIR of samples activated with tresyl chloride (CT_TRESYL_37 and CT_TRESYL_RT) and coated with chitosan at 37°C or at room temperature (CT_TRESYL_37_PBS and CT_TRESYL_RT_PBS)

5.1.3. Polydopamine activated samples

The FTIR analysis, in this case, showed with great evidence that the coating with chitosan dissolved in the MES buffer did not work, as visible in Figure 5.4. This can also be due to errors in the measurement, as emerges from the spectrum of CT_POLYDOP, but, according to the spectrum and to the difficulty of the dispersion of chitosan in the MES buffer solution, further analyses on this attachment are not performed. From this spectra, it is also evident that the best coating seems to be the chitosan dispersed in deionized water that produces, on substrates activated by polydopamine, the fundamental peaks expected at medium or high intensities as can be seen in Table 5.5.

Wavenumber (cm ⁻¹)	Type of peak	CT_POLYDOP_PBS	CT_POLYDOP_WATER	Description
3400	Broad	High	High	O-H of carboxylic acids
2900	Sharp	-	High	CH ₂
1650	Sharp	High	Small	Conjugated C=O of carboxylic acids
1560	Sharp	High	Small	NH
1375	Three sharp peaks	-	Medium	CH ₃
1100	Broad	Small	High	C-O of carboxylic acids
945-900	Two sharp peaks	Small	High	C-O-C

Table 5.5: type and intensity of functional groups obtained via FTIR on polydopamine activated samples coated with chitosan

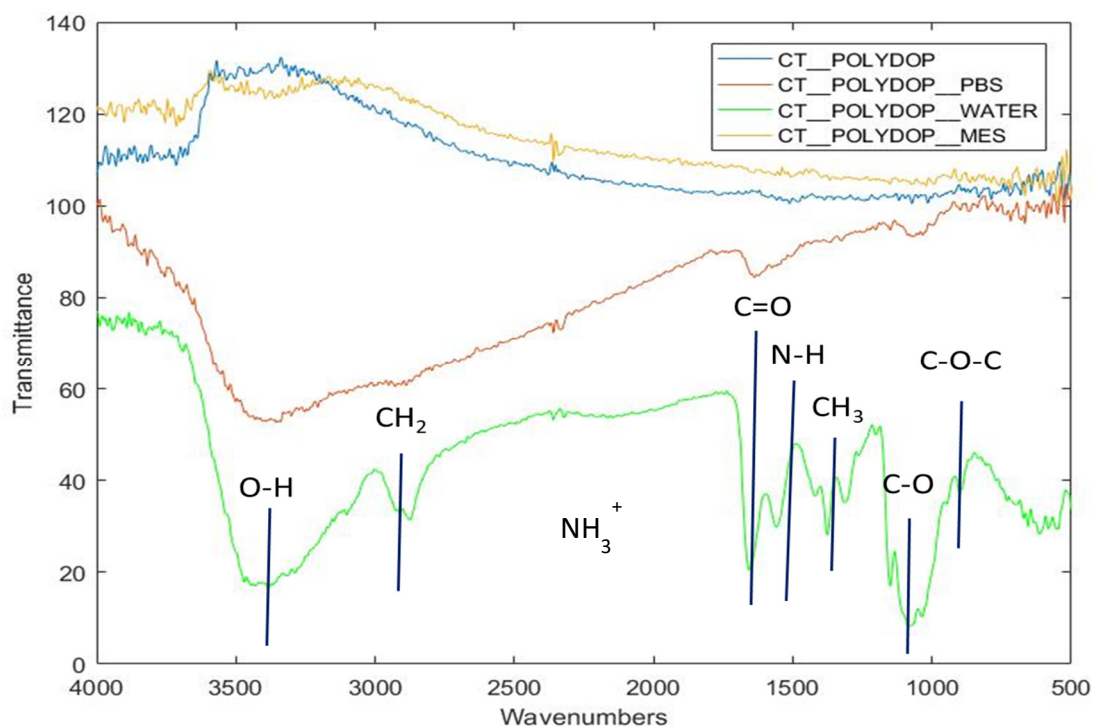


Figure 5.4: FTIR spectra of polydopamine activated samples (CT_POLYDOP) and coated with chitosan (CT_POLYDOP_PBS, CT_POLYDOP_WATER, CT_POLYDOP_MES)

5.1.4. Comparisons between different types of coatings

Selecting the best coating from each method, it can be seen in Figure 5.5 that the most intense peaks due to chitosan presence are obtained with chitosan dissolved in acetic acid physically attached to the surface. It is confirmed the presence of NH_3^+ groups only on the sample made in acetic acid.

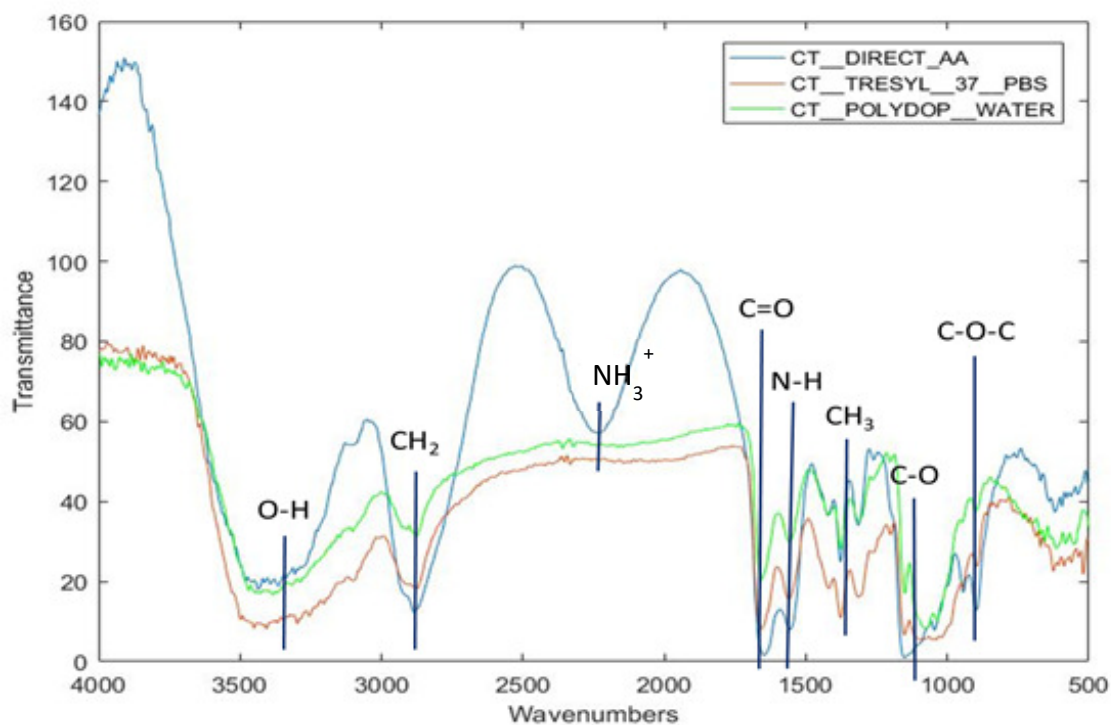


Figure 5.5: FTIR spectra of coated titanium: the spectrum with the most intense peak obtained by each preparation method is reported and compared

5.1.5. FTIR on samples stored in PBS at 37°C for two weeks

The FTIR taken on the samples stored in PBS, which simulates body fluids condition, still shows the presence of chitosan indicating a resistance of the coated samples to dissolution effects at physiologic temperature and pH. The samples stored were prepared by chitosan dissolved in acetic acid and physically attached to oxidised titanium (Figure 5.6), or by chitosan suspended in PBS and attached to oxidised titanium activated with tresyl chloride at 37°C (Figure 5.7) or, as last, by chitosan dispersed in deionised water and attached to oxidised titanium through polydopamine (Figure 5.8). In Figure 5.6 the sharp peak around 2400 cm^{-1} near the sine curve of NH internal reflectance, is due to a low compensation of CO_2 . CO_2 low compensation is also visible in Figure 5.7.

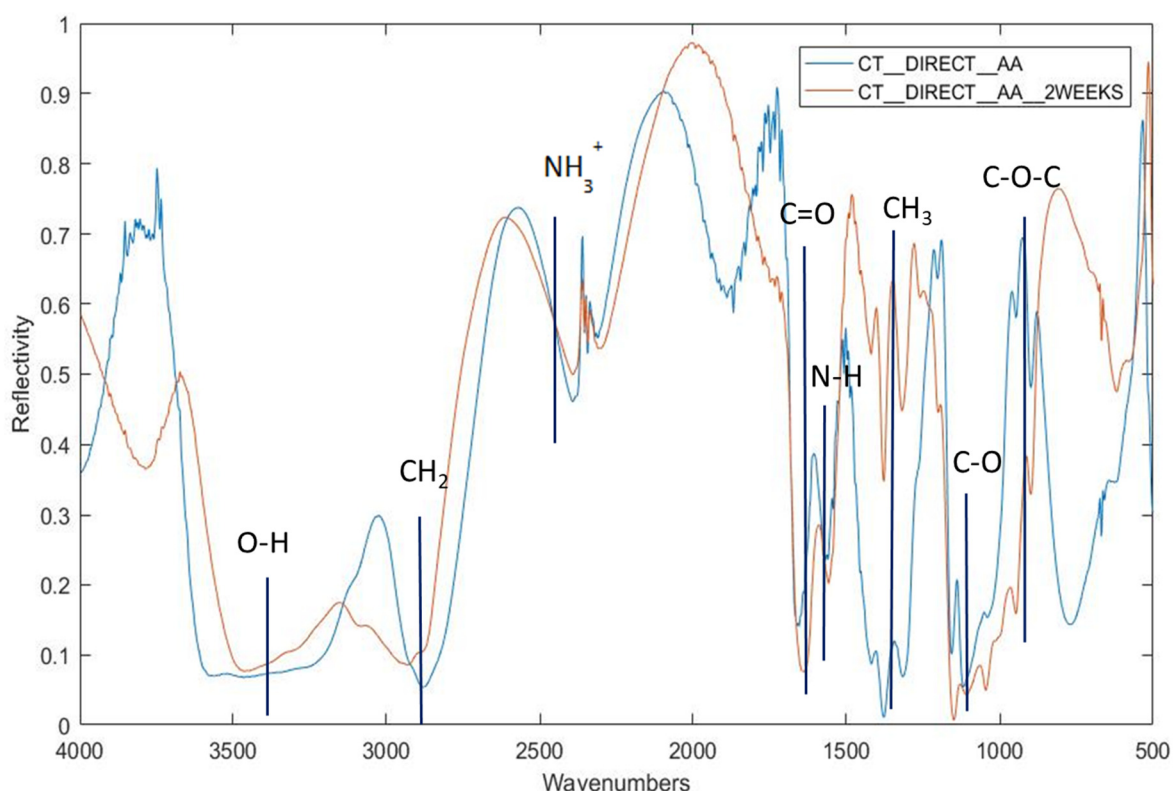


Figure 5.6: FTIR of physically attached chitosan, dissolved in acetic acid, before and after two weeks in PBS at 37°C

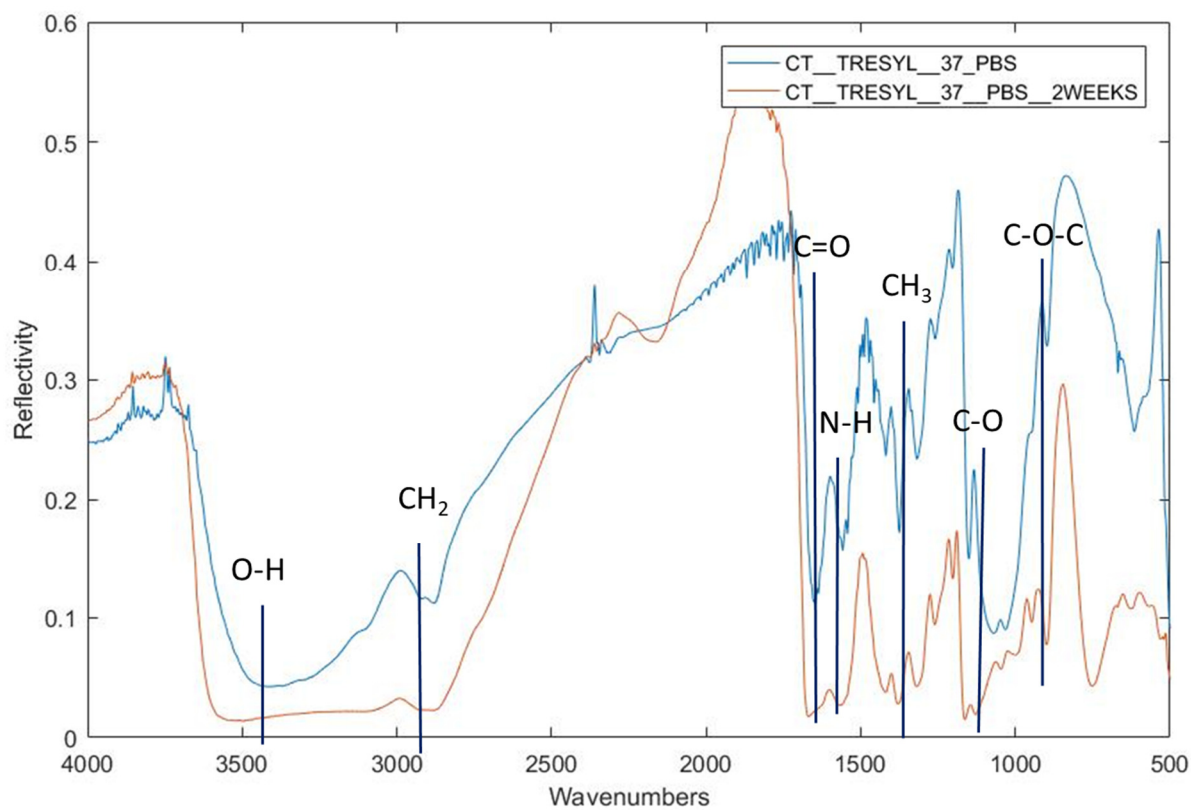


Figure 5.7: FTIR of sample, activated with tresyl chloride at 37°C, coated with chitosan suspended in PBS before and after two weeks in PBS at 37°C

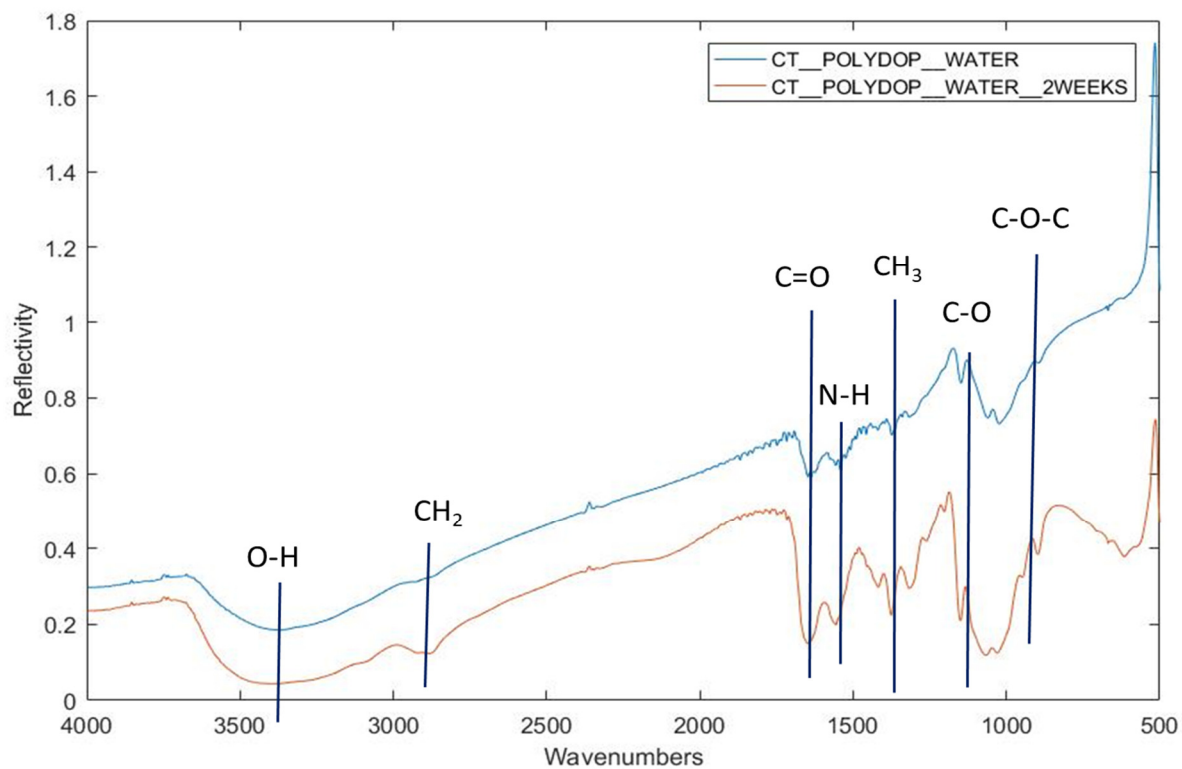


Figure 5.8: FTIR of polydopamine activated titanium coated with chitosan, dispersed in deionized water, before and after two weeks in PBS at 37°C

5.2. Scanning Electron Microscope analysis

The scanning electron microscope is used to observe morphology of the surfaces.

After importing the images in ImageJ, setting the threshold values needed, the software can identify differences in the color of each pixel to distinguish the area coated with the one uncoated and obtain, for each sample analysed, the results shown in Table 5.6. Physical adhesion of chitosan dissolved in acetic acid is the easiest technique to dissolve chitosan and produces a strong bond due to acid-base reaction between the substrate (that shows a negative charge) and chitosan (that shows a positive charge in this solution) as explained by Fowkes in 1981 [9]. Thresyl chloride activation at 37°C, on the other hand, improves the adhesion of chitosan suspended in PBS if compared to physical adhesion, while tresyl chloride activation at room temperature results in a low adhesion. The activation with polydopamine act as linker for chitosan dispersed in deionized water as desired but the efficacy is lower than physically attached chitosan dissolved in acetic acid

SAMPLE	% Area coated
CT_DIRECT_AA	100
CT_DIRECT_PBS	41
CT_TRESYL_37_PBS	72
CT_TRESYL_RT_PBS	25
CT_POLYDOP_WATER	65

Table 5.6: % of area coated

The image of the titanium substrate confirmed the nanoporous morphology due to the oxydation process as visible in Figure 5.9a with 100x magnification and 5.9b with 50000x magnification. The analysis of the surfaces coated with the physical attachment of chitosan showed that the chitosan dissolved in acetic acid covered the whole area (Figure 5.9c), while the chitosan suspended in PBS only 41% (Figure 5.9d).

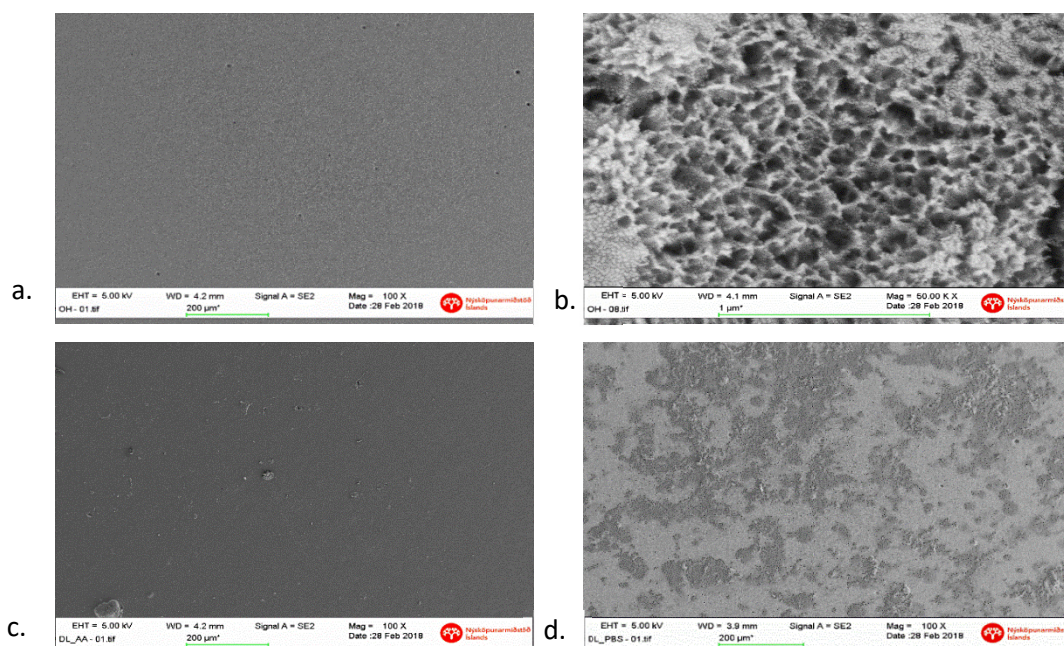


Figure 5.9: SEM images of the titanium substrate at different magnification (a-b), samples coated with chitosan dissolved in acetic acid (c) and suspended in PBS (d)

Samples activated with tresyl chloride at room temperature presented a low level of area coated as shown in Figure 5.10b, while samples treated at 37°C resulted in 72% of surface coated as in Figure 5.10a. From Figures 5.10c and 5.10d emerges that the coating obtained at room temperature is much more continuous than the one obtained at 37°C that seems spreaded on the surface and not properly attached. Further tests are needed to asses the mechanical adhesion of these coatings.

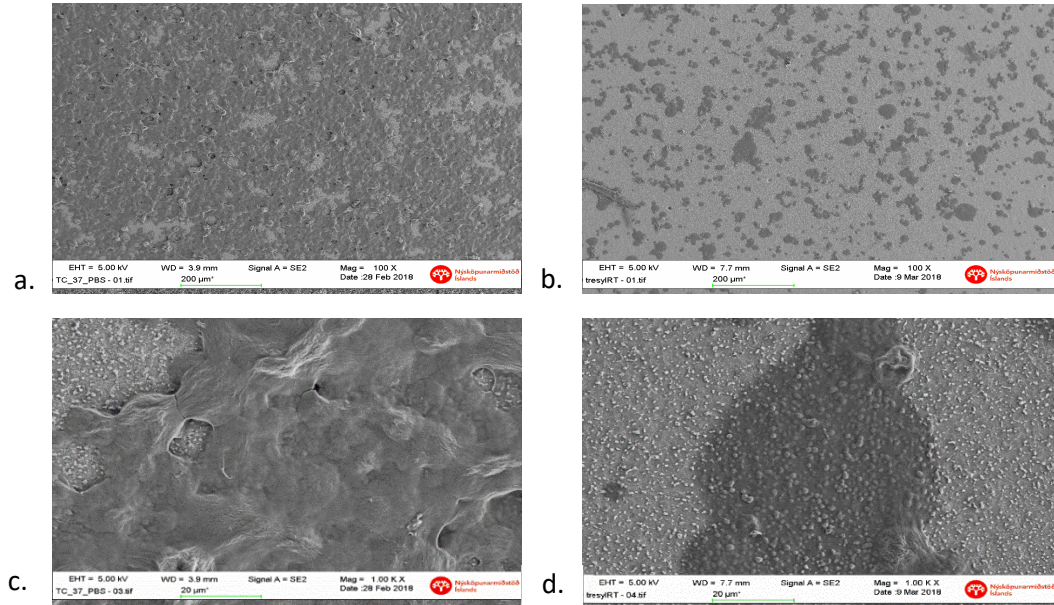


Figure 5.10: SEM images of tresyl chloride activated samples coated with chitosan at 37°C (a-c) and at room temperature (b-d)

In the samples activated through polydopamine, the area coated by chitosan dispersed in deionized water is around 65% (Figure 5.11a) while in the one with chitosan suspended in PBS was 29% (Figure 5.11b). As can be seen in Figures 5.11c and 5.11d, in both cases, further tests are needed to verify the mechanical adhesion.

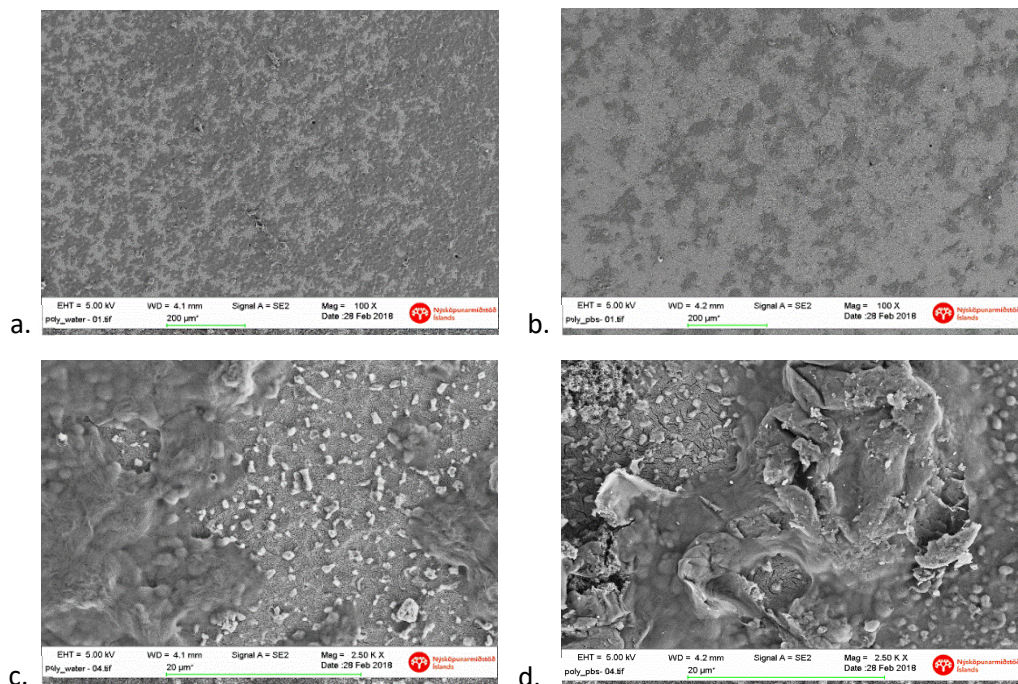


Figure 5.11: SEM of polydopamine activated samples coated with chitosan dispersed in deionized water (a-c) and suspended in PBS (b-d)

Particles deposited on the surfaces are observable on the samples activated through polydopamine, before the coating procedures; they were analysed by EDS to establish their chemical nature (Figure 5.12) and the spectrum evidenced the presence of Carbon, Nitrogen and Oxygen that are the primary components of every organic compound (Table 5.7). The presence of gold is due to the coating used to improve the quality of the SEM microscopy.

Element	Weight %	Atomic %
C	29.78	52.27
N	2.72	4.10
O	30.07	39.63
Au	37.43	4.01

Table 5.7: % of elements in the polydopamine activated sample

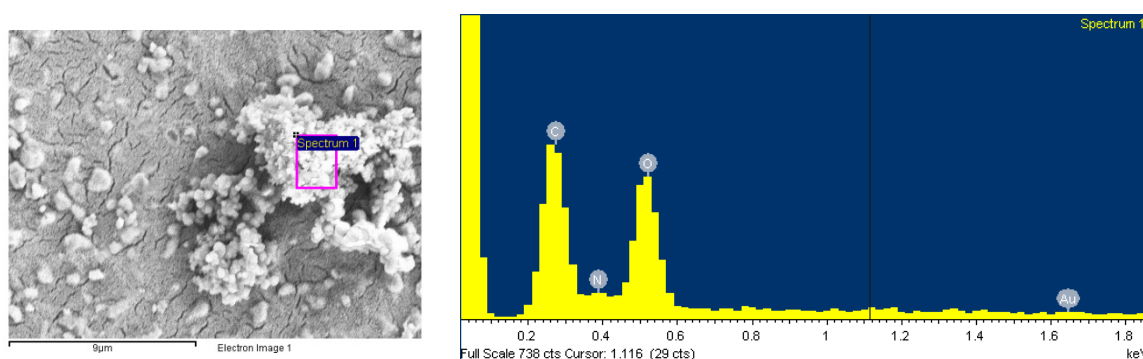


Figure 5.12: grain analysis of a sample activated with polydopamine

Considering the previous analysis and the SEM images, one procedure per method is further analysed after the AFM analysis, in particular: physically attached chitosan dissolved in acetic acid, tresyl chloride activated titanium coated with chitosan suspended in PBS at 37°C and polydopamine activated titanium with chitosan dispersed in deionised water. SEM images were also obtained after storing these samples in simulated body fluids for 2 weeks in incubator at 37°C and the results show that the coating is still in place as visible in Figures 5.13, 5.14 and 5.15.

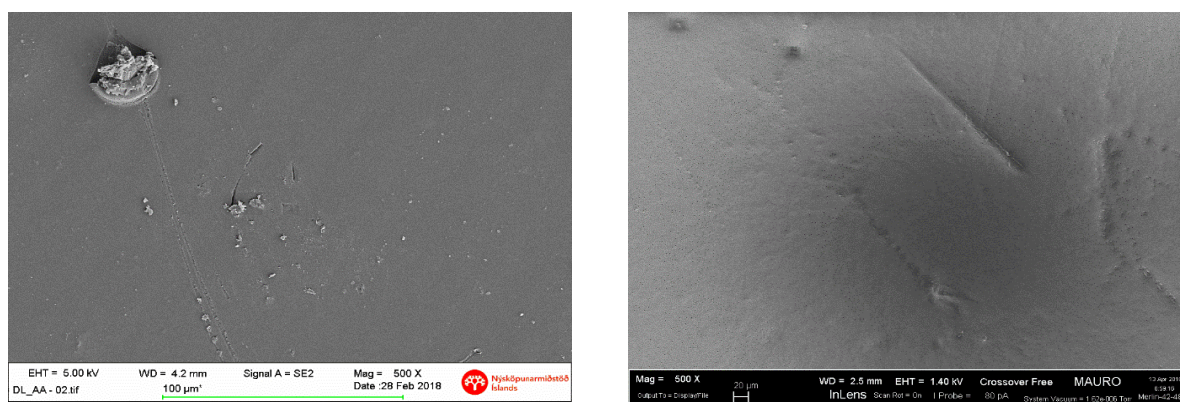


Figure 5.13: SEM images of titanium, coated with chitosan dissolved in acetic acid, before and after storage for two weeks in PBS at 37°C

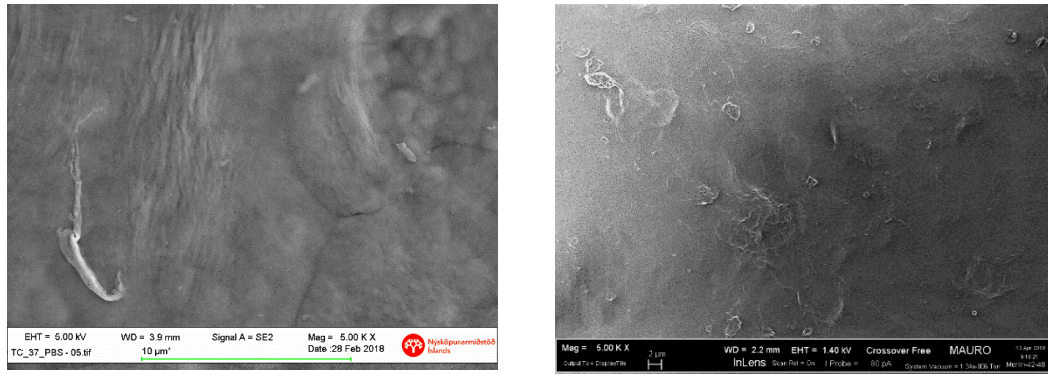


Figure 5.14: SEM images of titanium, activated with tresyl chloride, coated with chitosan suspended in PBS at 37°C, before and after 2 weeks in PBS at 37°C

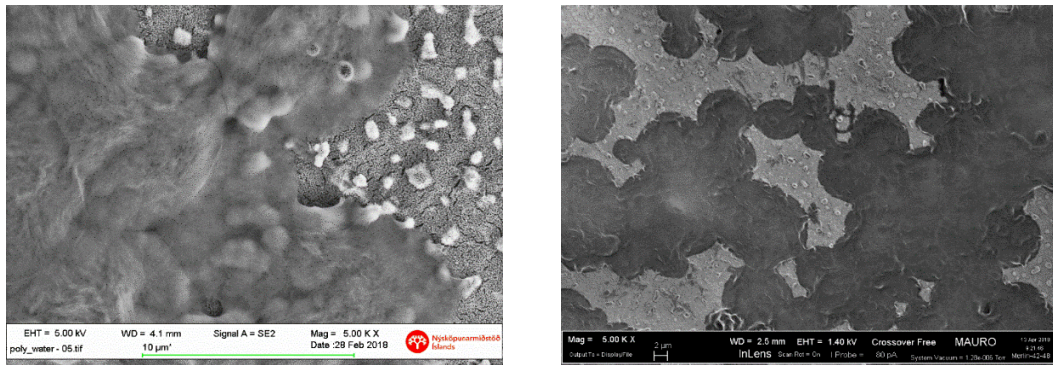


Figure 5.15: SEM images of titanium, activated with polydopamine, coated with chitosan dispersed in deionized water, before and after 2 weeks in PBS at 37°C

5.3. Atomic Force Microscope analysis

Table 5.8 illustrates the values of roughness obtained via Gwyddion from the AFM images and can be used for a comparison of the coated samples and in order to evaluate the formation/absence of a continuous coating. The substrate (chemically treated titanium) is characterized by roughness on the micro and nano scale: the presence of a continuous chitosan coating is expected to be associated to a significant decrement in surface roughness of the sample.

SAMPLE	S _q and S _a measured on 1 µm x 1 µm		S _q and S _a measured on 5 µm x 5 µm	
	RMS Roughness S _q [nm]	Mean Roughness S _a [nm]	RMS Roughness S _q [nm]	Mean Roughness S _a [nm]
Oxidised titanium	21.7	17.79	151.66	123.95
CT_DIRECT_AA	2.01	1.61	4.73	3.44
CT_DIRECT_PBS	10.22	8.14	-	-
CT_TRESYL_37	26.18	21.39	94.58	69.88
CT_TRESYL_RT	13.59	10.91	64.85	52.75
CT_TRESYL_37_PBS	58.59	49.3	144.2	116.56
CT_TRESYL_RT_PBS	23.4	18.24	131.38	110.59
CT_POLYDOP	19.73	15.15	78.55	63.41
CT_POLYDOP_WATER	16.85	14.19	160.57	136.8
CT_POLYDOP_PBS	30.86	24.14	158.79	129.61

Table 5.8: values of roughness for the samples taken for an area of 1 µm and 5 µm, the values of CT_DIRECT_PBS at 5 µm are not reported due to errors in the measurement

Table 5.8 indicates that the root mean square roughness values of samples coated by chitosan dissolved in acetic acid and physically attached to the surface showed a decrease of 97% compared to the same value for the uncoated titanium when the area is $5 \mu\text{m}^2$ and of 81% when the area is $1 \mu\text{m}^2$. On samples coated in the same condition, but with chitosan suspended in PBS, the decrease is lower (around 52%) confirming SEM images of a lower adhesion of the coating. CT_DIRECT_AA results in a uniform coating with very low roughness. Figures 5.16 and 5.17 shows the images obtained from AFM that were used in Gwyddion to determine the roughness values, while Figure 5.18 shows a 3D scale comparison between the oxidised uncoated titanium and the physically attached chitosan coatings giving evidence of the decrease of roughness due to a continuous coating: from 150 nm to 14-60 nm.

Figure 5.19 shows the image of tresyl chloride activated sample coated and uncoated with chitosan. The samples activated with tresyl chloride both at 37°C and at room temperature show differences in the roughness values compared to oxidised titanium probably depending on the area scanned, even if in the tresyl chloride mechanism this compound modifies the functional groups without introducing modifications in the surface roughness. Instead, sample coated with chitosan at 37°C show a valley visible in Figure 5.20 that increases the roughness probably because of the area scanned, that can be at the boundary between coated and uncoated parts. When the area scanned increases, RMS value of CT_TRESYL_37_PBS is similar to the oxidised titanium, indicating that the coating is not uniform as resulted from SEM. This assumption can be used also for roughness values of CT_TRESYL_RT_PBS that are similar to oxidised titanium for both the areas scanned.

The samples coated after polydopamine activation (Figures 5.23 and 5.24) showed opposite values of roughness when the area is $1 \mu\text{m}^2$, in the case of chitosan dispersed in deionized water there was a decrease, while in chitosan suspended in PBS the value is highly increased when compared both to the same activation condition, but with chitosan in water, and to oxidised titanium. These values of roughness confirmed the results and hypothesis based on SEM images that the surface, when chitosan is suspended in PBS is not well coated. A bigger area scanned ($5 \mu\text{m}^2$) shows RMS roughness values similar to oxidised titanium indicating that both CT_POLYDOP_WATER and CT_POLYDOP_PBS are not well coated as resulted from SEM.

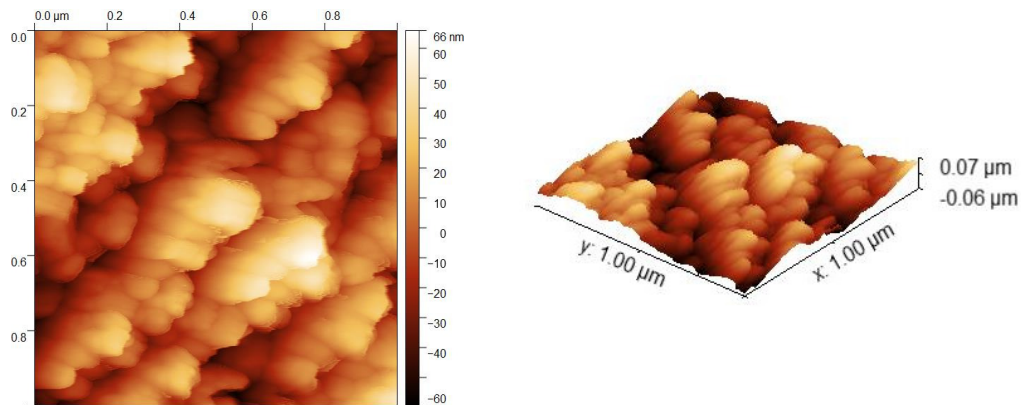


Figure 5.16: AFM images of oxidised sample

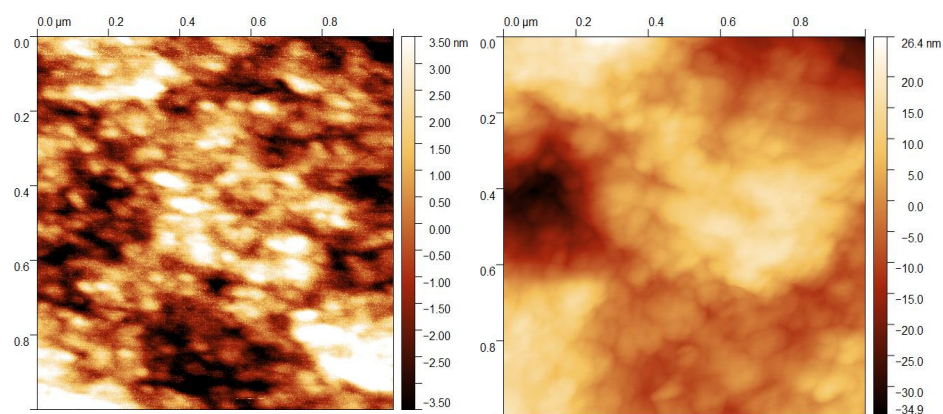


Figure 5.17: AFM images of samples coated with chitosan dissolved in acetic acid (left) and suspended in PBS (right)

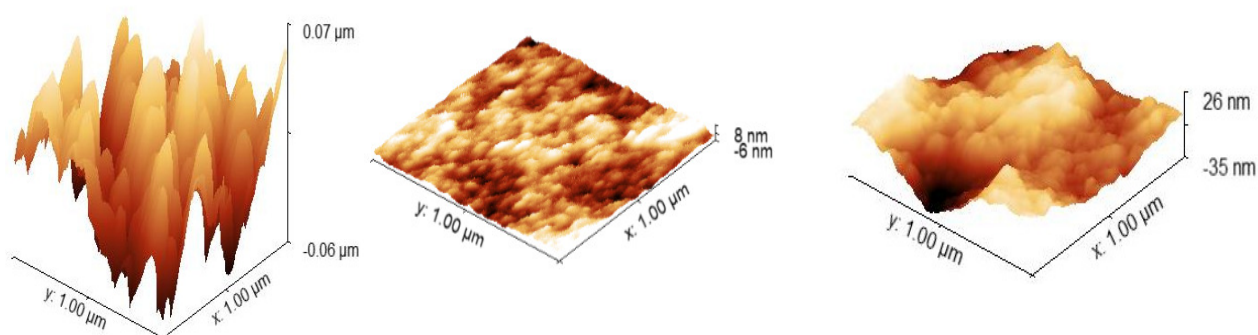


Figure 5.18: 3D view comparison between oxidised titanium (left) and physically attached chitosan dissolved in acetic acid (central) and suspended in PBS (right)

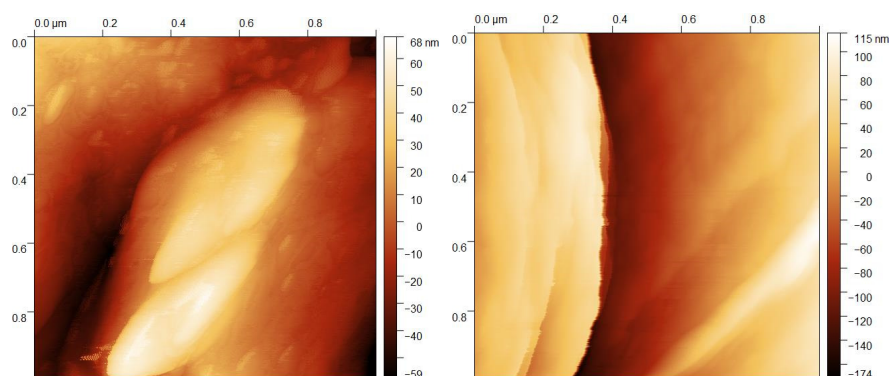


Figure 5.19: AFM images of tresyl chloride activated sample; uncoated (left) and coated with chitosan at 37°C (right)

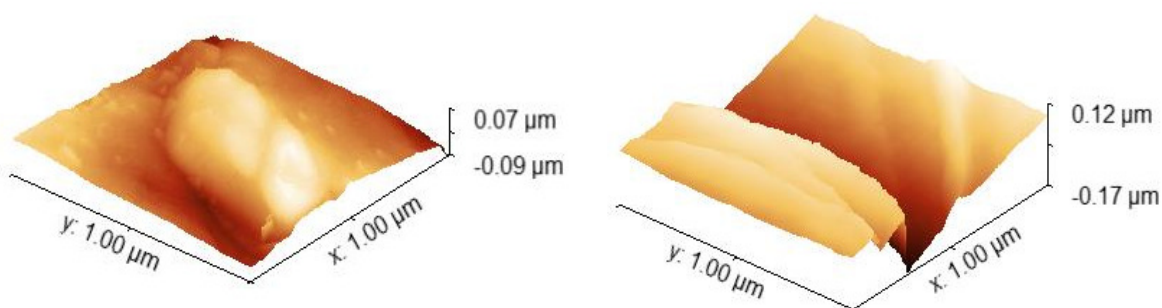


Figure 5.20: 3D view of tresyl chloride activated sample; uncoated (left) and coated with chitosan (right) at 37°C

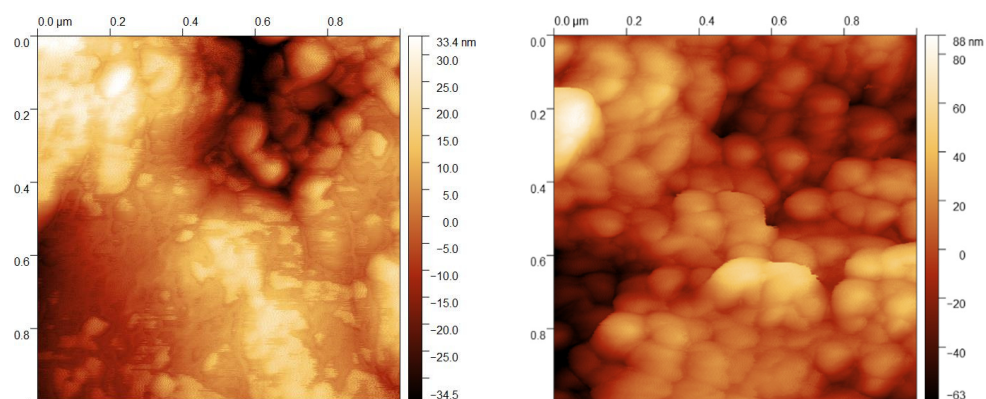


Figure 5.21: AFM images of tresyl chloride activated sample; uncoated (left) and coated with chitosan at room temperature (right)

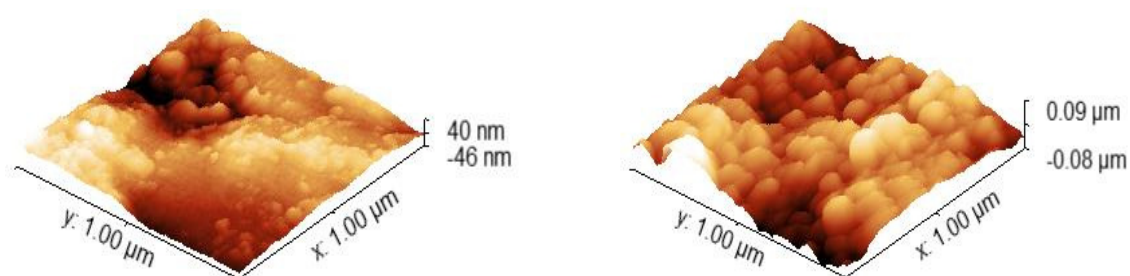


Figure 5.22: 3D view of tresyl chloride activated sample; uncoated (left) and coated with chitosan (right) at room temperature

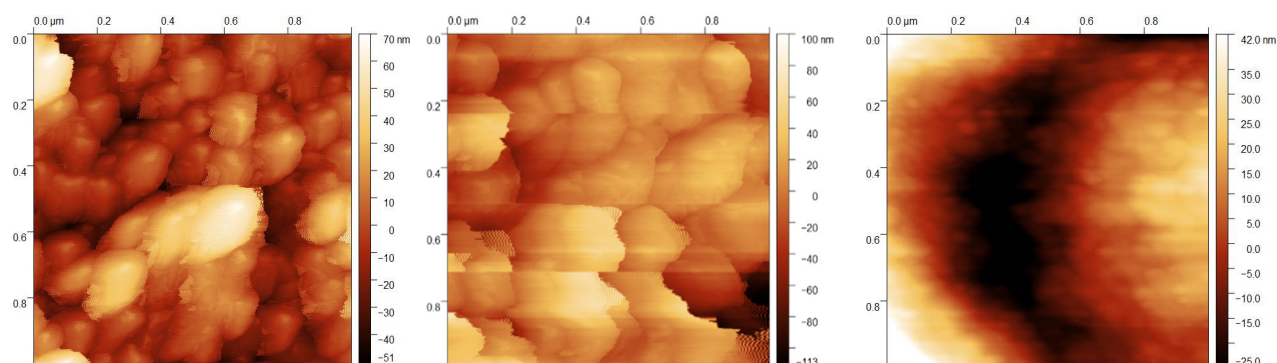


Figure 5.23: AFM images of polydopamine activated samples; uncoated (left), coated with chitosan suspended in PBS (centre) and dispersed in deionized water (right)

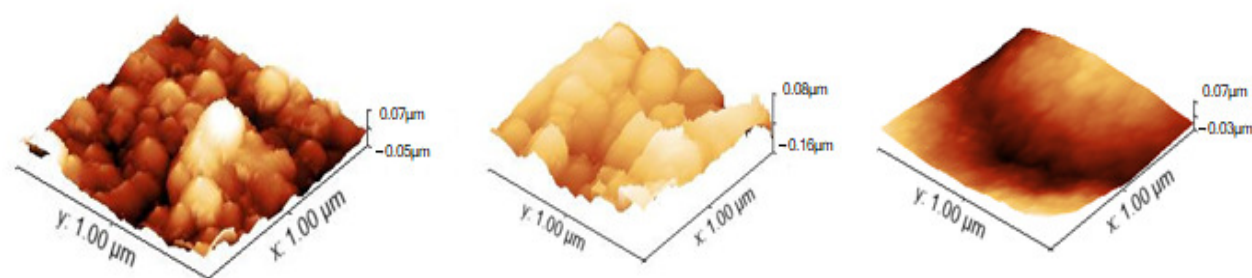


Figure 5.24: 3D view of polydopamine activated samples; uncoated (left), coated with chitosan suspended in PBS (centre) and dispersed in deionised water (right)

5.4. Zeta potentials

Zeta potential is a measure of the superficial charge on a sample via streaming potential. These measurements can also be used to estimate the quality of the coating by comparing the results with literature for chitosan's streaming potential assuming that the more the Isoelectric point value or zeta potential at a specific pH value is similar to the one of chitosan, the more uniformly coated is the surface.

In order to properly analyse the results obtained, zeta potential of oxidised Ti6Al4V, obtained by previous researches in the same laboratory with the same procedure of this thesis, is reported as comparison in Figure 5.26 [10]. Polished Ti6Al4V shows an isoelectric point at pH 4.7, while oxidised Ti6Al4V presents a shift of the isoelectric point to more acidic values compared to polished Ti6Al4V (around pH 2 – as visible in Figure 5.25) and a plateau in the basic region (onset at pH 4.5) [10]. This evidences the presence of acidic OH groups on the surface of the treated substrate which act as a strong acid and are completely deprotonated at pH above 4.5.

As can be seen in Figures 5.27, 5.28, 5.29 and especially in Figure 5.31, each sample has different zeta potential values due to differences among the coatings. The zeta potential for the polished titanium substrate coated with chitosan dissolved in acetic acid has an oscillatory behaviour with high standard deviation making this values highly inaccurate as shown in Figure 5.30. This effect could be due to higher reactivity or swelling of the coating on the polished substrate.

As comparison, *Amaral et al.* (2012) measured the zeta potential for chitosan with different deacetylation degree (DD), finding that the 50% DD form has a value around 15mV at pH 5.5 [11]. The zeta potential of chitosan at acidic pH is significantly positive due to the protonation of the amino groups in the chain. For high pH values, the material swelling introduces variation in the magnitude of the potential that needs to be taken into account. It is evident by Figure 5.31 that the sample with a zeta potential value at pH 5.5 that is more similar to the value measured by Amaral is the sample coated with chitosan dissolved in acetic acid and physically attached to oxidised titanium (16 mV), while for the other samples zeta potential is lower (6 mV for CT_TRESYL_37_PBS, 7 mV for CT_POLYDOP_WATER).

Presence (or absence) of a plateau in the measurements indicates that there are functional groups on the analysed surface with similar (or different) chemical reactivity and protonation (or deprotonation) behaviour; a plateau is always observable between pH 5.5 and 6 (Figures 5.27 - 5.29). This confirms, as expected, that chitosan has strong basic amine groups which are completely protonated at pH lower than 6: they are probably active when the coating procedure is performed in acetic acid and contribute to a strong attraction of the coating to the negative charged substrate. A plateau is also observable around pH 9 of the coated samples and it can be ascribed to OH groups which act as a very weak acid and are completely deprotonated at pH higher than 9.

The isoelectric point of a surface, the pH value at which there is equilibrium of charges and the potential is 0 mV, is an indication of the balance between acid and basic functional groups on the surface. In particular, Isoelectric point at pH values around 8 indicate a prevalence of basic functional groups. Table 5.9 shows the IEP for the tested samples. Considering that the substrate has a low isoelectric point, a shift of the IEP of the coated samples towards lower values can be related to a lower degree of covering of the surface by the coating. It can be deduced that the coating of chitosan is able to cover the substrate with an increasing trend moving from CT_POLYDOP_WATER (the lowest covering) to physically attached chitosan dissolved in acetic acid (the highest covering). As already underlined,

the polished titanium sample with physically attached chitosan dissolved in acetic acid had an anomalous behaviour.

SAMPLE	IEP
Polished titanium	4.7
Oxidised titanium	2
CT_DIRECT_AA	8.53
CT_TRESYL_37_PBS	8.17
CT_POLYDOP_WATER	7.33
MP_DIRECT_AA	8.5-9.5

Table 5.9: isoelectric point of samples

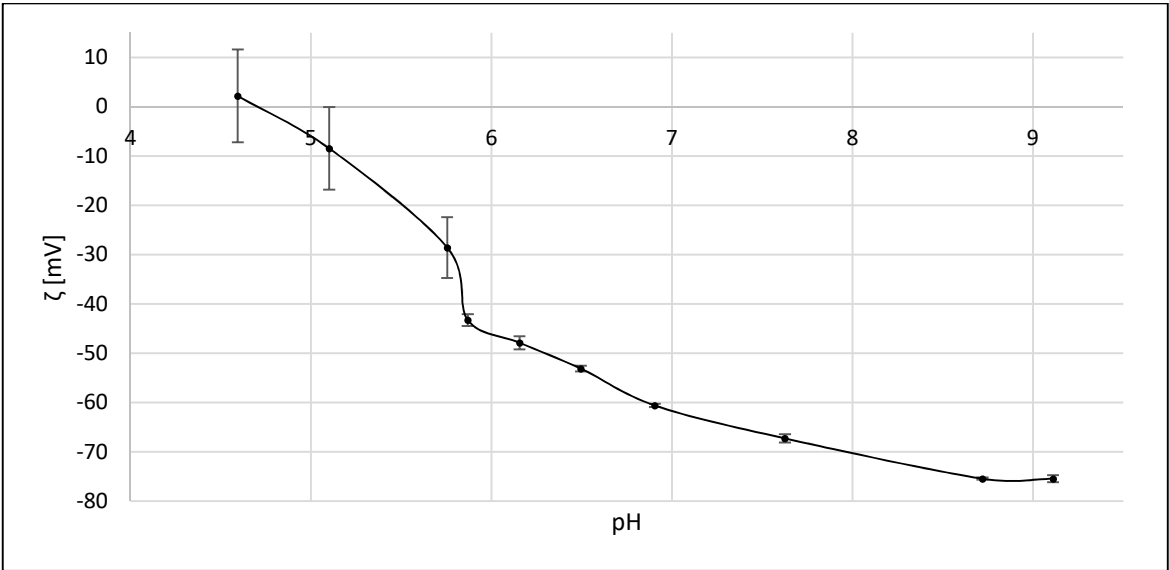


Figure 5.25: Zeta potential of mirror polished titanium

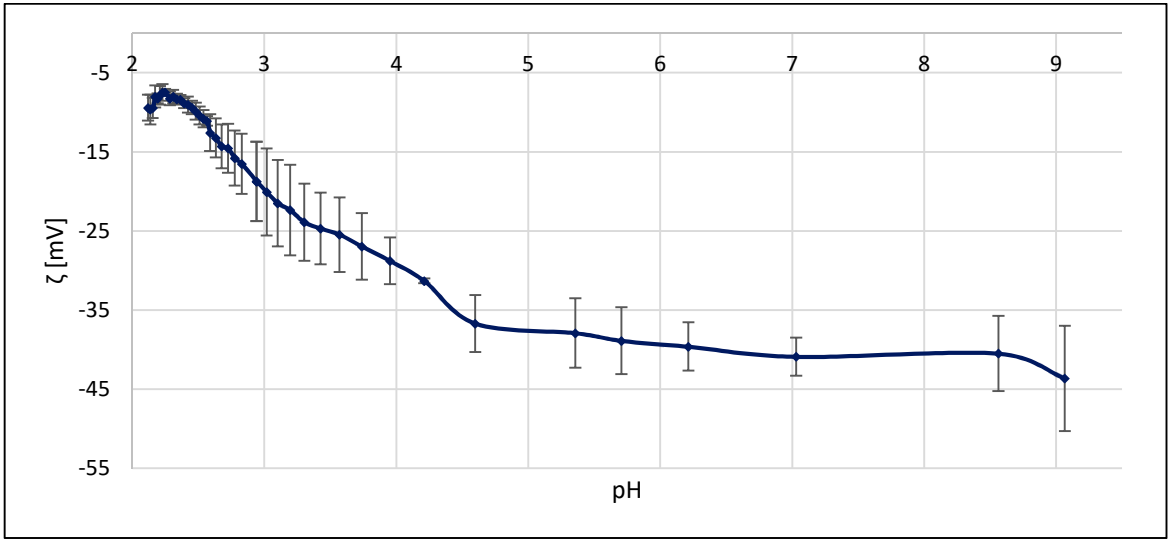


Figure 5.26: Zeta potential of chemically treated titanium

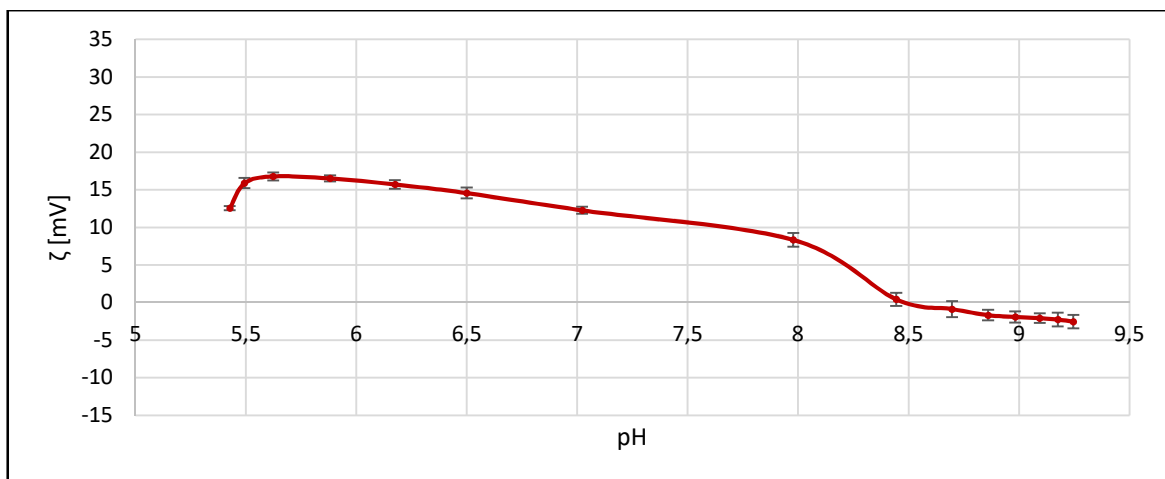


Figure 5.27: Zeta potential of oxidised titanium coated with chitosan dissolved in acetic acid

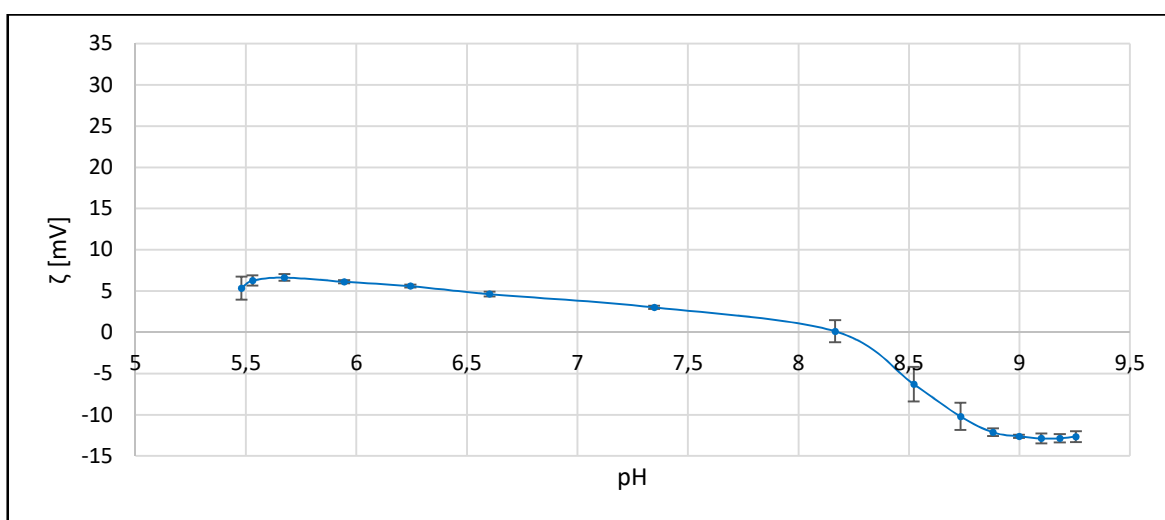


Figure 5.28: Zeta potential of oxidised titanium, activated with tresyl chloride, coated with chitosan suspended in PBS at 37°C

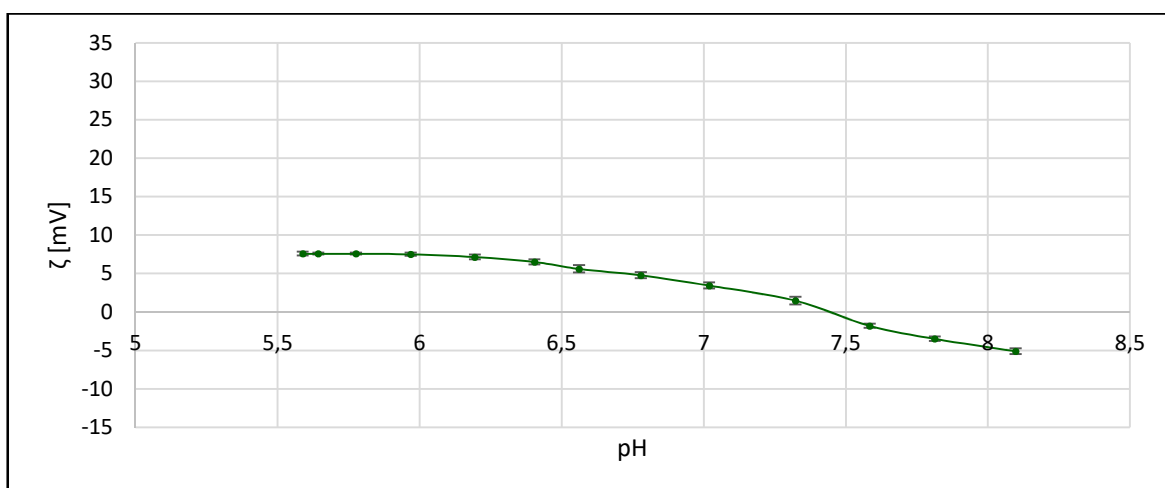


Figure 5.29: Zeta potential of oxidised titanium, activated with polydopamine, coated with chitosan dispersed in deionised water

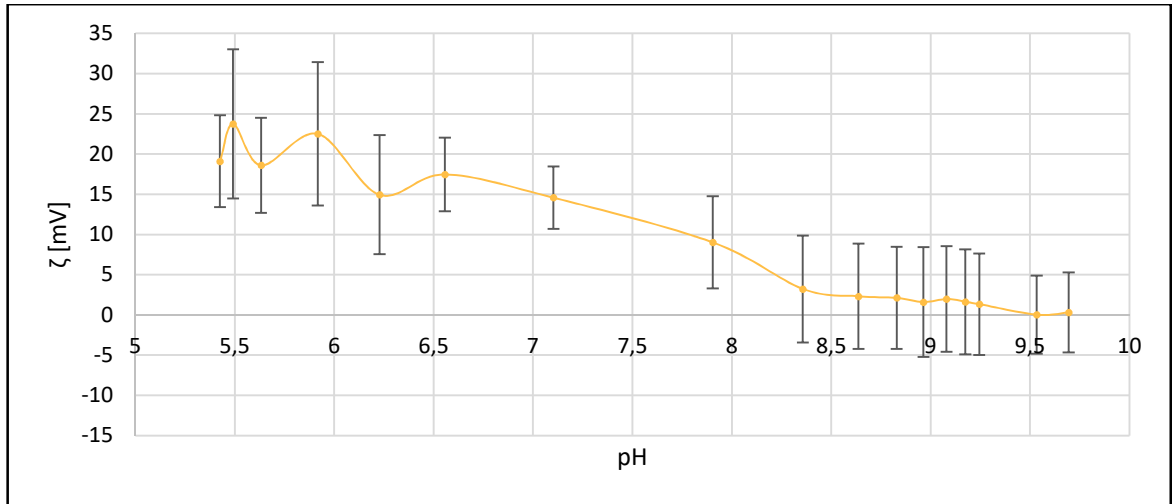


Figure 5.30: Zeta potential of polished titanium coated with chitosan dissolved in acetic acid

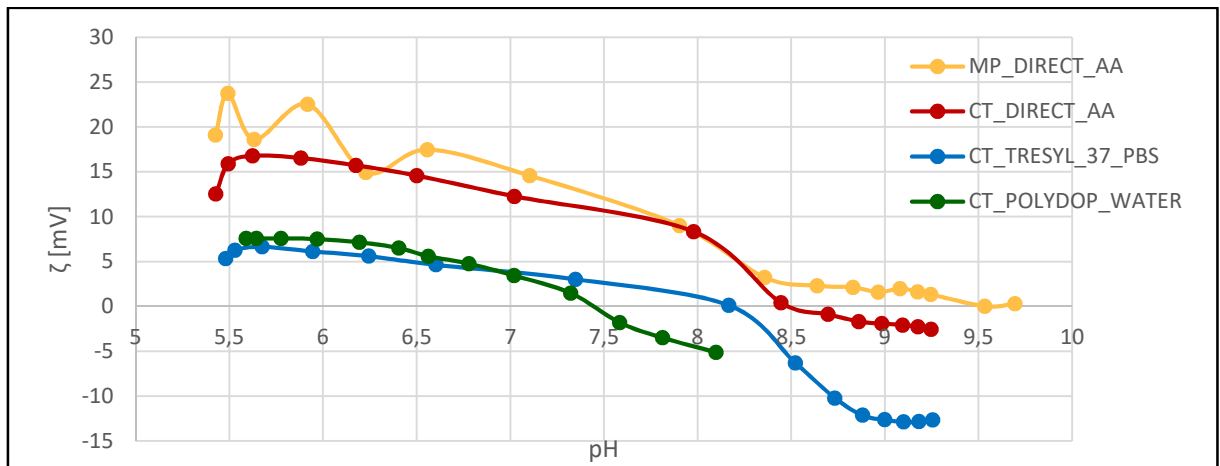


Figure 5.31: Basic zeta potentials of chitosan coated samples, MP_DIRECT_AA is the polished sample coated with chitosan dissolved in acetic acid, CT_DIRECT_AA is the oxidised sample coated with chitosan dissolved in acetic acid, CT_TRESYL_37_PBS is the oxidised sample, activated with tresyl chloride, coated with chitosan suspended in PBS at 37°C and CT_POLYDOP_WATER is the oxidised sample, activated with polydopamine, coated with chitosan dispersed in deionised water

5.5. Contact angle measurements

Previous analysis on polished Ti6Al4V and oxidised Ti6Al4V, obtained in the same laboratory and with the same procedure used in this thesis, report contact angles of $81.4^\circ \pm 0.77$ for polished titanium and $76^\circ \pm 5.59$ for oxidised Ti6Al4V according to the presence of OH groups on it [12]. These results can be compared to the one obtained after the coating with chitosan and on all the other treatments.

As shown in Table 5.10, the contact angles after coating indicate a hydrophobic behaviour of the samples in which chitosan is physically attached (CT_DIRECT_AA) and in the sample activated with tresyl chloride after the coating with chitosan (CT_TRESYL_37_PBS). Both these samples have an increase in contact angle after coating with respect to the value of the CT substrate, as expected due to the good covering of the coating and the hydrophobic nature of chitosan.

In the case of MP_DIRECT_AA, the contact angle value does not significantly change with respect to the MP substrate; in this case the contact angles of the MP substrate and the chitosan coating are

quite similar and this measurement is not indicative for evaluating the degree of coverage of the substrate by the coating.

In the sample activated with polydopamine the coating with chitosan (CT_POLYDOP_WATER) shows a hydrophilic angle. This effect can be seen in Figure 5.32a where the difference among the samples is evident. A hydrophilic behaviour of polydopamine is reported in literature [13]. It can be deduced that in some cases (as this specific sample) polydopamine was effectively graft while chitosan coating was not.

It can be concluded that contact angle measurements are useful for evaluate the presence/absence of the coating on the CT samples.

The measurement of the contact angle has been performed also on the samples after zeta potential measurements, in which the chitosan swelled in a basic aqueous solution, or tape test, in which the coating can be removed from the surface, in order to get complementary information about the residual covering of the samples after these tests.

It can be seen in Table 5.10 that the contact angle values are still higher after all the different treatments made to the chitosan physically attached to the oxidised substrate, indicating a resistance of the coating to the test conditions of zeta potential measurement (in a wide range of pH) and tape test. It can be concluded that this coating is both chemically and mechanically stable.

The oxidised substrate activated with tresyl chloride, even maintaining values higher than bare chitosan, shows a decrement in the values after all the treatments as a result of modifications occurred during the tests, in particular the removal of some parts of the coating after tape test.

Oxidised titanium, activated with polydopamine and then coated with chitosan shows a high decrease in the contact angle value after coating, due to the presence of polydopamine, while the sample after storage for two weeks in PBS at 37°C has a great value of contact angle. The value obtained after storage in PBS for the sample activated with polydopamine can be explained if we consider that that single sample was well covered and the coating was stable after soaking in PBS.

The polished titanium coated with chitosan shows a decrement in the values taken after tape test because the coating has been removed, while during zeta-potential analysis the swelling of chitosan modified the coating giving an increase in the value with a great standard deviation.

SAMPLE	Contact angle of the substrate	Contact angle measured after coating	Contact angle measured after 2 weeks in PBS	Contact angle measured after tape test	Contact angle measured after z-potential
Polished titanium	81,4°±0,77	-	-	-	-
Oxidised titanium	76°±5,59	-	-	-	-
MP_DIRECT_AA	-	83,2°±5,71	-	62,05°±7,84	110,9°±50,34
CT_DIRECT_AA	-	83,95°±4,4	93,35°±9,4	96,5°±2,26	99,8°±11,17
CT_TRESYL_37_PBS	-	103°±14,44	83,9°±0,14	93,85°±16,2	96,95°±1,06
CT_POLYDOP_WATER	-	16,7°±13,97	79,25°±9,12	-	-

Table 5.10: contact angle measurements

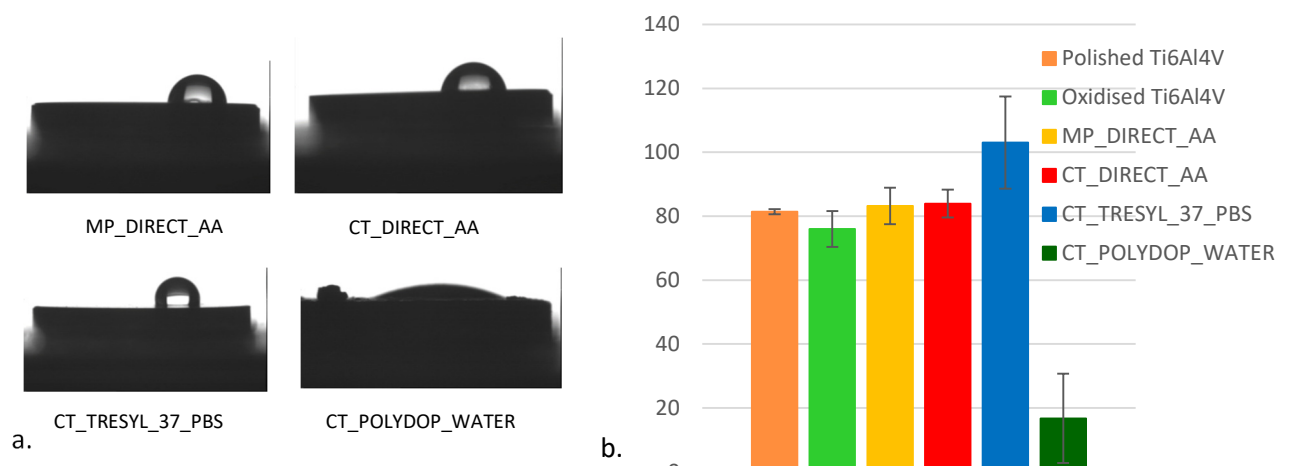


Figure 5.32: a. images of contact angle measurements on samples coated with chitosan, b. mean values of contact angles of the titanium substrates and of the samples coated with chitosan

5.6. Tape test

Classification of the coating adhesion on the basis of the tape test results depends on visible differences in the surface after the test. A scheme of the procedure is shown in Figure 5.33. Due to the transparent aspect of chitosan, it is rather difficult to assign a classification value to the sample with a coating through physical attachment on polished titanium (MP_DIRECT_AA in Figure 5.34). This analysis becomes simpler with the oxidised samples in which the cuts of the test are visible, as in CT_DIRECT_AA and CT_TRESYL_37_PBS in Figure 5.34.

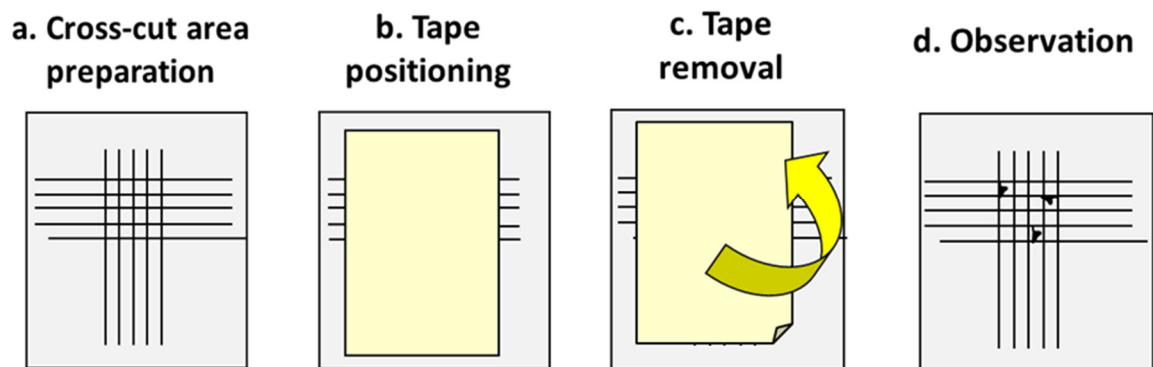


Figure 5.33: Scheme of tape test procedure

In the case of the coating through physical attachment of chitosan to the treated substrate (CT_DIRECT_AA in Figure 5.34), the test results in a 5B classification (ASTM Standard) with none removal of the coating, while for the chitosan coating on samples activated by tresyl chloride (CT_TRESYL_37_PBS in Figure 5.34), the classification is 0B because the cross-cut area is uncoated at the 83%.

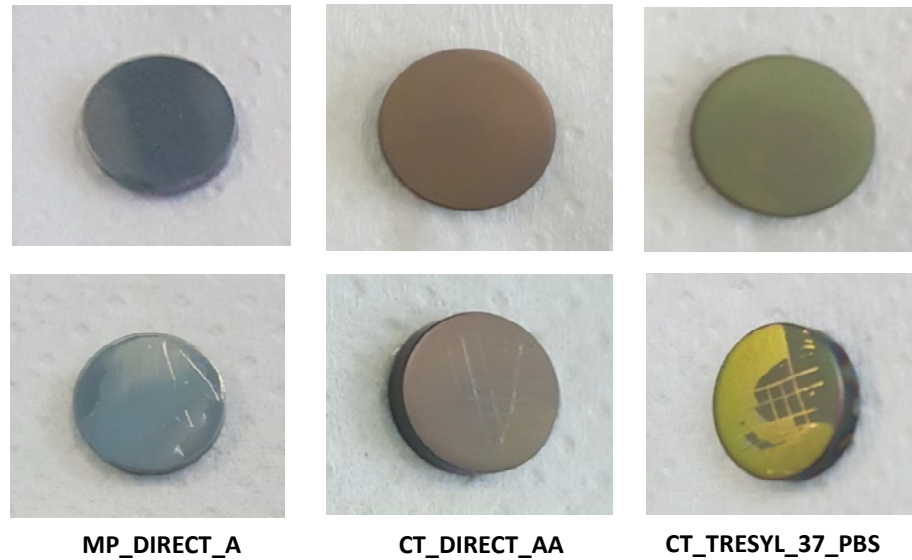


Figure 5.34: samples images before and after tape test

To further assess the tape test visive results, FESEM was performed on these samples. In Figure 5.35, it can be seen that the coating is removed only within the cross-cuts on the sample with a chemically treated substrate coated with chitosan physically attached. In Figure 5.36, it is shown the difference between the cross-cut sections on the coated and uncoated samples where coating was performed through tresyl chloride activation. In Figure 5.37, the external areas of the polished sample with chitosan physically attached, that still have the coating attached, are shown as comparison with the central area of the samples where the coating was removed: a low classification of the coating in the tape test results on these samples.

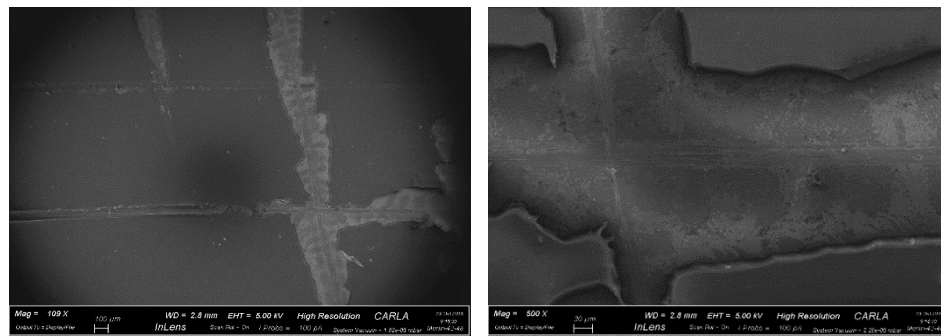


Figure 5.35: FESEM on CT_DIRECT_AA samples after tape, the cross-cuts evidence the presence of the coating

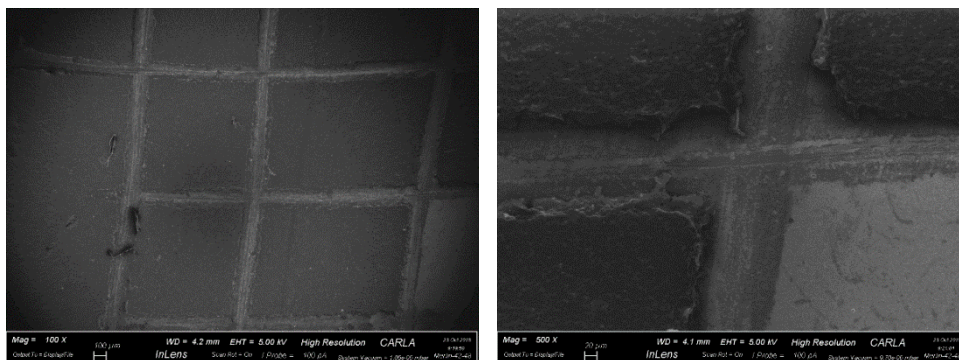


Figure 5.36: FESEM on CT_TRESYL_37_PBS samples after tape, it can be seen the difference between areas where the coating was removed and areas with the coating still present

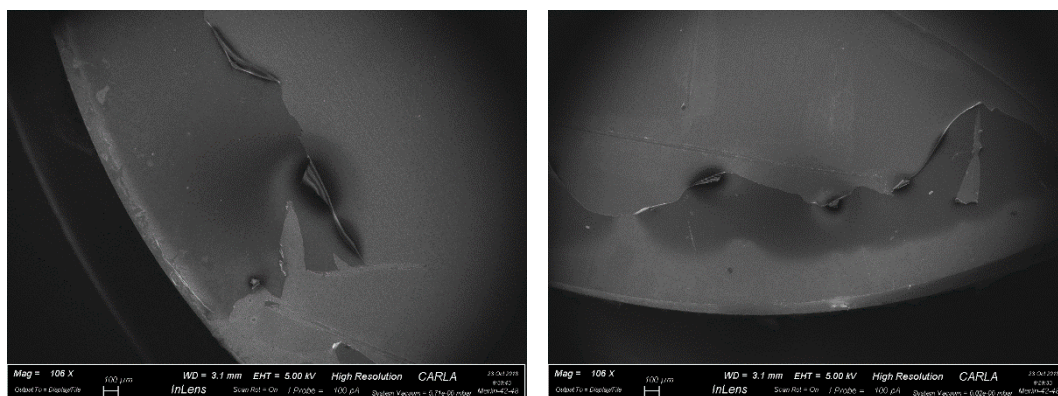


Figure 5.37: FESEM on MP_DIRECT_AA samples after tape, it can be noted that chitosan is still attached on the edges

5.7. Discussion

Douglas et al. in 2017 coated mirror polished titanium with chitosan. Titanium was ultrasonically cleaned with ethanol and acetone and then soaked into chitosan dissolved in acetic acid for 24h. On the chitosan-coated samples, FTIR showed a broad peak at $3500\text{--}3000\text{ cm}^{-1}$ attributed to N-H asymmetric stretching and O-H symmetric stretching. Adsorption band of C=O at 1655 cm^{-1} and bending of N-H at 1599 cm^{-1} indicated the presence of chitosan. N-H stretching also cause bands at 1423 cm^{-1} and 1381 cm^{-1} . C-O stretching resulted in two bands at 1081 cm^{-1} and 1033 cm^{-1} [14]. *Bumgardner et al.* in 2003 attached chitosan, dissolved in acetic acid, to mirror polished titanium via silane reactions and reported a contact angle of $76.4^\circ \pm 5.1$ [15]. *Zheng et al.* in 2013 studied the adhesion of carboxymethyl chitosan on titanium through silane adhesion, dopamine or polydopamine [6]. Carboxymethyl chitosan (CMCS) was synthesized soaking chitosan in isopropanol, NaOH and monochloroacetic acid. The mixture was heated at 60°C for 3h and was added cold distilled water. pH was adjusted to 7 with glacial acetic acid and the mixture was filtered and rinsed with ethanol to obtain solid CMCS. CMCS was dissolved in a NHS, EDC and MES buffer and attached to titanium treated with Kroll's reagent (7.2% HNO_3 , 4% HF and 88.8% H_2O acidic aqueous solution). To attach CMCS through silanization the substrate was immersed in APTES ((3-Aminopropyl)triethoxysilane) in toluene solution at 70° for 6h with stirring, then sonicated in toluene for 15 min and washed with toluene, isopropanol and distilled water respectively. To attach CMCS with dopamine, the substrate was soaked into aqueous dopamine solution overnight at room temperature. To attach CMCS through polydopamine was used the same procedure of activation of treated titanium used in this study (soak dopamine in a Tris buffer at room temperature for 4h with stirring). Contact angles for these procedures showed a hydrophilic behaviour for all the chitosan coated surfaces with values of $27^\circ \pm 3$ for CMCS attached via silane reaction and values $<10^\circ$ for samples activated with dopamine and polydopamine.

Tang et al. in 2014 used a mixture of chitosan and carbonated hydroxyapatite as a coating for titanium [16]. Titanium was treated with H_3PO_4 and HF. CaCO_3 particles are deposited on titanium through electrophoresis (CaCO_3 was dissolved in ethanol and then HCl was added), then transformed into carbonated hydroxyapatite by immersion in a PBS solution. Since carbonated hydroxyapatite forms nanoparticles, chitosan is added to remove cracks and obtain a uniform coating through interconnection of hydroxyapatite, leading to a roughness reduction. SEM images of the cross section demonstrated the presence of an oxide layer, due to the acids treatment, between the substrate and the coating that can improve physicochemical bonding. FTIR spectrum of chitosan present in this

compound showed the band due to OH at 3415 cm^{-1} , the bending vibration of N-H at 1571 cm^{-1} , the bending vibration of CH_2 at 1410 cm^{-1} and the stretching vibration of C-N at around 1030 cm^{-1} . Chitosan also reduced the hydrophilicity of the coating when compared to carbonated hydroxyapatite alone. Contact angle for the chitosan/carbonate hydroxyapatite layer is 29.4° and for the carbonated hydroxyapatite layer is 12.5° .

Zhong *et al.* in 2015 investigated the adhesion of zinc substituted hydroxyapatite nanoparticles (ZnHAP) mixed with chitosan attached to titanium with EPD [17]. HAP were prepared soaking silk fibroin (obtained from silk cocoons treated in sodium carbonate and CaCl_2 , water and ethanol) in a calcium nitrate solution at 37°C . ZnHAP were prepared adding a zinc nitrate solution to calcium nitrate solution. Then it was slowly added a disodium hydrogen phosphate solution. NaOH was used to adjust pH to 9 and the solution was incubated at 37°C in a water bath for 72h to obtain the precipitant ZnHAP. EPD was performed with chitosan dissolved in a solution of ethanol and acetic acid to which were added HAP and carbon nanotubes (CNT). FTIR showed a broad peak at 1021 cm^{-1} due to HAP presence, OH vibrations at 3200 cm^{-1} and C=O vibration at 1622 cm^{-1} due to chitosan. Tape test resulted in a 5B classification, according to ASTM Standard, without removal of the coating.

Electrophoretic deposition (EPD) can also be used to coat titanium with chitosan containing micro and nanoparticles of bioactive glass as reported by Avcu *et al.* in 2018 [18]. Chitosan was dissolved in acetic acid and ethanol. Bioactive glass particles were dispersed into chitosan solution with stirring. FTIR on these samples showed the bands associated to the analysed coating. Samples coated with chitosan alone showed C-O vibration at 1076 cm^{-1} , C-O stretching at 1381 cm^{-1} , CH bending at 1417 cm^{-1} , N-H stretching at 1555 cm^{-1} and C=O stretching at 1652 cm^{-1} . To promote osseointegration, the required average surface roughness has values between 0.6 and $2\text{ }\mu\text{m}$. These values are obtained on the grit blasted chitosan-coated titanium with minimal differences. Grit blasting modifies surface characteristic through acceleration, with compressed air inside a nozzle, of abrasive particles such as alumina, garnet and SiC. In particular, the grit blasted sample without coating has a value of surface roughness (S_a) for an area of 2 mm^2 of $1.95\text{ }\mu\text{m}$, the sample coated with chitosan $1.45\text{ }\mu\text{m}$ and the sample coated with chitosan and bioactive glass particles $1.87\text{ }\mu\text{m}$. The presence of chitosan influences the wettability of grit blasted EPD samples with an increase in the values of the contact angle measured. Grit blasted titanium has a contact angle of 15° , while the sample coated with chitosan shows a value of 78° . Bioactive glass particles influence the value of the contact angle, obtaining a surface more hydrophobic when chitosan presents nanoparticles of bioactive glass (92°) or more hydrophilic when chitosan presents both microparticles or nanoparticles (34° - 35°). As comparison, the contact angle for mirror polished titanium is 50° that becomes 60° when coated with chitosan and microparticles of bioactive glass [18].

Chitosan, alone or in combination with bioactive glass particles, has been attached to titanium after the transformation of the surface into titanium nanotubes (TNT) via anodization as reported by Mokhtari *et al.* in 2018 [19]. In order to produce the TNT layer, titanium was used as anode in combination with a platinum cathode and a direct current was applied between them. Before the application of chitosan, titanium was coated with alginate to improve the electrostatic interactions of chitosan. Samples were immersed in a solution containing chitosan, alone or in combination with bioactive glass particles (BG). FTIR spectrum of titanium coated with chitosan and BG showed that amide I, amide II and amide III bonds of chitosan are shifted to higher frequencies from their characteristic values of 1650 cm^{-1} , 1550 cm^{-1} and 1328 cm^{-1} . The average roughness (R_a) of titanium is 132 nm and decreases to 112 nm when titanium is coated with chitosan and BG, while TNT presents roughness of 449 nm , 86 nm when coated with chitosan and 143 nm when coated with chitosan and BG. It emerges that chitosan reduces the roughness of the substrate. It can also be noted that chitosan

blended with BG attached to titanium has similar roughness to TNT titanium coated with chitosan. It seems that TNT do not improve the reduction of roughness. The wettability highly depends on these values of roughness, contact angles for titanium with and without chitosan and BG coating are similar ($72.5^{\circ} \pm 4.3$ and $76.4^{\circ} \pm 5.6$ respectively), while chitosan applied to TNT titanium shows a high increase in the contact angles values ($34.1^{\circ} \pm 5.5$ for TNT layer, $91.5^{\circ} \pm 6.3$ for TNT layer coated with chitosan and $66.2^{\circ} \pm 2.9$ for TNT layer coated with chitosan and BG).

FTIR spectra obtained from the analysis of the samples studied in this thesis showed values as reported in literature, allowing the assessment of the presence of chitosan on the substrates.

Average roughness values obtained in this thesis for areas of $5 \mu\text{m}^2$ report values in the nanoscale (123 nm is the S_a for oxidised titanium). When chitosan is dissolved in acetic acid and is physically attached to the substrate, S_a has a value of 4.73 nm. Other coatings in this thesis showed roughness values similar to oxidised titanium and to coatings obtained with nanotubes on the surface.

Contact angles for the samples in this thesis showed values similar to the ones in previous literature, indicating a decrease in wettability when chitosan coats the substrates. For the case study, the substrates are hydrophobic with a contact angle of $81.4^{\circ} \pm 0.77$ for mirror polished titanium and $76^{\circ} \pm 5.59$ for the one oxidised. Chitosan coating with physical adhesion or with a leaving group maintain the hydrophobic behaviour of the samples ($83.95^{\circ} \pm 4.4$ and $103^{\circ} \pm 14.44$ respectively), while the adhesion with the coupling agent resulted in a hydrophilic behaviour with a contact angle of $16.7^{\circ} \pm 13.97$. This result is similar to the one obtained by *Zheng et al.* for titanium coated with chitosan through polydopamine and indicates the prevalence of polydopamine with respect to chitosan on the wettability of the coating.

SAMPLE	Roughness (μm)	Contact angle	Adhesion strength (ASTM Standard)	References
MP_Ti+Chitosan	-	$76.4^{\circ} \pm 5.1$	-	[15]
CT_Ti+HAP	-	12.5°	-	[16]
CT_Ti+HAP+Chitosan	-	29.4°	-	[16]
CT_Ti+Chitosan	-	$27^{\circ} \pm 3$	-	[6]
CT_Ti+Dopamine+Chitosan	-	$<10^{\circ}$	-	[6]
CT_Ti+Polydopamine+Chitosan	-	$<10^{\circ}$	-	[6]
MP_Ti+ZnHAP+CNT+Chitosan	-	-	5B	[17]
Grit blasted titanium (GB_Ti)	1,95	15°	-	[18]
GB_Ti+Chitosan	1,45	78°	-	[18]
GB_Ti+BG+Chitosan	1,87	34.5°	-	[18]
GB_Ti+nBG+Chitosan	-	92°	-	[18]
MP_Ti	0,132	$72.5^{\circ} \pm 4.3$	-	[19]
MP_Ti+BG+Chitosan	0,112	$76.4^{\circ} \pm 5.6$	-	[19]
TNT	0,449	$34.1^{\circ} \pm 5.5$	-	[19]
TNT+Chitosan	0,086	$91.5^{\circ} \pm 6.3$	-	[19]
TNT+BG+Chitosan	0,143	$66.2^{\circ} \pm 2.9$	-	[19]
Oxidised titanium	0,123	$76^{\circ} \pm 5.59$	-	-
CT_DIRECT_AA	0,0047	$83.95^{\circ} \pm 4.4$	5B	-
CT_TRESYL_37_PBS	0,116	$103^{\circ} \pm 14.44$	0B	-
CT_POLYDOP_WATER	0,137	$16.7^{\circ} \pm 13.97$	-	-

Table 5.11: values of roughness, wettability and adhesion strength reported from literature to compare the results of this study. Roughness values (S_a) for this study are obtained for an area of $5 \mu\text{m}^2$, *Avcu et al.* reported S_a for an area of 2 mm^2 and *Mokhtari et al.* reported R_a for a line

Since the aim of this study is to develop an antibacterial and antimicrobial coating with modulated host response and knowing from literature [20], [21] that macrophages prefer rough surfaces for adhesion and proliferation, the coating should have the lowest values. The challenge is to obtain a substrate that possess antibacterial behaviour and that is also capable to stimulate osteointegration.

The strength of adhesion, as resulted in tape test, can be explained by acid-base interactions as discovered by *Fowkes* in 1981 [9]. Titanium shows an acid surface as evidenced by zeta potentials. When chitosan is dissolved in acetic acid it becomes protonated with a positive charge that allows a strong adhesion with the negative substrate. When chitosan is suspended in PBS, instead, loses its charge and the adhesion is weaker.

The results obtained showed that the use of a leaving group or of a coupling agent did not produced the desired improvements on the coating and that the physical adhesion, when chitosan is dissolved in acetic acid, is sufficient to obtain a uniform coating with a simple procedure.

5.8. Bibliography

- [1] T. Hayakawa, "Biochemical surface modifications to titanium implants using the tresyl chloride activated method," *Dent. Mater. J.*, vol. 34, no. 6, pp. 725–739, 2015.
- [2] H. Lee, S. M. Dellatore, W. M. Miller, and P. B. Messersmith, "Mussel-inspired surface chemistry for multifunctional coatings," *Science*, vol. 318, no. 5849, pp. 426–430, 2007.
- [3] H. Li *et al.*, "Enhancement of growth and osteogenic differentiation of MC3T3-E1 cells via facile surface functionalization of polylactide membrane with chitooligosaccharide based on polydopamine adhesive coating," *Appl. Surf. Sci.*, vol. 360 Part B, pp. 858–865, 2016.
- [4] J. Liu *et al.*, "Simple and tunable surface coatings via polydopamine for modulating pharmacokinetics, cell uptake and biodistribution of polymeric nanoparticles," *RSC Adv.*, vol. 7, no. 26, pp. 15864–15876, 2017.
- [5] X. Yu, J. Walsh, and M. Wei, "Covalent Immobilization of collagen on titanium through polydopamine coating to improve cellular performances of MC3T3-E1 cells," *RSC Adv.*, vol. 4, no. 14, pp. 7185–7192, 2013.
- [6] D. Zheng, K. G. Neoh, Z. Shi, and E. T. Kang, "Assessment of stability of surface anchors for antibacterial coatings and immobilized growth factors on titanium," *J. Colloid Interface Sci.*, vol. 406, no. 1, pp. 238–246, 2013.
- [7] E. B. Ibitoye, I. H. Lokman, M. N. M. Hezmee, Y. M. Goh, A. B. Z. Zuki, and A. A. Jimoh, "Extraction and physicochemical characterization of chitin and chitosan isolated from house cricket," *Biomed. Mater.*, vol. 13, no. 2, p. 025009, 2018.
- [8] C. A. Breda, D. L. Morgado, O. B. G. Assis, and M. C. T. Duarte, "Processing and characterization of chitosan films with incorporation of ethanolic extract from 'pequi' peels," *Macromol. Res.*, vol. 25, no. 11, pp. 1049–1056, 2017.
- [9] F. M. Fowkes, "Acid-Base Interactions in Polymer Adhesion," *Tribol. Ser.*, vol. 7, no. 1, pp. 119–137, 1981.
- [10] S. Ferraris, M. Cazzola, V. Peretti, B. Stella, and S. Spriano, "Zeta Potential Measurements on Solid Surfaces for in Vitro Biomaterials Testing : Surface Charge , Reactivity Upon Contact With Fluids and Protein Absorption," *Front. Bioeng. Biotechnol.*, vol. 6, no. 9, pp. 6–60, 2018.
- [11] I. F. Amaral, A. L. Cordeiro, P. Sampaio, and M. A. Barbosa, "Attachment, spreading and short-term proliferation of human osteoblastic cells cultured on chitosan films with different degrees of acetylation," *J. Biomater. Sci. Polym. Ed.*, vol. 18, no. 4, pp. 469–485, 2007.
- [12] S. Ferraris, S. Spriano, G. Pan, and C. L. Bianchi, "Surface modification of Ti-6Al-4V alloy for biomineralization and specific biological response : Part I , inorganic modification," *J. Mater. Sci. Mater. Med.*, vol. 22, no. 3, pp. 533–45, 2011.
- [13] S. Kang *et al.*, "One-Step Modification of Superhydrophobic Surfaces by a Mussel-Inspired Polymer Coating," *Angew. Chem. Int. Ed. Engl.*, vol. 49, no. 49, pp. 9401–9404, 2010.
- [14] T. E. L. Douglas *et al.*, "Titanium surface functionalization with coatings of chitosan and polyphenol-rich plant extracts," *Mater. Lett.*, vol. 196, no. 24600, pp. 213–216, 2017.
- [15] J. D. Bumgardner, R. Wiser, S. H. Elder, R. Jouett, Y. Yang, and J. L. Ong, "Contact angle, protein adsorption and osteoblast precursor cell attachment to chitosan coatings bonded to titanium," *J. Biomater. Sci. Polym. Ed.*, vol. 14, no. 12, pp. 1401–1409, 2003.
- [16] S. Tang, B. Tian, Y.-J. Guo, Z.-A. Zhu, and Y.-P. Guo, "Chitosan/carbonated hydroxyapatite

- composite coatings: Fabrication, structure and biocompatibility,” *Surf. Coatings Technol.*, vol. 251, no. 1, pp. 210–216, 2014.
- [17] Z. Zhong, J. Qin, and J. Ma, “Electrophoretic deposition of biomimetic zinc substituted hydroxyapatite coatings with chitosan and carbon nanotubes on titanium,” *Ceram. Int.*, vol. 41, no. 7, pp. 8878–8884, 2015.
 - [18] E. Avcu, Y. Yıldıran Avcu, F. E. Baştan, M. A. U. Rehman, F. Üstel, and A. R. Boccaccini, “Tailoring the surface characteristics of electrophoretically deposited chitosan-based bioactive glass composite coatings on titanium implants via grit blasting,” *Prog. Org. Coatings*, vol. 123, pp. 362–373, 2018.
 - [19] H. Mokhtari, Z. Ghasemi, M. Kharaziha, F. Karimzadeh, and F. Alihosseini, “Chitosan-58S bioactive glass nanocomposite coatings on TiO₂ nanotube: Structural and biological properties,” *Appl. Surf. Sci.*, vol. 441, no. 1, pp. 138–149, 2018.
 - [20] Z. Sheikh, P. J. Brooks, O. Barzilay, N. Fine, and M. Glogauer, “Macrophages, Foreign Body Giant Cells and their response to implantable biomaterials,” *Materials (Basel)*, vol. 8, no. 1, pp. 5671–5701, 2015.
 - [21] B. Chehroudi, “Effects of Surface Topography on Cell Behavior,” in *Encyclopedic Handbook of Biomaterials and Bioengineering*, D. L. Wise, Ed. Marcel Dekker, 1995, pp. 813–842.

Conclusions

When developing a coating for a biomaterial, it needs to have high efficacy in terms of covering of the surface, proper roughness, strength of attachment, chemical stability, biocompatibility, biological efficacy and simplicity of the procedure. Covering of a coating is measured by the uniformity of the coating and it is maximised when it covers all the substrate. The strength of the attachment is important to avoid an easy removal. Simplicity of the procedure of attachment is useful on an industrial level to reduce time and costs of production. Chemical stability is required in a wide range of pH considering its variability in physiological conditions. Since leucocytes prefer rough surfaces, in order to control the host response and avoid the development of a chronic inflammation, a smooth surface is preferable when coating a substrate for the specific purpose of this work.

In this thesis the results obtained indicate that chitosan dissolved in acetic acid physically attached to a chemically treated titanium substrate matches the requirements for an efficient coating in terms of covering of the surface, proper roughness, strength of attachment, chemical stability and simplicity of the procedure. The use of an acidic environment for the coating procedure allows to effectively use the presence of positively charged amine groups for a stronger interaction of the coating to the substrate, that is negatively charged.

Further analysis should focus on realizing the attachment under sterile conditions and to test the microbial and cell response both *in vitro* and *in vivo*.

The coatings tested in this thesis can also be applied to other types of substrates to verify their attachment and properties on other biomaterials such as bio-glasses and hydroxyapatite.

Acknowledgements

This thesis would have not been finished without the help of many people.

First of all, I want to express my gratitude to Professor Silvia Spriano and Professor Sara Ferraris for the opportunity to study abroad and being part of this project.

My utmost gratitude goes to my co-supervisor Dr. Gissur Örlygsson at the Innovation Center Iceland for his enthusiasm, help and support during this work and to Dr. Ng Chuen How of GENIS for his knowledge of chitosan. I would like to thank Dr. Birgir Johansson for his assistance with Scanning Electron Microscope at Innovation Center and Dr. Unnar Arnalds with the Atomic Force Microscope at the University of Iceland.

I am also thankful to all the staff and employees at Innovation Center Iceland for their welcoming, for sharing their spaces and their stories about Iceland.

Thanks to Giulia Maggia, Alessia Di Nubila, Giovanna Di Sevo, Sara Saber Younes Mohamed, Giacomo Riccucci and all the new and old friends that contributed with friendship and advices during these years of studying together. Thanks also to Ella Nurmi, my Finnish flatmate in Iceland, for the great adventures shared.

And finally, and most importantly, my gratitude goes to my family. In particular, to my mother, in which memory this work was done and to which is lovingly dedicated, for sharing her passion for biology and human life while I was a child, to my father, who is the person I admire most in life for never giving up in any circumstance, and to my sister and my brother for their support and encouragement as family and as engineers.